UNIVERSITÀ DEGLI STUDI DI PADOVA

DIPARTIMENTO DI INGEGNERIA CIVILE, EDILE E AMBIENTALE

Department Of Civil, Environmental and Architectural Engineering

Corso di Laurea Magistrale in Environmental Engineering

TESI DI LAUREA

Study on the adsorption capacity and selectivity of magnetic adsorbents based on graphene oxide toward heavy metals

Relatore: Prof. Sgarbossa Paolo

Laureando: Russo Eleonora
2024143

ANNO ACCADEMICO 2021-2022

Contents

1 Introduction

The delicate historical period we are living clearly indicates that a lot of certainties are not so solid. Thus, if the lack of potable water has not been experienced up to now in the most developed areas, this could easily change in the next decades, making the protection of water resources of paramount importance. To sustain this endeavour, we must avoid returning to the environment any polluted wastewater. The 6th of the 17 goals established in the 2030 Agenda for Sustainable Development is about the need to "ensure availability and sustainable management of water and sanitation for all". In fact, 80% of wastewater in the world flows back into the ecosystem without being treated or reused. The correct management and treatment of wastewater is essential.

Figure 1.1 presents a simplified overview of water uptake and subsequent wastewater pathways back to the environment. The effluents from certain industries may require treatment that is not commonly available in urban wastewater treatment plants and may therefore be treated on-site before direct release to water (scenario A). Some industrial units, such as cooling systems, generate wastewater streams with low pollutant content that can be directly released into receiving waters without treatments (scenario B). Some industrial installations generate effluents those cannot be directly released to surface water (and not treated on site) and thus are transferred off site for treatment at an urban wastewater treatment plant or independently operated wastewater treatment plant (scenario C), the so-called indirect releases.

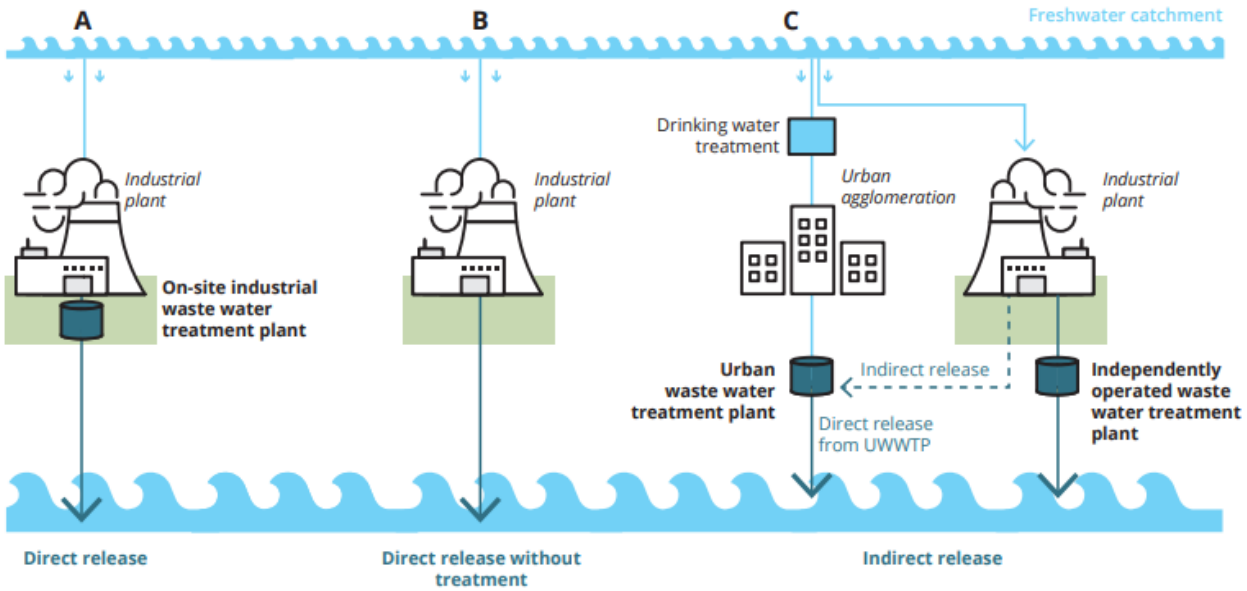

Figure 1.1: Simplified wastewater treatment cycle (Granger & Montalvo, 2018).

The treatment of industrial wastewater at an urban wastewater treatment plant is typically a commercial arrangement between the industry that generates the wastewater and the plant that treats it. This can be complex, but a charge is normally based on the quantity of wastewater and its

constituent pollutants. The operation will also typically restrict, or even, prohibit the receipt of pollutants that might comprise operation of the plant.

In this perspective, this work would investigate innovative possibilities for treating wastewater containing heavy metals ions. Up to now, the main problem regarding wastewater treatment is that traditional wastewater treatment methods suffer with high capital cost, high energy requirement, incomplete pollutant removal, and the disposal of secondary wastes. On the other hand, adsorption on the surface of solid adsorbents demonstrates a great perspective for the treatment of heavy metal ion contaminated water. It is more advantageous than other methods owing to its simple design and low investment in terms of initial cost and space required. Further, the adsorption process becomes highly cost effective if the adsorbent used is recyclable (Wadhawan et al., 2020). Ideally an adsorbent should provide sufficient binding sites for appropriate adsorption of heavy metal ions. Main conventional adsorbents used for heavy metal ion elimination are activated carbon, metal oxides, clay etc. to name a few. These traditional adsorbents suffer from certain constraints such as low adsorption capacities, lack of functional tunability, reusability and recyclability. To overcome such limitations, new sorbents in nano dimensions are being synthesized and adopted. Nowadays, a considerable attention has been drawn by nanomaterials as adsorbents in decontamination of wastewater. In fact, they possess high surface area, good adsorption capacity, high mobility in solution, reactivity, and their small size leads to use in wastewater treatment. Many of the research studies state that nanomaterials show great promise for applications in water and wastewater treatment and were able to remove organic, inorganic, and heavy metal pollutants. Furthermore, nanostructured adsorbents can be reused and recycled repeatedly which makes them cost-effective.

Mainly magnetite (Fe_3O_4) nanoparticles were investigated, for their easy synthesis and dispersion in water solution, either pristine or deposited on graphene oxide nanosheets. Graphene oxide possess a good dispersibility in aqueous solution and this makes it easily mixable with the polluted wastewater to be treated. Its good dispersibility during the first adsorption phase is then overcome, during the recovery phase, by the presence of magnetic nanoparticles in the composite structure. Moreover, to study a more effective and separable adsorption system, preliminary tests on the incorporation of the prepared materials in sodium alginate beads have been pursued. Sodium alginate is a natural polysaccharide which can be extracted from brown algae, which is nontoxic, biocompatible, and able to crosslink by coordinating metal cations. It has been used for the encapsulation of chemical and biological compounds in a wide range of applications such as agriculture, food technologies, pharmaceuticals, cosmetics, chemical and environmental engineering, paper and textile industry. It has several manufacturing advantages including water-based reaction, high cross-linking capability, economical and easily synthesized derivatives, and room temperature manipulation of gelation,

enabling simple and safe procedures. However, these polymers are generally not mechanically stable, their internal structure is dense, and swell significantly in aqueous solutions. On the other hand, they can be easily modified with the addition of nanoparticles or other compounds, giving composite with enhanced strength and improved adsorption capacity. The final goal is to obtain effective and separable magnetic adsorbents to be applied in the treatment of heavy metals polluted wastewater.

2 Water consumption and heavy metals in wastewater

The quantitative relevance of industry in the water cycle can be measured considering its water consumption or its water uptake. The term water consumption in industrial activities refers to the difference between the water that is taken from a source and the amount of water that is then released either into the environment or into the sewage system after the use. The most common water outputs are wastewater effluents, cooling system purges and evaporation and steam purges to release pressure. On the other hand, water uptake refers to the gross amount of water that enters a facility in a given period. Thus, water uptake is, by definition, greater than water consumed. While water consumption is a better metric to understand the potential distortion of the water cycle by a given industrial site, it is also a metric for which data are scarce and which presents methodological challenges in terms of data collection. Water uptake is a good proxy for understanding the relevance of the sector. Global data on water uptake per region in 2016 are presented in Figure 2.1. It shows that industry in Europe is a major consumer of water in relation to other sectors (54 %). The global average water uptake by industry is around 19 % (Granger & Montalvo, 2018).

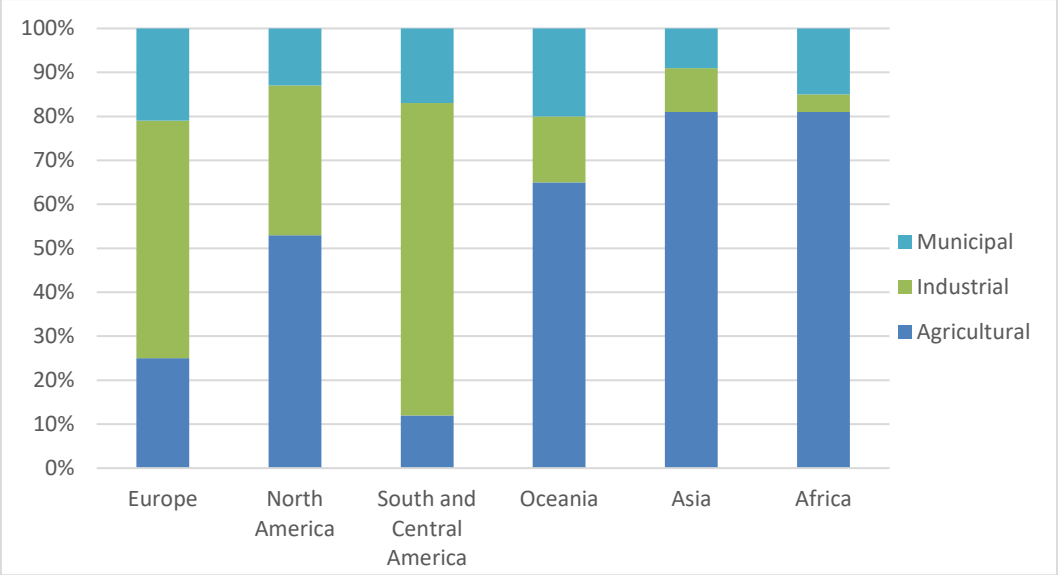

Figure 2.1:Estimated annual share of global water uptake activity and country.

The release of industrial wastewater is regulated in Europe both directly as part of the environment law on industry and indirectly by the EU policies on water issues. Under the Water Framework Directive (WFD, 2000/60/EC), specific directives regulate aspects that will influence industrial wastewater generation and management. The most relevant are the Urban Waste Water Treatment Directive (UWWTD, 91/271/EEC), the Groundwater Directive (2006/118/EC) and the Environmental Quality Standards Directive (2008/105/EC). Industry's direct or indirect releases of pollution to the environment are among the key aspects regulated by the Industrial Emissions

Directive (IED, 2010/75/EU). All these instruments combined constitute the main mechanism for protection regarding industrial wastewater and each regulates a specific element of the various pathways in which industrial wastewater can be released. Figure 2.2 is a simplified illustration of the interactions between the compliance points of the three directives.

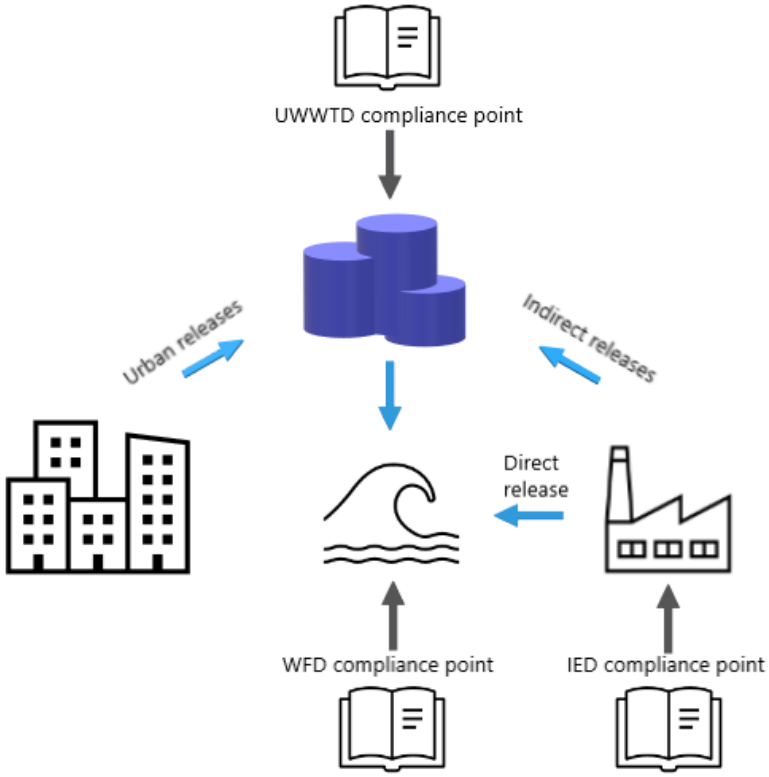

Figure 2.2: Compliance points for the three key directive protecting the environment from environmental pressures to water.

Heavy metals (HMs) are defined as those elements having an atomic number greater than 20 and atomic density above 5 g cm^{-3} and must exhibit the properties of metal. They can be broadly classified into two categories: essential and nonessential heavy metals. Essential heavy metals are those required in trace amounts by living organisms for carrying out the fundamental processes like growth, metabolism, and development of different organs. There are numerous essential heavy metals like Cu, Fe, Mn, Co, Zn, and Ni required by plants as they form cofactors that are structurally and functionally vital for enzymes and other proteins. Essential elements are often required in the level of 10–15 ppm and are known as micronutrients. Nonessential heavy metals like Cd, Pb, Hg, Cr, and Al are not required by living organisms, even in trace amounts, for any of the metabolic processes (Raychaudhuri et al., 2021).

Heavy metal pollution in water is a global environmental problem. This is mainly due to their excessive accumulation, biomagnification, toxicity, and persistency. In fact, they are not biodegradable and creates serious threat to human and nature. Heavy metals can derive from both

natural and anthropogenic sources. Natural sources mainly comprise bedrock weathering, while anthropogenic sources include industrial production, fertilizer use, and sewage discharge. Heavy metals are not easily removed in a standard wastewater treatment plant configuration. In 2016, 68 % of industrial emissions (1,402 tonnes) of heavy metals reported in the European Pollutant Release and Transfer Register (E-PRTR) were transferred to urban wastewater treatment plants. They, which also receive some input from municipal wastewater, released 1,276 tonnes of heavy metals directly to the environment.

Figure 2.3 illustrates the sectors and sub-sectors with the highest estimated pressure on the water environment from direct releases of heavy metals in terms of eco-toxicity. The dominance of the wastewater treatment sector is because wastewater treatment plants receive effluents from industry but also from surface run-off from impervious surfaces (such as roofs and roads) and domestic wastewater, which can both be rich in heavy metals. Despite larger direct releases of heavy metals in terms of mass, the estimated environmental pressure of emissions from metal processing industries is lower relative to other industry sub-sectors. That is due to the high emissions of copper from the energy supply sector and the high eco-toxicity of copper in freshwater (Granger & Montalvo, 2018).

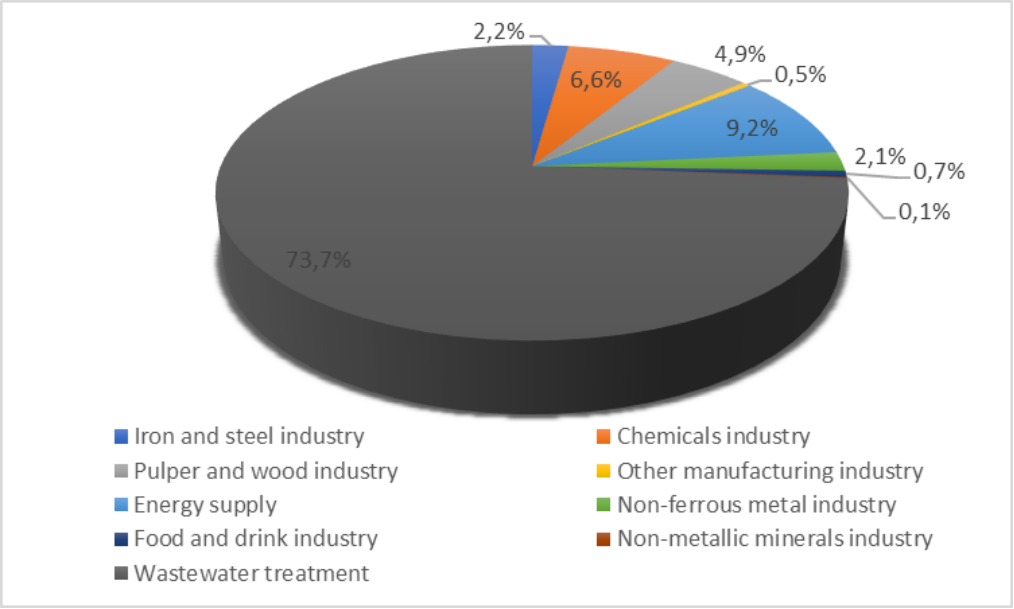

Figure 2.3: Direct releases of heavy metals by sector and sub-sector, expressed as eco-toxicity.

Figure 2.4 reports the industries' streams that contribute to enrich the wastewater treatment system of heavy metals, according to The European Pollutant Release and Transfer Register (E-PRTR), Member States reporting under Article 7 of Regulation (EC) No 166/2006 provided by European Environment Agency (EEA).

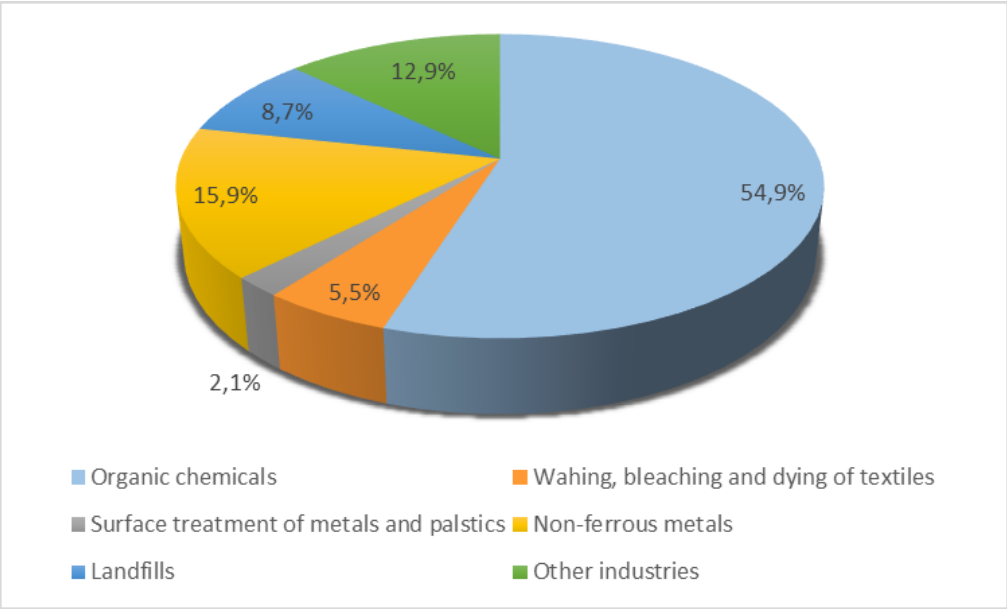

Figure 2.4: Sources of transfers to urban waste water treatment plants.

Based on the data reported in Figure 2.5, the largest industrial contributor of indirect releases of heavy metals is chemicals manufacturing, followed by non-ferrous metal processing and other manufacturing. Among industry, the energy supply sector is one of the highest direct emitters of heavy metals to water but does not appear to transfer much of the load off site for treatment. The shares of non-ferrous metal and other manufacturing sub-sectors in direct releases of heavy metals are low, yet these sub-sectors are responsible for 18 % and 11 % of indirect releases of heavy metals by industry. This suggests that the transfer of emissions is more common in sectors with a large number of smaller facilities than in sectors with a smaller number of larger facilities (Granger & Montalvo, 2018).

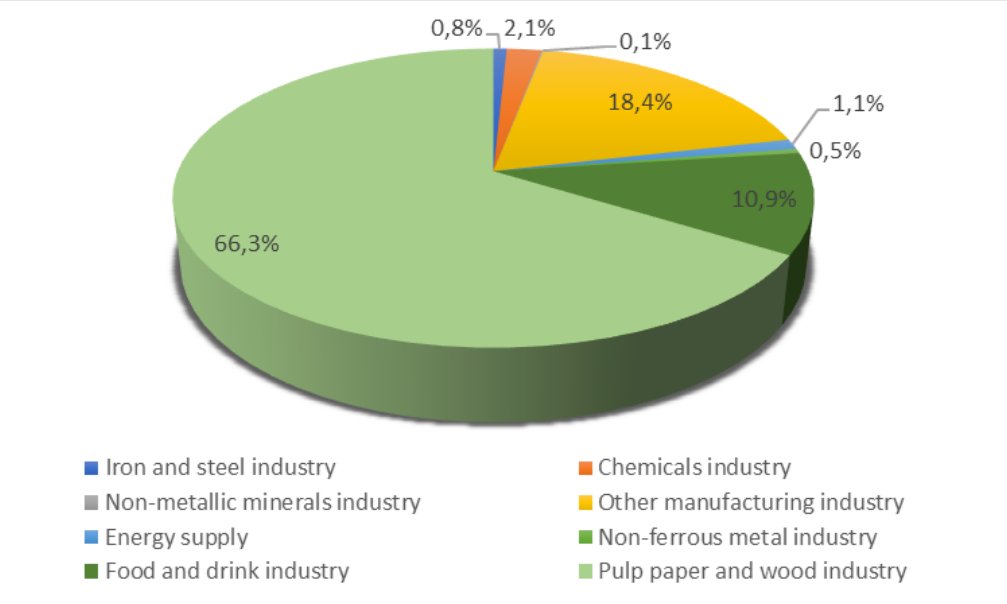

Figure 2.5: Indirect releases of heavy metals by sector and sub-sector, expressed as eco-toxicity.

The pressure on the environment from industrial activities is greatest where there are large-scale individual chemical or metal manufacturing sites, power plants or clusters of facilities with relatively small emissions, for example the chemical manufacturing plants in western Germany and northern Italy and the power plants in northern Spain and Germany. Furthermore, the pressure of heavy metals from wastewater treatment plants is highest near large cities such as London and Birmingham in the United Kingdom, Sofia in Bulgaria, Barcelona in Spain, and Munich and Cologne in Germany. Some parts of Europe particularly exposed to pressures from heavy metal emissions generated by both manufacturing and power plants include regions in northern England, western Germany, northern Italy and Spain (Granger & Montalvo, 2018).

In Italy, the limits for the discharge in superficial water or in the sewage system are stabilized by the D.lgs of April 3rd, 2006, n°152 (Table 2.1). These limits hold for each type of wastewater, including also all the industrial wastewater streams discharged in the environment. In specific cases, more stringent limits could be applied, by competent authorities.

Table 2.1: Limit values for the discharge in superficial water and in the sewage. (*Decreto Legislativo 3 Aprile, N°152, Parte Terza, Allegato 5, Tabella 3, 2006).*

Parameter	**Discharge in superficial water (mg L^{-1})**	**Discharge in the sewage system (mg L^{-1})**
Aluminum	≤ 1	≤ 2.0
Arsenic	≤ 0.5	≤ 0.5
Barium	≤ 20	-
Boron	≤ 2	≤ 4
Cadmium	≤ 0.02	≤ 0.02
Total chromium	≤ 2	≤ 4
Chromium (VI)	≤ 0.2	≤ 0.20
Iron	≤ 2	≤ 4
Manganese	≤ 2	≤ 4
Mercury	≤ 0.005	≤ 0.005
Nickel	≤ 2	≤ 4
Lead	≤ 0.2	≤ 0.3
Copper	≤ 0.1	≤ 0.4
Zinc	≤ 0.5	≤ 1.0

Table 2.2 reports the limits of some heavy metals acceptable for drinking water, in accordance to the United State Environment Protection Agency (US-EPA) and to the World Health Organization (WHO).

Table 2.2: Permissible limits for heavy metals.

Heavy metal	**Acceptable limit for the US-EPA (mg/L)**	**Acceptable limit for the WHO (mg/L)**
Arsenic	0.01	0.01
Cadmium	0.005	0.003
Chromium (total)	0.1	0.05
Copper	1.3	2
Nickel	-	0.07
Lead	0.015	0.01
Mercury	0.002	0.006

3 Common heavy metals removal techniques

In the last few decades, several methods have been developed and extensively investigated for heavy metal removal from water matrices. The most common techniques can be divided in chemical and physical ones. The first are based on the physical transfer of the pollutant from a phase (e.g., aqueous solution) to another phase (e.g., membrane surface). Membrane filtration, solvent extraction, and ion exchange are common example of physical removal techniques. The second ones are based on the chemical transformation of the pollutant. Chemical precipitation, and electrochemical treatment and are diffuse example of chemical removal techniques. Each of these techniques have their advantages and limitations.

3.1 Physical techniques

Membrane filtration is a method whose use is constantly increasing in the last years. It allows to remove a wide range of contaminants: suspended solids, organic and inorganic compounds (e.g., heavy metals), depending on the size of the particle that can be retained. There are three types of membrane filtration for removal of heavy metals: ultrafiltration (UF), nanofiltration (NF) and reverse osmosis (RO). This classification is based on the size of the particles that can be retained by the membrane: UF > NF > RO. Therefore, generally NF membranes separation efficiency is between the UF and RO ones. The three types of filtrations combined can be used to obtain multiple barriers in order to increase the efficiency. Ultrafiltration presents some advantages such as lower driving force and a smaller space requirement due to its high packing density. It utilizes permeable membrane to separate compounds on the basis of the pore size (5-20 nm) and the molecular weight. With a metal concentration ranging from 10 to 112 mg/L, UF can reach a removal efficiency higher than 90%. However, fouling has many adverse effects on the membrane (e.g., flux decline, increase in transmembrane pressure), which result in high operational costs. Reverse osmosis is sometimes used to remove low levels of heavy metals from drinking water. However, this method is costly and easily subject to clogging (the same metal oxides tend to clog the membrane). It is a separation process that uses pressure to force a solution through a membrane that retains the solute on one side and allows the pure solvent to pass to the other side. For what concern solvent extraction, it is used for heavy metal removal, but it is considered to be economical only for concentrated solutions. Specifically, it is used for the recovery of economically valuable heavy metals from ores or from waste. The other main technique applied to the physical removal of heavy metals is ion exchange, a reversable chemical reaction wherein an ion from a wastewater solution is exchanged for a similarly charged ion

attached to an immobile solid particle. These solid ion exchanges are either naturally occurring inorganic zeolites or synthetically produced resins. So, ion exchangers are capable of exchanging ions with the surrounding solution. They attract soluble ions from the liquid phase to the solid phase. It is a physical reparation method, they cannot change the ions chemically. The most common are synthetic organic resins, which generally can be regenerated on site by treatment with acid or caustic soda. The positively charged ions in cationic resins such as hydrogen and sodium ions are exchanged with positively charged ions, such as nickel, copper, zinc, copper, chromium, iron in the solutions. This method is very efficient, low-cost, small sludge producing, and selective. However, it has many drawbacks, the most important being that it cannot treat water with high metal concentration, because of fouling of the matrix by organics and other solids present in the wastewater. Furthermore, ion exchange is nonselective and highly sensitive to pH.

3.2 Chemical techniques

Chemical precipitation is an effective technique for remove heavy metals from wastewater. In the process, chemicals react with the heavy metals present in wastewater with the formation of insoluble precipitates. These precipitates are removed using sedimentations technique and the cleaned water is decanted. The removal percentage of metal ions in the solution may be improved to optimum by changing major parameters such as pH, temperature, and initial concentrations. The method of chemical precipitation can be summarized by the following precipitation equation (M^{2+} are the dissolved metal ions, OH^- represents the precipitant and $M(OH)_2$ is the insoluble metal hydroxide):

$$M^{2+}+2OH^- \leftrightarrow M(OH)_2$$

The major parameter affecting this method is the pH, which needs to be adjusted to basic conditions, which affect the solubility of metals, and these conditions helps convert heavy metals into hydroxides, sulphides, and other less soluble compounds. The most common precipitant agents used are lime and limestone (composed of calcium carbonate, $CaCO_3$). Lime precipitation is efficient to treat inorganic effluents with concentrations higher than 1000 mg/L. Other inorganic precipitants used for heavy metal precipitation are caustic soda (NaOH), soda ash (Na_2CO_3), sodium bicarbonate ($NaHCO_3$), sodium sulphide (Na_2S) and sodium hydrogensulphide (NaHS). Although the technique is cheap, safe, and simple, it requires the use of a large amount of chemicals in order to reduce metal content to an acceptable level. The chemical agents employed in this technique might pollute the water supply even more. Furthermore, it creates a lot of sludge needing treatment and sludge treatment is very expensive. Other minor drawbacks are slow metal precipitation, poor settling, aggregation of metal

precipitates, and long-term environmental impacts of sludge disposal. Electrochemical treatment is a promising technique for the treatment of heavy metal containing wastewater because of its efficiency, compatibility, and versatility. Major benefits are the treatment of lower concentrations of heavy metals and effluents with complex composition. But these techniques might consume a lot of electricity. This process includes electrochemical oxidation and reduction, electrodeposition, electrocoagulation, electroflotation, and electrodialysis. In electrochemical removal, electricity is used in an aqueous metal-bearing solution containing a cathode plate and an anode. Heavy metals are deposited on the negatively charged surface and are removed in the elemental metal state. However, there is a high sludge production and low metal precipitation which leads to long-term environmental impacts on sludge disposal. Moreover, the efficiency depends on the cell parameters such as mass transport, temperature, conductivity, pH, water composition. Other limitations are the short lifetime of electrode material, a rise of temperature, and low mass transfer rates.

Table 3.1 summarizes the comparisons of the tradition methods for the removal of heavy metal ions.

Table 3.1: Comparison of traditional methods for the removal of heavy metal ions (Gao et al., 2020).

Technology	**Advantages**	**Disadvantages**
Ion exchange	- Metal selective - High regeneration	- High initial capital cost - High maintenance cost
Membrane filtration	- Low solid waste generation - Low chemical consumption - Small space requirement - Possible to be metal selective	- High initial capital cost - High maintenance and operation cost - Membrane fouling - Limited flow rates - Large amount of sludge containing metals
Chemical precipitation	- Process simplicity - Inexpensive capital cost	- Sludge disposal cost - High maintenance cost - Not metal selective
Electro deposition	- High purity metal generation - Might generate nanoparticles - Applicable at room temperature	- High energy requirement - Time consumption - Pollution on the solution

4 Adsorption

Adsorption is a physical separation process in which certain components of a fluid phase are transferred to the surface of a solid adsorbent. In our case, it can be seen as a physicochemical treatment process which operates the effective removal of heavy metals from contaminated wastewater and is one of the most preferred and efficient method. This even if the cost of the carbon-based adsorption materials is rising due to the depletion of coal-based commercial carbon (Thakur et al., 2022). In fact, adsorption has certain advantages over conventional methods such as they minimize chemical and biological sludge, low cost, high efficiency both at high and low contaminant concentration, regeneration of adsorbents and possibility of metal recovery. Adsorbents which have been already used for heavy metal removal are activated carbon, zeolite, chitosan, carbon nanotubes, manganese oxides, agricultural waste product such as water hyacinth, hazelnuts shells, orange peel pith, sunflower, coconut coir pith, bacterial biosorbent, fungal biosorbent, marine algae, microbial and plant derived biomass.

4.1 Process description

Basically, adsorption is a mass transfer process of substances which bind by physical and/or chemical interactions to a solid surface. It consists in the transfer of a substance from the liquid or gas phase to the surface of a solid. The substance may be bound by physical (electrostatic interaction, diffusion, and van der Waals force) and/or chemical interactions (coordination interaction, chemical bonding, and acid-base interactions). The process is composed of three main steps:

1. Transport of the pollutant from the bulk solution to the sorbent surface;
2. Adsorption on the solid surface;
3. Transport within the sorbent particle.

4.1.1 Adsorption isotherms

Adsorption isotherms correlate the extent of adsorption of heavy metal ions with their concentrations at constant temperature. To characterize adsorption mechanism, Langmuir and Freundlich isotherms are used. Langmuir model depicts the monolayer adsorption of the solute on the adsorbent surface with fixed number of adsorption sites with equivalent affinity towards the adsorbate molecules. This model is represented by the following equation:

$$q_e = \frac{q_m K_l C_e}{1 + K_l Ce} \quad [1]$$

where C_e (mmol/g or mg/g) is the adsorption capacity or amount of material adsorbed per gram of substrate; q_m (mmol/g or mg/g) refers to the maximum adsorption capacity of the material at saturation and K_l is the equilibrium adsorption constant for the adsorbent-adsorbate system. The Langmuir model does not give any idea about the heterogeneous adsorption and roughness of the adsorbent surface. However, the Freundlich model describes the multilayer adsorption and roughness of the adsorbent surface (non-uniform adsorption energies). Thus, the Freundlich isotherm is based on multilayer sorption by assuming that the adsorbent has a heterogeneous surface with nonuniform distribution of sorption sites. This empirical model can be described using the following equation:

$$q_e = K_f C_e^{1/n} \quad [2]$$

The surface heterogeneity is described by the exponential term (1/n). The major difference between the two models is that the Freundlich model assumes that an infinite amount of adsorbate can be adsorbed onto the adsorbent surface, where the strength of the interactions is dependent on the degree of surface coverage. This is in contrast to the Langmuir model that assumes monolayer adsorption by the adsorbate occurs until saturation of the independent sites is attained (Agbovi & Wilson, 2021).

Considering instead the evaluation of the experimental results, the adsorption capacity of the adsorbent at different times and equilibrium are ascertained by the following equations:

$$q_e = \frac{(C_0 - C_e)V}{W} \quad [3]$$

$$q_t = \frac{(C_0 - C_t)V}{W} \quad [4]$$

where q_t (mg/g) is the adsorption capacity at time t; q_e (mg/g) is the adsorption capacity at equilibrium; C_o (mg/L) is the initial concentration of heavy metal ions solutions; C_e (mg/L) is the equilibrium concentration of heavy metal ions solutions; C_t (mg/L) is the concentration of heavy metal ions solutions at time t (min); V (mL) is the volume of heavy metal ions solution; W (mg) is the weight of dry adsorbent.

4.1.2 Adsorption kinetics

The kinetic predictions are significant and vital for understanding the adsorption mechanism and for the determination of adsorption equilibrium time and adsorption rate. Adsorption kinetics describes the rate of the adsorption process with respect to time and reactant concentration. The rate of adsorption can be described by various kinetic models depending on the rate of solute uptake and reactant concentration. Kinetic adsorption studies provide information about the optimum conditions (contact time, temperature, adsorbent dosage, and pH) and mechanism of adsorption, and are investigated using kinetic models to test the experimental isotherm results. The most commonly used kinetic models are the pseudo 1st order and the pseudo 2nd order. Mathematically, the pseudo 1st order and the pseudo 2nd order kinetic models are defined according to the following two equations:

$$q_t = q_e(1 - e^{-k_1 t}) \quad [5]$$

$$q_t = \frac{k_2 q_e^2 t}{1 + k_2 q_e t} \quad [6]$$

Here, q_e and q_t (mg/g) are the adsorption removal capacity at equilibrium and at a specific time (t), respectively; k_1 and k_2 are the rate constants for the pseudo 1st order and pseudo 2nd order kinetic models. The linearized forms of the pseudo 1st order and pseudo 2nd order are defined respectively by the following equations:

$$\ln(q_e - q_t) = lnq_e - k_1 t \quad [7]$$

$$\frac{t}{q_t} = \frac{1}{k_2 q_e^2} + \frac{1}{q_e} t \quad [8]$$

According to these equations, a plot of $\ln(q_e\text{-}q_t)$ as a function of time (t) provides an estimate of q_e and k_1 from the intercept and the slope terms, respectively. Similarly, a plot of t/q_t versus t provides values of k_2 and q_e from the intercept and slope, respectively.

4.1.3 Adsorption mechanisms

Figure 4.1 shows the five main types of adsorption for heavy metal on carbon-based materials:

- Physical adsorption: the process of diffusion and deposition of the heavy metal ions in the pore of the adsorbent material, without the formation of chemical bonds, which depends on the pore size distribution and surface area of the adsorbent itself. The increase of

microporosity and mesoporosity can in turn increase the surface area and facilitate contaminant diffusion, which can promote physical adsorption and accelerate adsorption kinetics.

- Electrostatic interaction: when negative or positive charges diffuse to the adsorbent surface, the electrostatic attraction would play a role in adsorption process between adsorbent and opposite charged ions. This mechanism acts during the adsorption of heavy metals by active carbon, carbon nanotubes and graphene oxide, which present charged moieties on the surface.
- Ion exchange: usually occurs between divalent metal cations (M^{2+}) and the protons of oxygen containing functional groups (−COOH, −OH). For example, alkaline metal ions (such as K^{+}, Na^{+}, Ca^{2+}, Mg^{2+}) contained in exchange resins show good capability to exchange with heavy metal cations.
- Surface complexation: functional groups (such as −OH, −COOH, -O-, and −CO-NH-) can coordinate with heavy metal ions (especially M^{2+}) and form multiatom structures on the adsorbent surface.
- Precipitation/coprecipitation: heavy metal ions can form solid precipitates or coprecipitate with other ions and groups on adsorbent surface. Coprecipitation can be observed in system with high concentration of heavy metal ions, and it can occur on carbon-based adsorbents surface repeatedly.

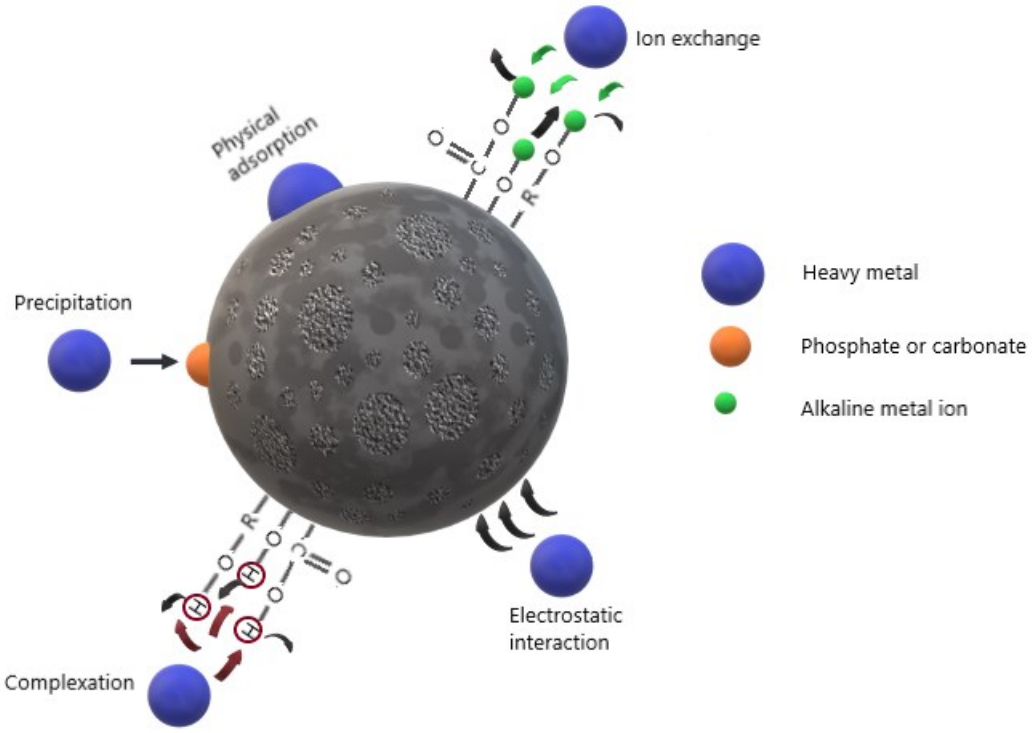

Figure 4.1:Main mechanism of heavy metal by carbon-based materials.

Sometimes, reduction plays a role in the heavy metal removal: some high-valent heavy metal ions are not directly adsorbed but reduced to low-valent states firstly (such as Cr(VI) being reduced to Cr(III)) as an effect of the presence of reducing groups on the carbon materials themselves, and then removed by complexation and ion ex-change.

4.2 Common adsorbents

The selection of material is always a challenging task for researchers to develop a good-performing adsorbent for heavy metal removal. Factors required for the adsorbent material are high selectivity, high surface area, appropriate pore size, regenerating capacity, easy to produce, low cost, reusability, and high adsorption capacity. Adsorbents materials can be subdivided in inorganic, polymer-based, and composite as shown in Figure 4.2.

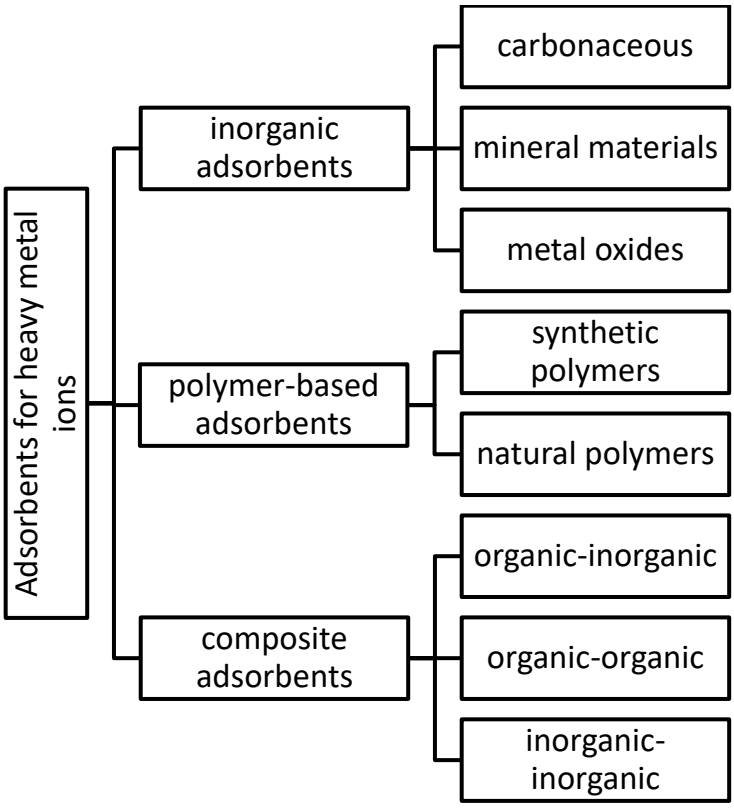

Figure 4.2: Classification of heavy metal adsorbents.

The most widely used adsorbents for heavy metal removal are:

- Activated carbon (AC). It refers to highly porous carbonaceous materials and is the most widely used adsorbent due to its large surface area (500–3000 m^2/g), cost-effectiveness, and good charge-holding abilities, as well as the potential to create various functional groups, which may be vital for the proper elimination of a variety of pollutants from the environmental matrix (aqueous or gaseous media). Activated carbon has well developed pores and high internal surface area for adsorption. It is an amorphous carbon solid presented as black powder formed by pyrolysis and activation of wood, coal, lignite, and other carbon-containing resources. In principle, activated carbon can be created by pyrolysis and activation of almost any carbon-rich substance; therefore, its sources are numerous, such as industrial wastes and agricultural wastes. The second ones are of course cheaper. Raw material preparation, pelletizing, carbonization, and activation are the four essential phases in preparing activated carbon. Thermal and chemical activation are two types of activation methods used to create a porous structure from a low-surface-area material.

  Anirudhan & Sreekumari (2011) have prepared activated carbon from waste coconut button for removal of lead, mercury and copper from wastewater. The authors have found maximum adsorption capacity for Pb(II) and Cu(II) at pH 6.0 and for Hg(II) at pH 7.0. The adsorption

capacities of the activated carbon decreases as Pb(II) > Hg(II) > Cu(II). The adsorption capacity was reported to be 94.35 mg/g, 82.09 mg/g and 75.78 mg/g respectively. The percent removal obtained for lead is > 90% while for copper and mercury it is > 95%. However, Lo et al. (2012) has prepared activated carbon by using moso and ma bamboo activated carbons for removal of lead, copper, chromium and cadmium. Removal efficiency was found in the decreasing order: Pb > Cu > Cr > Cd for bamboo activated carbons and the removal efficiency obtained for lead, copper, chromium and cadmium are 99.9%, 100%, 100% and 96.4%. Sardella et al. (2015) has prepared activated carbon from grape industry wastes such as grape stalk, lex and pomace and used for the removal of lead and cadmium. The adsorption capacity found for lead and cadmium are 1.93 mmol/g and 0.67 mmol/g, respectively. However, Bohli et al. (2015) prepared activated carbon using olive stones for removal of Cu(II), Cd(II), Pb(II), with adsorption capacity of 17.667 mg/g and 57.098 mg/g for copper and cadmium respectively (Singh et al., 2017).

Ma et al. (2019) prepared corn straw porous carbon from maize straw as material and conducted a Cr(VI) adsorption experiment. After three adsorption-desorption cycles, the highest adsorption capacity of Cr(VI) was 175.44 mg/g, with a removal efficiency of 70.65%. The adsorption process includes many mechanisms: (1) $HCrO_4$ and $Cr_2O_7^{2-}$ were confined in micropores; (2) Cr (VI) and oxygen-containing functional groups (e.g. COOH, OH, and -C-O-C) exchanged ions and complexed; (3) Cr(VI) was reduced to Cr(III) by R-O-R or R–OH. Shahrokhi-Shahraki et al. (2021) conducted single and competitive batch adsorption studies for the removal of three synthetic heavy metal ions [Pb(II), Cu(II), and Zn(II)] from an aqueous solution to compare the effectiveness of Tire-derived Activated Carbon (TAC) to that of commercial activated carbon (CAC). TAC had a high potential for adsorption of heavy metals, with monolayer adsorption capacities of 322.5, 185.2, and 71.9 mg/g for Pb(II), Cu(II), and Zn(II), respectively. Significantly higher than CAC' adsorption capacities of 42.5, 15.0 and 14.0 mg/g for Pb(II), Cu(II) and Zn(II), respectively (Mahesh et al., 2022).

- Carbon nanotubes (CNTs). Carbon nanotubes are made of one or more shell structures classified as single-wall carbon nanotubes (SWCNTs) or multi-wall carbon nanotubes (MWCNTs). CNTs are available in a variety of diameters and lengths. The length of a typical nanotube might vary between 10 nm and 100 mm. SWCNTs and MWCNTs have sizes ranging from 0.7 to 2.5 nm and 4–150 nm, respectively. In the past decade, carbon nanotubes have gained much attention because they have stability, large specific area, excellent adsorbent properties and excellent mechanical and electrical properties. CNTs are a perfect adsorbent with high adsorption capacity for removing organic and inorganic pollutants due to

their enormous specific surface areas, hollow and covered architectures, and the presence of functional groups like –COOH, –OH, and –NH_2. More functional groups can be added to CNTs via oxidation using a catalyst such as Pd, Ni, or Pt (Mahesh et al., 2022).

- Biochar (BC). It is a porous, stable, insoluble, highly carbon-rich solid substance made by pyrolysis (250-700°C) in an oxygen-free or -limited environment. BC can be manufactured from a wide range of botanical materials and agricultural waste, hence expanding its possible production sources and lowering production costs and energy consumption. In studies and applications of HM adsorption, BC is identical to AC, or there is no evident distinction between the two. One notable distinction is the temperature at which they produce their products. BC was typically formed from biomass at temperatures below 700◦C under anaerobic conditions, whereas AC was made from prepared carbon/biomass at temperatures over 700 ◦C (e.g., 800-1000 ◦C). As a result, their properties differ depending on the surface area(physical) and functional groups (chemical). AC usually has a higher specific surface area, whereas biochar has more surface functional groups. Besides, BC has several advantages, including a unique pore structure and chemical stability. A wide variety of agro-wastes (fruit peels, wheat waste, sawdust, coconut waste, rice husk, straw wastes, etc.) have been employed for the preparation of BC, which could be an effective adsorbent for the removal of HM from aqueous media. Das et al. (2021) studied the elimination of the most common heavy metal ions (Cd, Pb, Ni, Zn, Cu, and As) by adsorption on BC produced from four distinct plant sources (black gram, pine needle, Lantana camara, and maize stalk). The average HM removal rate from aqueous solution was 52.7-64.2% (As), 49.5-66.1% (Cd), 49.3-63.2% (Cu), 47.3-60.0% (Pb), 46.6-60.8% (Zn), and 45.5-60.6% (Ni). Additionally, before and after passing through a charcoal bio-filter, the wastewater Cu, Zn, Pb, Cr, As, and Cd levels were 93.3-95.5%, 90.1-94.5%, 94.6-77.8%, 83.1-88.1%,78.5-86.5%, and 52.6-94.7%, respectively. In addition to BC obtained from agricultural and botanical waste, other attempts have been undertaken to create BC from other botanical sources such as sludge, manure, and other similar substances. The competitive adsorption of Pb (II) and Cd (II) on anaerobic digestion sludge biochar (ADSBC) was investigated by Ni et al. (2019). Because Pb(II) has a higher affinity for adsorption sites than Cd(II), some Pb(II) arriving at the ADSBC surface would replace deposited Cd(II) and occupy the sites, preventing Cd(II) adsorption. Ho et al. (2017) pyrolyzed ADSBC for the utilization to remove HM from water and the adsorption capacities were in the order of Cr(VI) < Ni(II) < Zn(II) < Cu(II) < Cd(II) < Pb(II). A single type of BC cannot remove all heavy metals from an aqueous solution due to variance in the adsorption characteristics of BC made utilizing different raw materials and

manufacturing conditions. Furthermore, the amount and type of heavy metals present in the solution affect the adsorption efficacy of BC. As a result, BC's adsorption ability on various heavy metals tends to vary. Although there are numerous BC-based adsorbents for removing heavy metals from polluted water, basic BC has low adsorption capacity and poor adsorption selectivity for some heavy metal's contaminants (Mahesh et al., 2022).

5 Sodium alginate as emerging technology

Alginate is an anionic polysaccharide found in the outer cell wall of brown algae, such as kelps. The major component of alginate is alginic acid while sodium alginate (SA) is the Na-salt of alginic acid, which is a polymer with abundant free hydroxyl and carboxyl groups distributed along the backbone chain of the polymer (Figure 5.1).

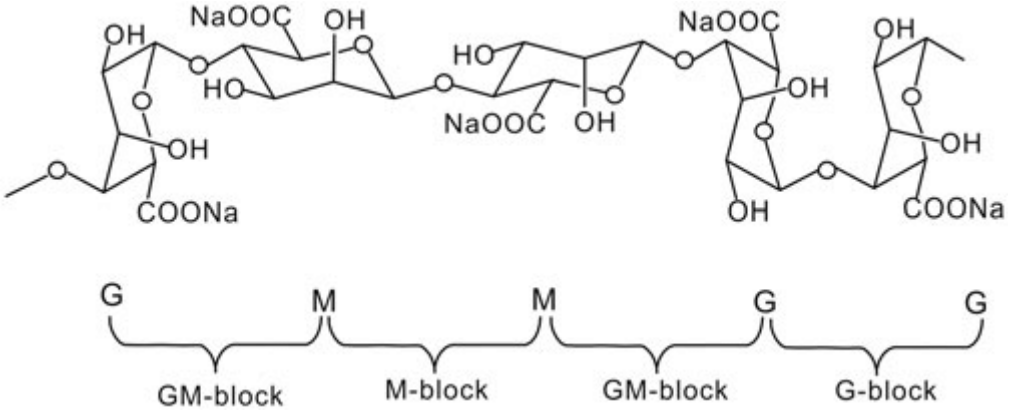

Figure 5.1: The molecular structure of sodium alginate (SA) (B. Wang et al., 2019).

The linear, anionic polysaccharide consists of two kinds of 1,4-linked hexuronic acid residues, namely β-d-mannuronopyranosyl (M) and α-1-guluronopyranosyl (G) residues, arranged in blocks of repeating M residues (MM blocks), blocks of repeating G residues (GG blocks) and blocks of mixed M and G residues (MG-blocks). The alginate polymer is hydrophilic in nature due to the presence of oxygen-containing functional groups over its molecular structure. Carboxyl and hydroxyl functional groups (hard bases) along the polymer skeleton allow high affinity toward strong and intermediate acid (Bilal et al., 2022).

Due to its nontoxicity, biocompatibility, and the ability to form crosslinks with cations, alginate has been utilized for encapsulation of chemical and biological compounds with a wide range of applications in agriculture, food technologies, pharmaceuticals cosmetics, chemical engineering, environmental engineering, paper and textile industry and many other areas. Alginate-based hydrogel are used in biomedical sensors, model extracellular matrices, as scaffolds for tissue engineering, drug cell deliveries, and biomaterials capable of removing toxic metals. Hydrogel-based alginate has several manufacturing advantages including high cross-linking reactions, economical and easily synthesized Na-alginate polymers, and room temperature manipulation of gelation, enabling a simple and safe procedure. Alginate hydrogel is thermally stable and possesses adjustable mechanical properties (Duc et al., 2021). The use of alginate in heavy metals decontamination has evoked a great interest among researchers due to the distribution of bulky carbonyl and hydroxyl groups along the

polymer chains. These functional groups can serve as excellent sites for anchoring heavy metals. Nevertheless, alginate tends to swell and dissolve in water as well as in alkaline solutions. A common technique that has long been used to overcome this problem is by turning alginate into gel materials. In fact, sodium alginate itself is soft and it can go through an irreversible chemical process with polyvalent cations to form a crosslinking bond and finally the formation of a thermo-irreversible gel. The simplest gelation way is the ionotropic gelation method, carried out by the introduction of cations: a solution of alginate salt (most often Na-alginate) is extruded dropwise into a gelation bath with a soluble calcium salt, e.g., $CaCl_2$. Gelation occurs rapidly preserving spherical shape of the droplets. So, when Ca^{2+} is added to the SA solution, Ca^{2+} displaces part of H^+ and Na^+ to form a calcium alginate (CA) gel (B. Wang et al., 2019). More specifically, sodium ions from G blocks are exchanged with divalent cations and generate hydrogel in the form of beads (Bilal et al., 2022). The gelation mechanism is often referred to as the "egg-box" where the calcium ions coordinatively interacting with the G block regions form a three-dimensional network (Figure 5.2).

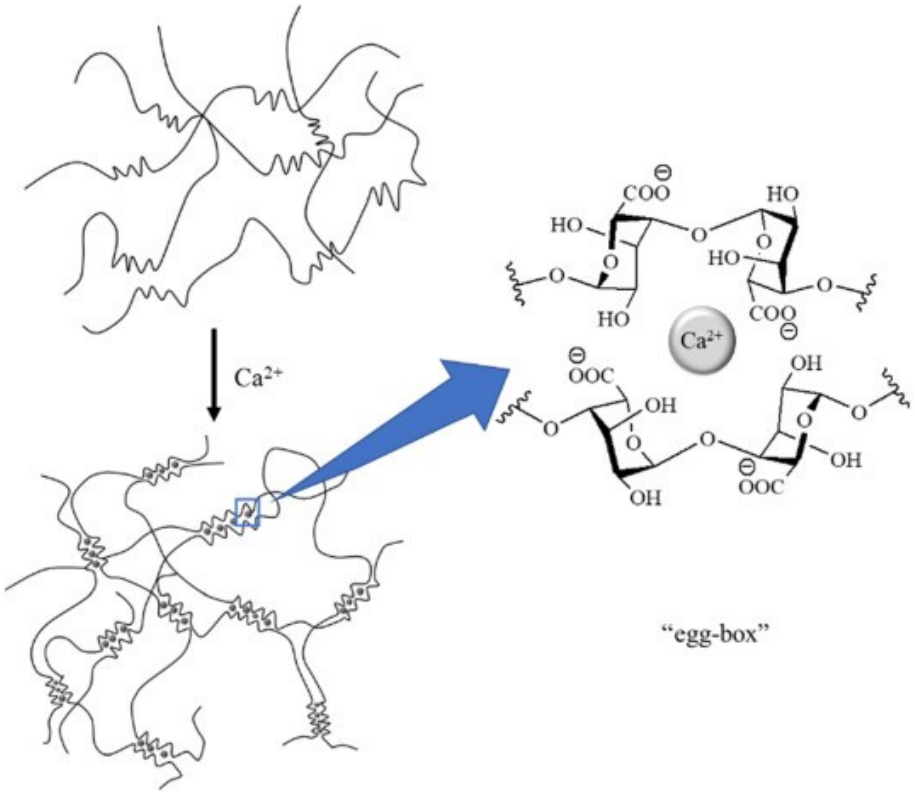

Figure 5.2: Schematic representation of the calcium-induced gelation of alginate in accordance with the "egg-box" structure (Sutirman et al., 2021).

The ability of alginate to bind divalent cations follows the order of $Pb^{2+} > Cu^{2+} > Cd^{2+} > Ba^{2+} > Sr^{2+} > Ca^{2+} > Co^{2+} > Ni^{2+} > Mn^{2+}$. Among them, Ca^{2+} is the most commonly used cation to prepare alginate gel. This affinity for specific ions to the alginate structure must be considered also when introducing the metal ions into the alginate matrix. Thus, a mixture of cations can be introduced simultaneously,

but if the goal is to achieve a somewhat similar uptake, the binding strength of the cations must be considered. The binding strength of Cu^{2+} is, for instance, much greater than that of Co^{2+}, and consequently, the molar ratio of the $Cu^{2+}Co^{2+}$ system must be tuned to obtain close to equimolar uptake in the alginate gel (Tafjord et al., 2021).

However, alginate gel has disadvantages such as high rigidity and fragility with poor elasticity and mechanical properties. Organic and inorganic alginate-based composites have been synthesized to enhance the mechanical and thermal stability and swelling properties of pure alginate gels. These composites possess unique physicochemical properties and excellent biocompatibility (B. Wang et al., 2019). In fact, traditional alginate-based hydrogels still have inherent defects in terms of intrinsic properties, such as compositions, gelation process, and system architectures. It has always been an interesting topic for researchers to investigate alginate derivatives through surface functionalization of the polymer, with the goal of improving its mechanical strength and stability for environmental applications. Surface functionalization also brings beneficial characteristics for alginate as adsorbent since it introduces additional functional groups which serve as active sites, improve selectivity of heavy metal ions, and increase the adsorption capacity. The selection of materials to be incorporated in alginate plays a huge role in determining adsorption performance towards target pollutants. Up to now, a wide range of materials have been explored for this purpose and they can be classified into few groups including organic molecules, polymers or copolymers, biomass, and inorganic materials.

Functionalization of alginate with organic compounds shows a clear improvement compared to unmodified alginate in terms of functional properties such as mechanical and adsorption capacity. Alginate has also been incorporated with polymers or copolymers to produce new composites with the advantages from both materials. These polymers, either natural or synthetic, contain a large number of functional groups such as methyl, amine, sulphate, and aldehyde which interact strongly with alginate and serve as additional active site for heavy metals. In recent years, different polymers or copolymers have been used to functionalize alginate. They include polyacrylonitrile, poly(itaconic acid), xanthan gum, cellulose, chitosan, and gelatine. These composites have demonstrated excellent adsorption efficiencies towards various heavy metals from aqueous solutions by providing multiple adsorption mechanisms. Carbonaceous materials (e.g., carbon nanotube, activated carbon, graphene, biochar) are well-known for their outstanding features such as ultrahigh specific surface area, well-defined pore structure, and high mechanical and thermal stability. Therefore, combination of carbonaceous material and alginate should substantially improve the adsorption performance and overcome the limitations of the pristine materials. In recent years, considerable efforts have been made to developing magnetic based-materials due to their physicochemical properties and advantages in size being in the nanometre range. Hybrid materials composed of magnetite and alginate not only

exhibit good morphology and chemical stability, but also easily separation from the solution using an external magnet without the need of centrifugation or filtration. All the afore mentioned reports show that selection of material to design an alginate-based adsorbent is of great importance as it determines the whole adsorption performance of the adsorbent for heavy metals. Therefore, it is necessary to choose a suitable system having high adsorption efficiency, good stability under operating conditions, high selectivity towards target pollutants and being inexpensive. It would also be useful if the approaches or technologies in preparing the adsorbent are easy to performe and simple as well as environmental-friendly (consume less chemicals and solvents, produce no waste, etc.). Considering GO (see section 6), a type of carbon-based nanomaterial with a 2D plane honeycomb like structure possessing a large surface area and good mechanical properties, it contains abundant O-containing groups and is rich in π electron system, thereby suggesting a great potential in removing pollutants. However, the size and hydrophilicity of GO limits its separation and recycling in actual applications. By encapsulation, GO can not only be immobilized on the surface of the polymer and supply reactive sites but also participate in network formation via strong interfacial interactions. For example, GO provides enhancement of the adsorption performance toward Pb(II)/Cu(II) and mechanical strength by incorporating on the alginate matrix (Zhang et al., 2021). Table 5.1 shows some examples of tested alginate-based adsorbents for the removal of metal from aqueous solution.

Table 5.1: Adsorption capacities and experimental conditions of alginate-based adsorbents for the removal of metal from aqueous solutions (Sutirman et al., 2021).

Adsorbent	**Metal ion**	**pH**	**Adsorption capacity (mg/g)**	**Isotherm**	**Kinetic**
Magnetic alginate beads	Pb(II)	2.3-6	99.5	Langmuir	Pseudo 2nd order
Activated carbon-alginate composite	Pb(II)	5	15.7	Langmuir	Pseudo 2nd order
Tetraethylenepentamine functionalized alginate beads	Cr(VI)	2	76.92	Langmuir	Pseudo 1st order
Alginate-graphene oxide hybrid gel beads	Cu(II)	-	60.2	Langmuir	Pseudo 2nd order
Magnetite graphene oxide encapsulated in alginate beads	Cr(VI)	7	14.9	Freundlich	Pseudo 2nd order

Adsorbent	Metal ion	pH	Adsorption capacity (mg/g)	Isotherm	Kinetic
Graphene oxide encapsulated polyvinyl alcohol/sodium alginate hydrogel	Cu(II)	4	147.16	Langmuir	Pseudo 2nd order
Glycine functionalized magnetic nanoparticle-calcium alginate beads	Cu(II)	6	120	Langmuir	Pseudo 2nd order

J. Wang et al. (2021) synthesized magnetic SA-based polyelectrolyte nanospheres via Ca^{2+} ion crosslinking reactions and electrostatic interactions between SA and amino modified Fe_3O_4 nanoparticles. They characterized and discussed the chemical structure, surface properties and morphology of the new magnetic polyelectrolyte. The tests and modelling of the Pb(II) adsorption were conducted, and the recovery performance was evaluated. Isothermal adsorption curves were drawn to determine the maximum Pb(II) ion adsorption content. Based on ion uptake, the thermodynamic characteristics of the adsorbent were investigated by modelling of the adsorption curves. Freundlich and Langmuir models were used for deriving the adsorption isotherms. Micromorphology of the magnetic nanoparticles (MNPs), amino-based magnetic nanoparticles (AM), and magnetic SA-based polyelectrolyte nanosphere (SA@AM) were investigated by TEM. The MNPs were spherical and uniform in size, and those particles tended to be clustered. The surface of 3-amnopropyl-trimethoxysilane (APTES) modified nanosphere (AM) become compact, irregular, and amorphous, with MNP cores darker because of their high electron density. It was proved that APTES was successfully grafted onto the MNPs for yielding AMs. Regular circular nanosphere were detected by TEM for the SA@AM, possessing smooth surfaces and uniform sizes ranged between 15 and 22 nm. According to the BET analysis, the surface areas of the products MNP, AM, and SA@AM were 58.72, 72.69 and 104.85 m^2/g, respectively. Compared with the original magnetic particles MNP, the specific surface area of the final product SA@AM was greatly increased, and the chance of contact with ions higher, which provides more opportunities for ion coordination and chelation. Therefore, the adsorption capacity was improved, which helped to improve the adsorption capacity for ions. Concerning the adsorption capacity of SA@AM for Pb(II) was increased by 50.1% compared to the SA control without MNP core. Through the comparison of Pb(II) adsorption capacity with other magnetic adsorbents, it was learned that the Pb(II) adsorption capacity was much higher than the others, i.e. from 20% to 150%. This was probably due to the abundant surface groups (-COO and -OH) from the SA shells, which could strongly adsorb Pb(II) ions. Further studies demonstrated

that the Langmuir model well fits the Pb(II) isothermal adsorption of SA@AM and showed a Pseudo-second-order for its kinetic adsorption. Using the Langmuir linear fitting results, the SA@AM demonstrated maximum Pb(II) adsorption capacity at 105.8 mg/g. The equilibrium Pb(II) adsorption of SA@AM was 91.7 mg/g, which was 47.0% higher than that of SA (62.4 mg/g), demonstrating a great enhancement after the SAs being coated onto MNPs. The magnetic sodium alginate polyelectrolyte microspheres have good magnetic separation performance, which resulted from the modified magnetic particles coated in the sodium alginate micro-spheres. With the increase of adsorption-desorption cycles, the adsorption performance was gradually decreased from 92.3% (first cycle) to 77.3% (fifth cycle). It was confirmed that the recycling performance of SA@AM was good, benefiting the repeated adsorption of heavy metal ions. This research can provide a reference for the subsequent development of magnetic adsorption materials.

Jiang et al. (2020) synthetised a novel bio-adsorbent hydrogel composite named SA-PAM/GO through free radical polymerization. Under optimal conditions, the maximum adsorption capacity of Cu(II) and Pb(II) were 68.76 mg/g and 240.69 mg/g, respectively. In addition, the kinetics and isotherms displayed that the pseudo-second-order kinetic model and the Langmuir isotherm model fitted the data well. Chemical adsorption accompanying the ion exchange process was confirmed as the principal adsorption mechanism. Furthermore, the adsorbent still maintained good adsorption capacity after 5 cycles of adsorption-regeneration. Therefore, the SA-PAM/GO hydrogel composites have potential to be applied in the removal of heavy metal ions from water bodies effectively.

Zhang et al. (2021) prepared novel porous alginate-based nanocomposite hydrogels by incorporating polyaniline-polypyrrole modified graphene oxide (GO@PAN-PPy) as reinforcing fillers into the alginate matrix (GO@PAN-PPy/SA) and applied them in Cr(VI) and Cu(II) removal from water. With an adsorption ability superior to that of plain SA and GO/SA, the optimized GO@PAN-PPy/SA exhibited good experimental maximum adsorption capacities for Cr(VI) (~133.7 mg/g) and Cu(II) (~87.2 mg/g) at pH 3.0, which were better than those of many other similar sorbents. The sorbents possessed excellent adaptability for 0.2 M salt for Cr(VI) removal but poor for Cu(II) removal. Pre-swelling treatment and co-adsorption could enhance their performances. The excellent reusability of hydrogel was demonstrated after five cycles in single/binary system. Overall, this work reveals that the resultant hydrogel holds potential as candidate sorbent to remove anionic- cationic heavy metal ions from water.

Ma et al. (2022) incorporated MIL-121 (Al- based MOF) crystals into biodegradable alginate matrix to form composite beads with enhanced recyclability and adsorption capacity. A systematic adsorption study for Cu(II) and Cd(II) was conducted and the optimal sample (with a MOF loading

of 50 wt%) presented an adsorption capacity of 204.5 mg/g for Cu(II) and 88.7 mg/g for Cd(II). Moreover, the composite beads can be regenerated effectively by hot water (80 °C). The desorption is attributed to the carboxyl-rich MIL-121, which could release high concentrations of protons (H^+) at elevated temperature. Compared with the traditional desorption using strong acids, this chemical-free thermal desorption strategy holds a great potential for adsorbent regeneration and practical wastewater treatment.

Duc et al. (2021) exploited a microfluidic system as an emerging technology to fabricate uniform spherical microparticles. The resultant hydrogel particles were spherical in shape with diameters ranging from 70 to 100 μm. Observations of dried calcium alginate microparticles using scanning electron microscopy showed a homogeneously corrugated surface. The resultant biomaterials were further examined and evaluated in terms of removal of toxic metals ions (Cu(II) and Ni(II)); they demonstrated an excellent removal performance. The highest adsorption capacities of the prepared calcium alginate microparticles toward Cu(II) and Ni(II) ions were 360 and 810 mg/for g of alginate microparticles, respectively. There was evidence of an ion exchange mechanism between the metal ions from the solution and the free carboxylic groups of the calcium alginate hydrogels. This study demonstrates a simple approach to produce small and uniform alginate-based hydrogel particles for applications in environmental treatments. Thus, these calcium alginate microparticles demonstrated the potential for toxic metal treatment at different concentrations with short duration and stability.

Shi et al. (2022) used hydrazide modification for preparing a new potential adsorbent for the separation and removal of heavy metal ions. In this study, DSA-AAD@Ca^{2+} was prepared using AAD and DSA to obtain functional hydrazone structure which can sensitively capture heavy metal ions. The equilibrium adsorption capacity based on chemical and monolayer adsorption of DSA-AAD@Ca^{2+} for Hg(II), Pb(II), Cd(II), and Cu(II) was 7.833, 2.036, 4.766, and 3.937 mmol/g, respectively, whereas the maximum adsorption capacity was 8.633, 1.968, 5.062, 4.068 mmol/g, respectively. Further analysis revealed the combination of chelation interactions and ion exchange between nitrogen, oxygen atoms, and heavy metal ions. Moreover, after 10 times adsorption–desorption recycles, the adsorption efficiency of the adsorbent was slightly decreased. In conclusion, the as-prepared adsorbent has great potential in practical water purification.

Jiao et al.(2016) fabricated an ordered porous sodium alginate/graphene oxide(SAGO) aerogel by in situ crosslinking and freeze-drying method. GO, as reinforcing filler, can be easily incorporated within the SA matrix by self-assembly via hydrogen bonding interaction. Compared with pure SA aerogel, the prepared SAGO exhibited excellent mechanical properties. The outstanding mechanical strength and satisfactory elasticity can be attributed to the strong hydrogen bonding interactions

between GO sheets and SA chains. SEM results showed that the addition of GO improves the porous structures of aerogel, which is beneficial for the enhancement of strength–toughness and absorbability. The adsorption process of SAGO is better described by pseudo-second-order kinetic model and Langmuir isotherm, with maximum monolayer adsorption capacities of 98.0 mg/g for Cu(II) and 267.4 mg/g for Pb(II). The results in terms of microstructures, mechanical properties and adsorption capacities of SAGO aerogel confirm that the embedding of GO and in situ crosslinking technology make SAGO aerogel a promising candidate in wastewater treatment.

Majdoub et al. (2021) used GO as a precursor for the covalent bonding of hexamethylenediamine (HMDA) molecules via the nucleophilic substitution/amidation reactions on epoxy (C-O-C) and carboxyl (-COOH) groups to yield hexamethylenediamine functionalized graphene oxide (GO-HMDA) with multiple binding sites such as oxygen and nitrogen. Afterwards, GO-HMDA was encapsulated in alginate hydrogel beads with different loadings 5, 10, 15 and 20 wt% to produce Alg/GO-HMDA hybrid adsorbents for the removal of trace heavy metal ions from aqueous solution. Batch adsorption studies showed remarkable adsorption rates reaching 100% for Pb (II), 98.18% for Cu (II) and 95.19 for Cd (II)(~1mgL1) with only 15 wt% of GO-HMDA incorporated into the alginate beads. Moreover, Alg/GO-HMDA showed high removal efficiencies of heavy metals from tap water with a removal order of(Pb > Cu > Cd) similar to that observed in single aqueous solution. In addition, the Alg/GO-HMDA adsorbents displayed excellent regeneration ability for six consecutive adsorption–desorption cycles, confirming their high performance and potential for real heavy metals remediation in environment and drinking waters. The adsorption mechanism of traces heavy metals resulted from several phenomena including electrostatic interactions.

6 Graphene oxide (GO)

Graphene is a single-atom-thick two-dimensional (2D) sheet of sp^2 hybridized carbon atoms organized in a hexagonal lattice by sigma and pi bound connections. It is a fundamental building block for other carbon allotropes such as carbon nanotubes and fullerenes. It comes in various forms, including graphene oxide (GO), which can be synthesized by chemical exfoliation of graphite, in oxidizing conditions. The latter is a 2D sheet with plentiful oxygenated functional groups on its basal plane and edges. GO itself has fascinated researches due to its many interesting characteristics and its role as a promising precursor for the bulk production of graphene-based nanomaterials. The fabrication method of GO disrupts the π-conjugated network and thus makes it highly water dispersible, reducing the stocky combination between the individual sheets, which indicates a wider perspective in wastewater treatment. Chemical exfoliation can be done in a two-step procedure. Firstly, increment of inter-layer spacing is obtained by reducing the van der Waals forces between the layers, usually by oxidation. Then, fast heating process or sonication is carried out to exfoliate graphene into single to few layers. For instance, ultrasonication is required to extract monolayer GO. Some consolidated synthetic methods of GO are the Brodie, Staudenmaier, and Hummers methods, or advanced modified approaches based on them (Figure 6.1). The improved Hummers method proves to be the most suitable method to be applied due to its reduced toxicity and its ability to produce more organized graphene structure.

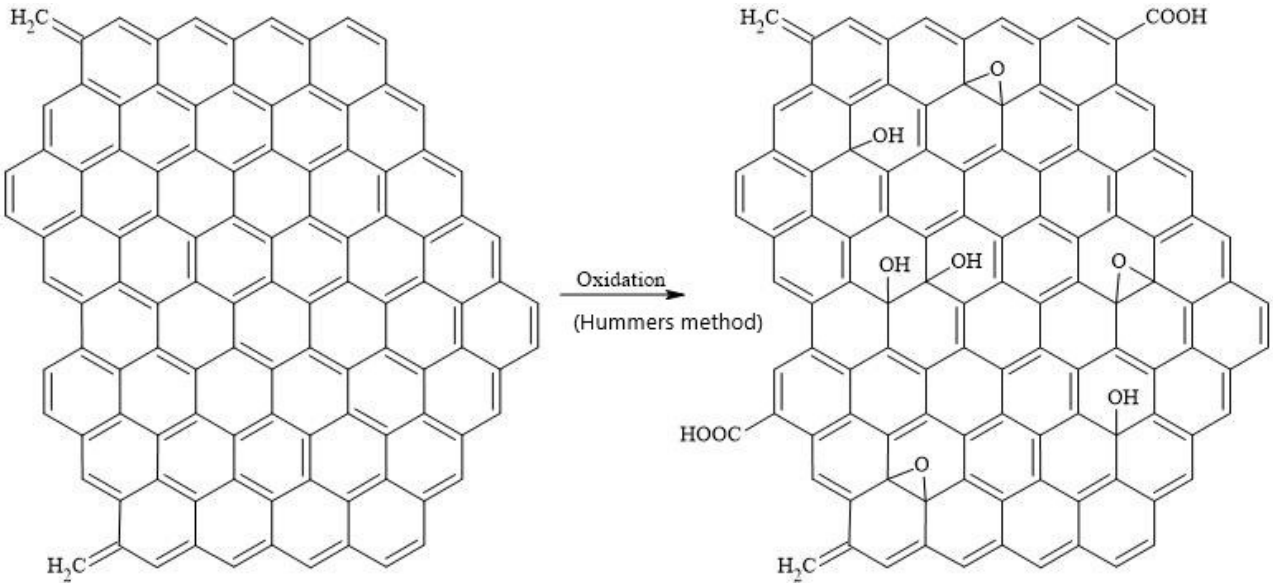

Figure 6.1: Graphene and graphene oxide structure.

Because of its relatively large specific area, rich functional groups, and exceptional mechanical strength, GO is a promising material for the adsorption of heavy metal ions. Because of the oxygen functional groups present, it possesses a high negative charge density and hydrophilicity. Especially,

GO has a very widespread activity in removing various heavy metal ions from aqueous solutions, such as Pb(II), Cu(II), Co(II), Cd(II), Cr(VI). GO, with a pore size of roughly 0.9 nm, emerges as the most cost- effective graphene-based material. The regeneration and reusability of adsorbents are critical elements for the commercial application of the adsorption process. Several investigations have shown that by employing either a strong acid (HCl) or strong alkali (NaOH), the desorption process can replenish graphene-based adsorbents. Magnetite/non-oxidative graphene composites (M-nOG) retained more than 92% of the first cycle arsenic ions, As(V), capacity after 5 regeneration cycles, showing that it is a cost-effective and efficient adsorbent. Due to the hydrophilic characteristics of GO, chemisorption involves the superficial complexation of heavy metal ions with oxygen-containing groups, since they can share an electron pair. Although pure GO has some adsorption capacity for heavy metals in aqueous solution, they have several flaws, including easy agglomeration due to strong intermolecular forces and limited adsorption capacity. A series of graphene-based functional materials were developed to address these issues. The use of organic molecules with O, N, and S functional groups to modify GO can increase the type and number of functional groups on its surface, hence boosting its ability to remove heavy metal ions. Oxidation (–CO–, –OH, –COH, –COOR), nitrogenation (-NH, $–NH_2$, CN-R, –CNH, –CONH), and sulphuration (-S-, –SH, CS, $–CSNH_2$, –COSH, –CSSH, etc.) are the most common functional modifications of graphene-based materials (Mahesh et al., 2022). Also, many polymers and metal oxides were combined to the graphene-based sheets and are currently developed as adsorbent nanomaterials. These nanomaterials show standout structural properties and multifunctional abilities by combing both characteristics of the components.

Specific adsorption mechanisms of graphene oxide-based nanomaterials are discussed in Table 6.1.

Table 6.1: Specific adsorption mechanism of graphene oxide-based nanomaterials for metal ions removal (Lim et al., 2018).

Graphene oxide-based nanomaterials	**Adsorption mechanisms included for metal ions removal**	**Advantages**	**Drawbacks**
Graphene oxide (GO)	- Electrostatic interactions - Ion exchange	- Good dispersion in water - Great colloidal constancy - Contains rich oxygenated functional groups	- Restricted number of sorption sites
Magnetic graphene oxide nanocomposites	- Electrostatic interactions with GO - Interactions with the particles surface - Magnetic properties of the nanoparticles	- Bigger surface area compared to the pure GO - Increased number of binding sites compared to pure GO - Ease the recovery process from solutions	- Combination of the particles weakens the colloidal stability
Graphene oxide materials functionalized with organic molecules	- Electrostatic interactions - Complexation with organic molecules	- Bigger surface area compared to pure GO - Great colloidal stability - Greater number of functional groups ($-NH_2$, -OH)	- Large variations of the stability of the loaded molecules

Many investigations have been reported to evaluate the heavy metals removal capability of graphene oxide materials. Liu et al. (2018) synthesized nanocomposites of manganese dioxide (MnO_2), GO, iron oxide (Fe_3O_4), and polypyrrole (PP_y) nanoparticles for the adsorption of hexavalent chromium from wastewater. They reported an adsorption capacity of 374.53 mg/g Cr(VI) at pH 2.0, with contact time 1400 min. The X-ray photoelectron spectroscopy suggested that the Cr(VI) removal mechanisms were effected by electrostatic attraction. They finally concluded that these nanomaterials had high potential as a cost-effective adsorbent of Cr (VI) from wastewater.

Table 6.2 shows an overview on graphene-based adsorbents used in Cu(II) removal from wastewater.

Table 6.2: Operative conditions, maximum adsorption capacities and/or percentage of removal of Cu(II) of graphene-based nanoadsorbents (de Beni et al., 2022; Lim et al., 2018).

Material	**Operative pH**	**Operative temperature (K)**	**Adsorption capacity (mg/g)/percentage of removal**
GO	5	298	29.4/99%
GO	5.7	303	72.6
Fe_3O_4-GO (MWCNTs)	5	298	574.71
GO/Fe_3O_4	5.3	293	18.26
GO/Fe_3O_4	6	-	62.89/92.43%
GO/Fe_3O_4	5.3	293	18.26
Ca-Alg_2/GO	-	-	60.2
Alg-MGO	5-6	298	294.11
GO/ZnO	4-5	-	45.5/92.9%
Chitosan/GO	6	318	423.8
PAH/GO	6	293	349.03
PAMAMs/GO	4.5	298	68.68

The main GO composites used as adsorbents are GO-chitosan, GO-alginate, and magnetic GO composites. Among them, functionalized magnetic GO (Fe_3O_4-GO (MWCNTs)), alginate bound on magnetic GO (Alg-MGO), chitosan/graphene oxide, poly(allylamine hydrochloride)/graphene oxide (PAH/GO), showed to have adsorption capacities greater than 200 mg/g. A good removal performance is obtained by the use of magnetic GO (GO/Fe_3O_4), and GO decorated with zinc oxide

nano-particles (GO/ZnO). GO/polyamidoamine dendrimers (PAMAMs/GO) shows a performance lower than 98.7 mg/g.

The adsorption capacities of adsorbents used in Cr(VI) adsorption is presented in Table 6.3.

Table 6.3: Operative conditions, maximum adsorption capacities and/or percentage of removal of Cr(VI) of graphene-based nanoadsorbents (de Beni et al., 2022; Lim et al., 2018).

Material	**Operative pH**	**Operative temperature (K)**	**Adsorption capacity (mg/g)/percentage of removal**
GO	3	-	49.01
PPy/GO	3	-	497.10
$MnO_2/Fe_3O_4/GO$	2	298	193.1
GO/Fe_3O_4	4.5	293	32.33
Chitosan/GO	3	318	310.40
$GO/mTiO_2/Fe_3O_4$	2	303	117.94
Fe_3O_4/GO	4.5	293	32.33

Generally, the adsorption capacity has a negative correlation with the increase of pH. This phenomenon can be attributed to the presence of different forms of Cr(VI) ion in aqueous solution. Chromic acid (H_2CrO_4) is predominant in strong acidic conditions (pH <1), hydrogen chromate ($HCrO_4$) and dichromate ($Cr_2O_7^{2-}$) are formed at pH values ranging between 2 and 6.8, and chromate (CrO_4^{2-}) is usually found at pH above 6.8. The results have showed the pseudo 2nd order model matched the adsorption kinetics behaviour of both GO and functionalized-GO toward Cr(VI), implying that the rate-determining step was most likely to be controlled by chemisorption. Among the variety of materials that have been added to GO, the most prevalent functionalization are polymers and magnetic materials. Polypyrrole (PPy)/GO composite nanosheets has been implemented successfully, displaying that the adsorption capacity toward Cr(VI) (around to 497.10 mg/g) is much higher than those of other adsorbents. Magnetic GO materials were produced by using magnetic materials such as Fe_3O_4 and Fe_2O_4. Finally, chitosan/GO provided efficient adsorption properties (310.4 mg/g at 318 K and pH of 3) for Cr(VI) ions.

The adsorption capacities of adsorbents used for Ni(II) is presented in Table 6.4.

Table 6.4: Operative conditions, maximum adsorption capacities and/or percentage of removal of Ni(II) of graphene-based nanoadsorbents (de Beni et al., 2022).

Material	**Operative pH**	**Operative temperature (K)**	**Adsorption capacity (mg/g)/percentage of removal**
GO	5.7	303	62.3
GO	9	298	20.19
GO	6	298	38.61
GO	6	308	52.63
$MnFe_2O_4$/GO	8	-	152.67
Mg Fe_2O_4-GO	-	-	100
Fe_3O_4/GO (MWCNTs)	5	298	384.62
GNS/MnO_2	9	298	46.55
Fe_3O_4-GS	6-7	313	22.07
MGA	5	298	190.8
GO/Fe_3O_4	8	-	51.02/92.23%

The optimum pH for Ni (II) removal is in the range of 5–9. The adsorption process is well-fitted to pseudo 2nd order kinetic, because of the electro-static interactions between the negative charges of GO surface and positive Ni^{2+}. The maximum adsorption capacity was found to be 62.3 at 303 K and pH of 5.7 for unfunctionalized GO and 384.62 at 298 K and pH of 5 for Fe_3O_4/GO (MWCNTs). Magnetic GO composites demonstrated adsorption capacities in the order: Fe_3O_4-GO-(MWCNTs) (384.6 mg/g) >MGA (190.8 mg/g) >$MnFe_2O_4$/GO (152.7 mg/g) >Mg Fe_2O_4-GO (100 mg/g) >GO/Fe_3O_4 (51 mg/g) >GNS/MnO_2 (46.5 mg/g) >Fe_3O_4-GS (22 mg/g).

Jiang et al., (2020) studied a novel sodium alginate grafted PAM/GO hydrogel. Polyacrylamide (PAM) is a linear organic polymer, which is wider used in wastewater purification. Previous research has shown that PAM expressed a good affinity toward heavy metal ions through electrostatic interactions. The morphology and the structure of the adsorbents were characterized and the adsorption performances toward Cu(II) and Pb(II) were affected by pH, ionic strength, adsorption time, and concentration. Furthermore, as a kind of promising adsorbent, the adsorption-regeneration ability was also studied. To assess the recyclability of SA-PAM/GO hydrogel composite, adsorption and regeneration experiment were performed. The scanning electron microscopy (SEM) and energy

dispersive spectrometer (EDS) result on the morphological structure of SA and dry SA-PAM/GO hydrogel composites showed that the surface morphologies of sample SA were smooth and had flat wrinkles, with low porosity. However, the surface of SA-PAM/GO hydrogel composite appeared with three-dimensional folds and possessed significantly more pores and more cavities. Hence, the new structure after modification could provide more specific surface areas and active sites, which are beneficial for heavy metal ions adsorption. This proved that the modification was successful, as further confirmed by EDS analysis. For the adsorption experiments, the pore sizes and BET surface areas are shown in Table 6.5.

Table 6.5: Parameter related to the surface area of SA, GO and SA-PAM/GO hydrogel composites.

Category	**SA**	**GO**	**SA-PAM/GO**
Surface area (dm^2/g)	63.1	607.16	190.89
Average pore size (nm)	6.7949	11.4177	19.8052
Total pore volume (dm^3/g)	1.072	17.311	9.451

The surface area increased from 63.1 dm^2/g to 190.89 dm^2/g after modification, which was more than three times higher than the starting materials. The average pore size between SA and SA-PAM/GO hydrogel composite increased from 6.7949 nm to 19.8052 nm, which also was more than tripled. The change of specific area and average pore size increased the active sites for adsorption. At the same time, it was clear that GO played a significant role in increasing the specific area and average pore size. Therefore, it was apparent that a 3D network structure was formed and the increase in specific surface area and pore size was consistent with the SEM results, accordingly. The SA-PAM/GO displayed the highest adsorption abilities than the other three materials. In optimal condition, the Cu(II) and Pb(II) maximum of adsorption capacity reached up to 68.76 mg/g and 240.69 mg/g, respectively. The adsorption data could be well fitted with pseudo-second-order kinetic model. The adsorption isotherm showed that the Langmuir isotherm could be well fitted with the experimental data and the adsorption rate of heavy metal ion was fast. The experiment of desorption-adsorption showed that there were more than 80% for Cu(II) and about 60% for Pb(II) of adsorption capacity after 5 cycles. Therefore, the adsorbent of SA-PAM/GO hydrogel composite, with a simple preparation process, fast adsorption rate, excellent removal efficiency, and good regeneration, has good potential to be applied in the removal of heavy metal ions in aqueous solution.

7 Magnetic nanoparticles

Nowadays, a considerable attention has been drawn by nanomaterials as the adsorbents in decontamination of wastewater due to their large specific surface area, and availability of large number of active groups for binding heavy metals. Furthermore, nanostructured adsorbents can be reused and recycled repeatedly which makes them cost effective and highly attractive. But their difficult removal from treated water and their challenging regeneration has restricted their commercial use. Therefore, researches are aiming to solve these issues by functionalization of nanoparticles.

In the past few years, metallic and metal oxide nanoparticles have emerged as an encouraging material in heavy metal ions removal. Bare metallic nanoparticles are less commonly used as adsorbents because they tend to agglomerate. In addition to this, separation of bare nanoparticles from wastewater is a complicated process. Therefore, there is a need of capping or functionalization of these nanostructured adsorbents to enhance their stability and to make the separation process easy. Among the metallic nanoparticles, Fe^0 (nano zero valent iron, NZVI) is of immense significance due to its high stability, greater surface area, non-toxicity, reducing nature, and higher adsorption capacity. Furthermore, the stability of the NZVI can be improved by their entrapment or functionalization with some stabilizing agent. Sikder et al. (2014) entrapped NZVI in a non-toxic and biodegradable stabilizer, i.e. chitosan carboxymethyl β-cyclodextrin complex. The synthesized material was used for the complete removal of Cr(VI) and Cu(II), which involves physisorption followed by reduction of Cr(VI) to Cr(III) and also Cu(II) to Cu(0) whilst oxidizing Fe^0 to Fe(III). In addition to metallic nanoparticles, numerous scientific investigations have been carried out by different research group to demonstrate the role of metal oxide nanoparticles in wastewater decontamination. Based upon their inherent magnetic character, these have been classified as magnetic and non-magnetic metal oxide nanoparticles. Magnetic nanomaterials constitute a major category of advanced nanomaterials which combine advantages of magnetic separation and nanotechnology for the better heavy metal ion removal. Magnetic separation technique is being widely used in the case of ecological issues, because the magnetic nanoparticles exhibit brilliant reusability after magnetic separation. Non-magnetic nanoparticles have less surface area and are difficult to separate from the aqueous phase that limits their applicability in wastewater decontamination. Alternatively, magnetic nanoparticles have a comparatively grater surface area, biocompatibility, chemical inertness, less toxicity, and easy dispersion ability. Hence, the application of magnetic nanoparticles in the wastewater treatment is more reliable, efficient and cost effective (Wadhawan et al., 2020).

Various magnetic nanoparticles have been used by the researches for the effective removal of heavy metal ions. Nano sized iron oxide particles are an important member of this family. These offer increased adsorption capacity, rapid adsorption rate, easy separation and renewal. In this regard, Iconaru et al. (2016) synthesized magnetite nanoparticles and compared their removal efficiency with commercial magnetite towards As(II) and Cu(II). The results indicated the higher adsorption capacity of synthesized magnetite as compared to commercial magnetite. In another study, Fe_3O_4 magnetic nanoparticles prepared by Giraldo et al were examined for the removal of Pb(II), Cu(II), Zn(II) and Mn(II) ions. The adsorption capacity of Fe_3O_4 magnetic nanoparticles towards Pb(II) was found to be maximum and for Mn(II) it was minimum.

Generally, bare magnetic nanoparticles are prone to oxidation and are easily agglomerated in aqueous media which restricts their practical application. Besides the significant developments in synthesises of magnetic nanoparticles, maintenance of their stability by preventing them from agglomeration and precipitation is an important issue. To overcome this limitations, bare magnetic nanoparticles can be functionalized with different moieties. Surface modification of magnetic nanoparticles increases adsorption capacity and stability towards oxidation with enhanced selectivity towards a particular metal ion. Functionalization provides complex formation, chemical binding and ligand combination in addition to electrostatic and Van der Waals interactions liable for the metal ion adsorption on the surface of adsorbent. These improved electrostatic interactions are responsible for adsorption selectivity. Further, surface functionalization of MNPs with hydrophilic coating using Polyethylene glycol (PEG), Poly vinyl alcohol (PVA), and Poly vinyl pyrrolidine (PVP) as capping agents, prevent them from agglomeration. It leads to larger surface area to volume ratio and increases the homogeneity of MNPs into the solution. The manipulation of the properties of MNPs by tailoring their surface results into selective adsorption of heavy metal ions. The type of surface functionalization and the geometric array of coating molecules decide the overall size and surface area of MNPs which play an important role in enhanced and selective adsorption of heavy metal ions from wastewater. Many investigations have been carried out for the functionalization of magnetic nanoparticles with various materials like polymers, organic or inorganic species, biomolecules, carbonaceous materials, etc. Polymeric support provides a number of advantages for nanoparticles functionalization such as better chemical stability, high mechanical strength and bio-compatibility. For example, Huang & Chen (2009) demonstrated the use of a new magnetic nanoadsorbent fabricated by the functionalization of Fe_3O_4 nanoparticles with polyacrylic acid (PAA) and diethylenetriamine (DETA) for the adsorption of Cu(II) and Cr(VI). The higher adsorption capacity was calculated for Cu(II) ions as compared to Cr(VI) ions. Functionalization of MNPs with biomolecules enables their safe and eco-friendly use in metal ion remediation process in addition to

in-creased adsorption capacity. Many researchers investigated the use of biomolecule functionalized MNPs in heavy metal ion adsorption. In a contribution by M. Verma et al. (2017) and R. Verma et al. (2017) glycine modified magnetic Fe_3O_4 nanoparticles (GF-MNPs) enclosed in alginate polymer in the form of beads were used. The adsorbent demonstrated excellent removal efficiency for Pb(II) owing to the amino and carboxylate groups on the surface of beads. Another adsorbent, containing iron oxide magnetic nanoparticles and calcium alginate embedded on the surface of a biomass strain pellets was prepared by Xu et al. (2012) for effective removal of Pb(II) with adsorption capacity 167.36 mg/g. Organic molecules provide various functional groups for the complexation with heavy metal ions which greatly enhance the adsorption capacity of magnetic nanoparticles. .Shen et al. (2013) explored the mechanism of adsorption of Cr (VI) on the surface of nanosized magnetic polymer functionalized with tetraethylene pentaamine (TEPA-NMPs). Experimental data confirmed the adsorption of Cr (VI) on these NMPs due to the electrostatic interaction, and also because of the reduction of Cr (VI)into Cr (III) through charge transfer on the adsorbent surface. In another category, Shen et al. (2012) synthesized a number of core-shell Fe_3O_4 nanoparticles functionalized with various multi-amino groups i.e. NH2-NMPs for the adsorption of Cu (II) and Cr (VI) ions in sole metal ion system and coexisting metal ion system. The adsorption process was found to be highly dependent on pH of the medium for both Cu (II) and Cr (VI) ions. It was due the fact that adsorption process was mainly based on electrostatic interactions. Adsorption capacities were maximum at pH values between 2–4. At pH lower than 2, protonation of $-NH_2$ to $-NH_3^+$ results into lesser availability of $-NH_2$ binding sites which reduces adsorption efficiency. At pH higher than 2, greater availability of $-NH_2$ binding sites results into increase in adsorption of Cu (II) ions. On the other hand, at pH above 4 precipitation of Cu (II) occurs. Similarly, adsorption of Cr (IV) i.e. $HCrO_4^-$ was maximum at pH 2–4 due to electrostatic attractions between $HCrO_4^-$ and $-NH_3^+$. A higher pH reduces adsorption capacity because of competition between $HCrO_4$ and OH^- ions. Further, it was observed that adsorption process was competitive at higher concentration of metal ions and low pH values in coexisting system. Lower concentrations and higher pH values did not affect the adsorption efficiencies of coexisting systems (Wadhawan et al., 2020). Furthermore, functionalization of MNPs with carbonaceous materials like graphene oxide and activated carbon is also an effective method to improve the adsorption efficiency of nanoadsorbents. In this way, the removal efficiency of the adsorbent is consistently increased, and overcomes the drawback due to the high dispersibility of graphene oxide in aqueous solutions. This high dispersibility is an advantage during the treatment phase, but it becomes a disadvantage once the adsorption process ends. The presence of magnetite on the surface of graphene's nanosheets consents an easy recovery using an external magnetic field. For example, magnetite graphene oxide/lauric acid (LA) nanocomposite containing ethylenediamine tetra

acetic acid (EDTA) NPs (GO/Fe_3O_4/LA/EDTA) prepared by Danesh et al. (2016) was used for the sorption of Pb(II) ions. Strong coordination ability of EDTA and the presence of −COOH and −OH on GO surface resulted in their enhanced electrostatic interactions with metal ions which improved adsorption performance. In another study, magnetite NPs modified with powder activated carbon i.e. (Fe_3O_4@C) were used as an adsorbent for Pb (II) (Wadhawan et al., 2020).

Researchers have also explored magnetic nanocomposites of different metal oxides as nanosorbents. In this respect, flower shaped Fe_3O_4/MnO_2 nanocomposite was synthesized by Kim et al. (2013). The adsorbent displayed a significant enhanced adsorption capacity for Cd(II), Cu(II), Pb(II) and Zn(II) than Fe_3O_4 nanoparticles. Another important category of magnetic nanomaterials is metal ferrite nanoparticles where any metal is coupled with the ferrite structure to acquire the property of magnetic separation. Metal ferrite, in general, is represented as $M(Fe_xO_y)$ where M denotes any metal which makes divalent bonds. In a series of investigations, Mn-Zn ferrite (Tu et al., 2013), copper ferrite (Tu et al., 2016), and zinc ferrite (Tu et al., 2017) nanoparticles were synthesized for heavy metal ion elimination. Mn-Zn ferrites were employed for removing As(V), Cd(II), and Pb(II) with high removal efficiencies. Subsequently, copper ferrite and zinc ferrite nanoparticles were used for the recovery of Mo(II) and Pb(II) from water, respectively.

Owing to the distinctive physical and chemical properties, carbonaceous based functional materials have emerged as one of the most favourable nanoadsorbents. They are attaining great attention of present researchers because of immense scope in treatment of wastewater decontamination. Several endeavours to obtain a variety of carbon-based nanostructures like carbon nanotubes (CNTs), carbon-based nanocomposites, and graphene have been performed in the past for the removal of various kinds of pollutants. Among these, CNTs are more promising due to their large surface area, small size, cylindrical hollow structure, and electrical conductivity. Basically, CNTs are of two main categories: single-walled (SWCNTs) and multi-walled (MWCNTs). Various studies describe the use of CNTs in heavy metal ion removal from wastewater. For example, Rahbari & Goharrizi (2009) described the adsorption of Pb(II) from water on CNTs with adsorption capacity of 70.1 mg/g. Similarly, Stafiej & Pyrzynska (2007) demonstrated the use of CNTs for the adsorptive removal of ions with removal capacities in the order of Cu(II) > Pb(II) > Co(II) > Zn(II) > Mn(II). In another investigation, oxidized multi-walled carbon nanotube with coating of MnO_2 (MnO_2/oMWCNTs) were used for the efficient removal of Cd(II) ions from aqueous solution with adsorption capacity of 41.6 mg/g (D. Liu et al., 2013). Graphene, another member of carbon-based nanomaterials, has gained a significant attention in the field of environmental remediation. The presence of oxygen containing functional moieties on graphene oxide surface provides a strong hydrophilic nature to it which lead to its fine dispersion in water (as seen in the previous section). The distinctive functional groups and high surface area of GO

makes it a prospective candidate for the wastewater decontamination. These nanomaterials are effective against various pollutants present in wastewater. Removal of heavy metal ions is based on the adsorption via complexation of metal ions with the oxide binding site in graphene (Wadhawan et al., 2020).

8 Experimental part

The final aim of the work was the study of the adsorption capacity of different adsorbent media, in several polluted aqueous solutions. Both pristine magnetite nanoparticles and beads have been tested. TEM and ESEM characterizations have been conducted in order to determine the size and the structure of the produced composites. Their isotherm and adsorption kinetic behaviour have been analysed and the removal capacity was calculated in the different conditions. Some research is still ongoing for what concerns the adsorption kinetics of the beads.

The experimental section of this thesis can be subdivided in three main sections:

1. The first concerns the synthesis of graphene oxide and of magnetite nanoparticles. These two compounds were then used for producing GO sheets decorated on the surface with the magnetite nanoparticles (Fe_3O_4@GO).
2. The second concerns the production of the beads. Different types of beads were produced with the incorporation of magnetite nanoparticles or Fe_3O_4@GO, using different concentrations of calcium chloride in the hardener solution.
3. The third concerns the adsorption tests. Adsorption tests were conducted for investigating both the isothermal and the kinetic behaviour of both nanoparticles and the different kind of beads.

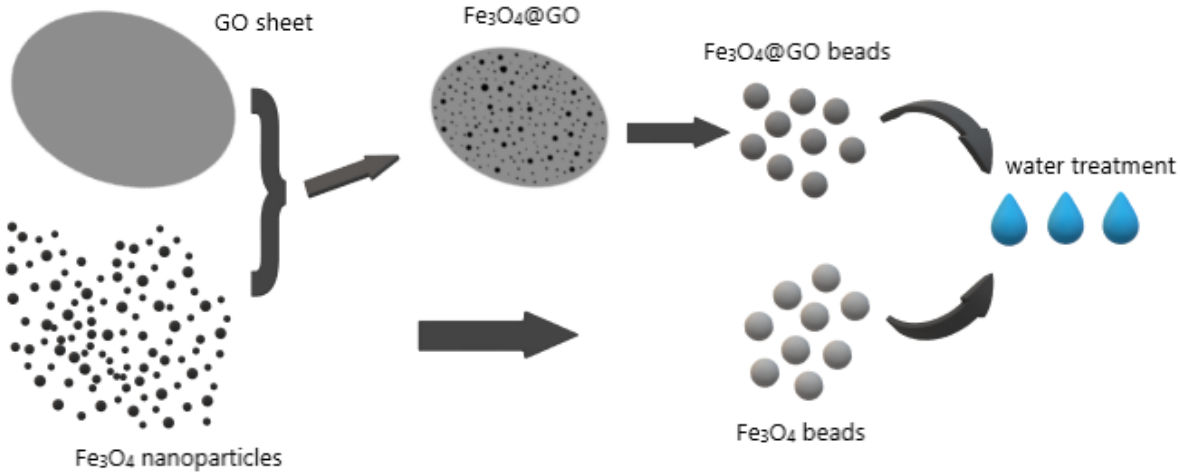

Figure 8.1: Schematic procedure of the experimental conducted during this work.

8.1 Synthesis

The graphene oxide solution, magnetite nanoparticles, and the composites with magnetic nanoparticles on graphene oxide were synthetised starting from the materials reported in section 8.1.1 and according to the following methods.

8.1.1 Materials

Table 8.1: Materials used for the first synthesis part.

Composites	**Chemical formula**	**Molecular weight (g/mol)**	**Purity**	**Productor**
Expanded graphite	-	-	-	ECOPHIT
Potassium permanganate	$KMnO_4$	158.03	≥ 99%	Sigma -Aldrich
Sulfuric acid	H_2SO_4	98.08	98%	Sigma -Aldrich
Hydrochloric acid	HCl	36.46	37%	Sigma -Aldrich
Ammonium hydroxide	NH_4OH	35.05	28-30%	Sigma-Aldrich
Ethanol	C_2H_6O	46.07	> 99.8%	Scharlau
Iron(II) chloride	$FeCl_2 \cdot 4H_2O$	198.81	≥ 99%	Sigma-Aldrich
Iron(III) chloride	$FeCl_3 \cdot 6H_2O$	270.30	≥ 99%	Honeywell Fluka

8.1.2 Synthesis of graphene oxide

The graphene oxide solution was obtained through a modified Sun method. 5 g of expanded graphite and 15 g of potassium permanganate powders were mixed and stirred in a beaker until homogeneity. The beaker was placed in an ice bath, adding slowly and under vigorous mechanical stirring 100 mL of H_2SO_4 (98%) until a petrol-dark green liquid sludge was obtained. The system was left reach room temperature under continuous stirring for about 30 min, until a foam-like material was formed. The beaker was placed again in the ice bath, and 400 mL of distilled water was added very slowly to avoid any uncontrolled temperature increase. The liquid was then placed in a 90°C water bath for 1 h and a dark suspension was obtained. The suspension was filtered on paper in a Buchner funnel and washed

subsequently with 500 mL of distilled water, 200 mL of HCl for removing any manganese traces, and finally again with 500 mL of distilled water to reach neutrality (Pendolino et al., 2014). Figure 8.2 shows the suspension obtained at the end.

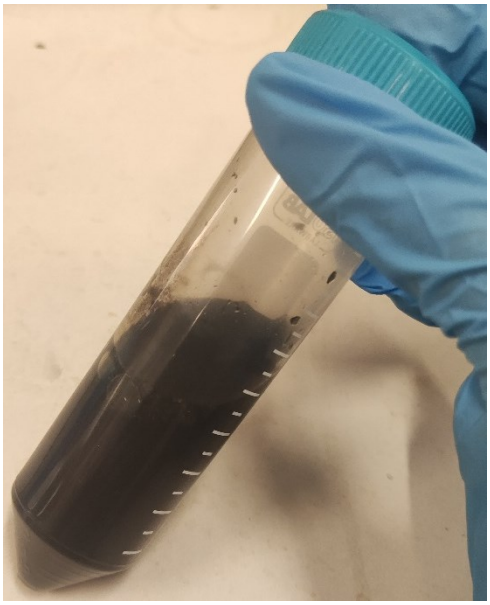

Figure 8.2: GO suspension obtained.

8.1.3 Synthesis of magnetite nanoparticles (Fe_3O_4)

Magnetite nanoparticles were synthetised through the coprecipitation method, starting from iron salts in basic conditions. The procedure followed was based on Ghasemi et al. (2008). Making use of both Fe(II) and Fe(III) chlorides, the coprecipitation requires that the two salts are in the stoichiometric proportion 2:1 (Fe(III)/Fe(II)). Their mixing has to be carried out in aqueous solution, without oxygen, with the successive precipitation in presence of a strong base.

1.0301 g of $FeCl_2 \cdot 4H_2O$ and 2.7813 g of $FeCl_3 \cdot 6H_2O$ were mixed in a 250 mL balloon with two necks under N_2 atmosphere. The solution obtained adding 100 mL of water was magnetically stirred for 20 minutes until the dissolution of the iron salts. Under a nitrogen flow, 12 mL of ammonia hydroxide (25% w/v) were added in order to increase rapidly the pH over 11 and provoke the precipitation of Fe_3O_4. The mixture was left stirring at ambient temperature, for 1 h. The equation of the reaction that describes the formation of magnetite, starting from the iron (II/III) chlorides with NH_4OH as precipitating agent, is:

$$2FeCl_3 \cdot 6H_2O + FeCl_2 \cdot 4H_2O + 8NH_4OH \rightarrow Fe_3O_4 + 20H_2O + 8NH_4Cl$$

Successively, the magnetic stirring was stopped, and the system was left decanting over a permanent magnet, for 1 h (Figure 8.3).

Figure 8.3: Magnetic deposition of the magnetite nanoparticles at the bottom of the beaker.

The solution containing the by-products of the reaction was removed with a pipette and the nanoparticles were washed with deionized water for three times and separated every time by centrifugation (80000 rpm per 5 min two times and 80000 rpm per 15 min). After two more washings with ethanol (8000 rpm for 15 min and for 5 min), the product was dried in a desiccator (Figure 8.4).

Figure 8.4: Magnetite nanoparticles powder, attracted by a permanent magnet.

8.1.4 Synthesis of the magnetite graphene oxide composite (Fe_3O_4@GO)

Fe_3O_4@GO was produced directly by coprecipitation of the magnetite nanoparticles on the graphene oxide sheets. Starting from iron (II/III) chlorides, 1.6038 g of $FeCl_3 \cdot 6H_2O$ and 0.4029 g of $FeCl_2 \cdot 4H_2O$ (molar ratio of Fe^{3+}/Fe^{2+} of 2:1) were put in a round bottom flask and magnetically stirred for 10 minutes, under a flow of nitrogen. They were dissolved in the balloon of 50 mL of deionized water. Once the solution was homogeneous, 25 mL of graphene oxide solution (concentration of the solution 2.23 g/L, thus 55.75 mg of GO) were added. The stirring continued for 30 minutes, after which, 7 mL of NH_4OH were added, in order to increase pH>11. The suspension was kept stirring for other 30 minutes (Figure 8.5).

Figure 8.5: Solution after the base introduction.

Then the stirring was stopped, and the nanoparticles were left to precipitate in a beaker, over a magnet. The precipitate was clearly visible on the bottom of the beaker after 1 h. We removed the solution, repeated the washing with 50 mL of deionized water, and sonicated. The sample was then washed one time with water and three times with ethanol (8000 rpm for 15 min). The sample was put in the desiccator (Figure 8.6).

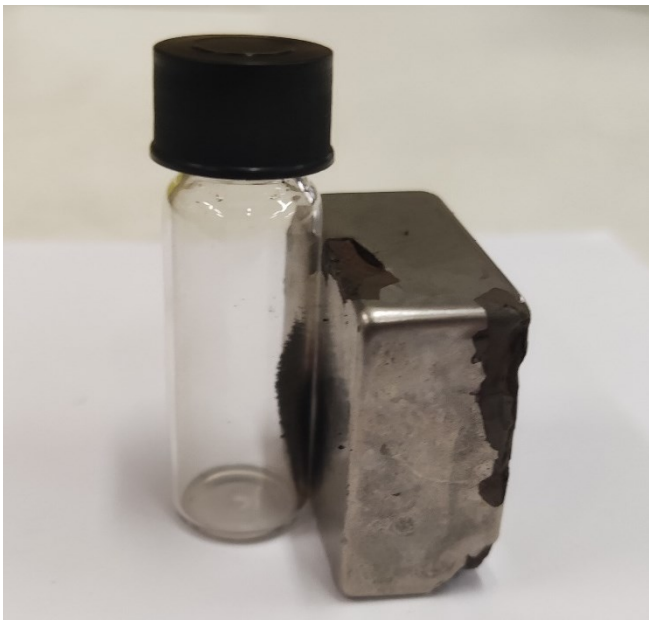

Figure 8.6: Fe_3O_4@GO produced, attracted by a permanent magnet.

The synthetic procedure was repeated reducing the concentrations of the iron salts for the same mass of GO. One quarter of the previous iron (II/III) molar quantities was used.

8.2 Production of beads

The magnetic properties of the nanoparticles are useful for us also as an engine for the collection of the sodium alginate beads from the treated solution, once the adsorption process is complete. Thus, we prepared different kinds of beads testing the effects of different concentrations of both nanoparticles and calcium chloride inside the hardener solution. In fact, we wanted to optimize the adsorption capacity, maintaining a good mechanical stability and a good removability of the adsorbent.

8.2.1 Materials

Table 8.2: Materials used for the production of the different kinds of beads.

Composites	**Chemical formula**	**Molecular weight (g/mol)**	**Purity (%)**	**Productor**
Calcium chloride	$CaCl_2 \cdot 2H_2O$	147.02	98%	Normapur
Sodium alginate	$(C_6H_7O_6Na)n$	1000-600000	90.8-106%	BioChemica-ITW Reagents

8.2.2 Preparation of sodium alginate solution

In 300 mL of deionized water, 3 g of sodium alginate powder were added (10 mg/mL). At this point the mixture was heated at 40°C and mechanically mixed for 1 h, until a homogeneous solution was obtained.

8.2.3 Beads with Fe_3O_4

Two different beads production methods were tested, both based on the same procedure. The first one used a higher concentration of calcium chloride in the hardener solution and longer contact time (during which the beads are left stirring and adsorbs calcium), while in the second, a lower concentration of calcium chloride was used, and the beads were collected from the solution, immediately after the formation. The beads obtained with the first method will be called type I, while those obtained with the second type II.

Considering the type I beads, in order to study the effects of the magnetic nanoparticles on the adsorbent medium, the beads were produced using different Fe_3O_4 nanoparticles concentrations: 5 mg/mL; 3 mg/mL; 1 mg/mL. Thus, 0.1502 g, 0.0914 g and 0.0298 g of nanoparticles respectively were added in 30 mL of the prepared sodium alginate solution. Once the suspension of alginate and nanoparticles was well homogenized (by mechanical agitation and sonication), a solution of calcium chloride with a concentration of 3 g of $CaCl_2 \cdot 2H_2O$ for 100 mL of deionized water was prepared as hardener solution (Figure 8.7). Beads of type I produced with a concentration of nanoparticles of 5 mg/mL were called B2, during the adsorption tests.

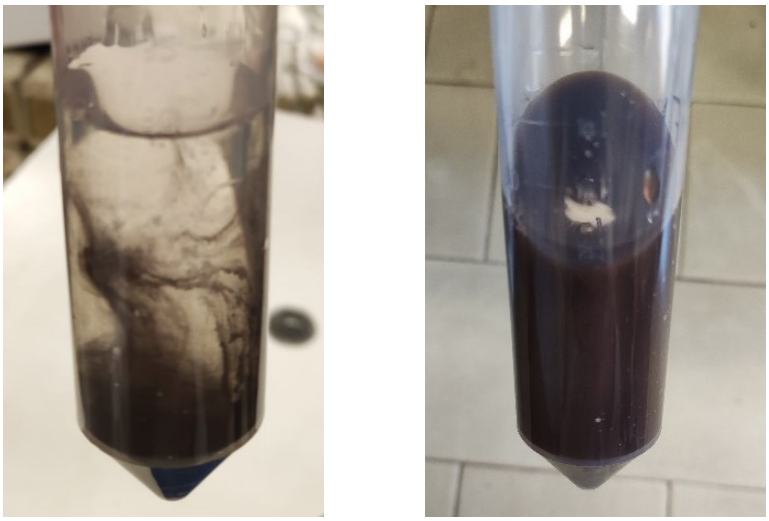

Figure 8.7: Solution of sodium alginate and Fe_3O_4 nanoparticles, before sonication (on the left). Solution of sodium alginate and Fe_3O_4 nanoparticles, after sonication (on the right).

The beads were produced by drop-wise addition of the alginate nanoparticles suspension in the hardener solution, under stirring. The formed beads were kept in the hardener solution for 1 h for aging (Figure 8.8).

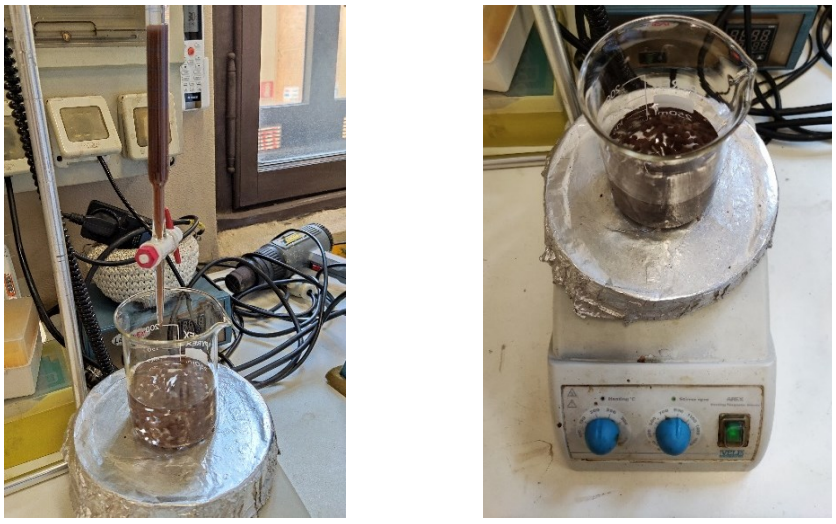

Figure 8.8: Apparatus for the bead's formation (on the left). Successive continuous stirring of the beads inside the calcium solution (on the right).

The beads were then recovered from the solution, washed four times with deionized and stored in a Falcon® tube, with 50 mL of deionized water, until used for the treatment experiments. Beads are dark in colour (Figure 8.9). The beads synthesized using a concentration of 5 mg/mL of nanoparticles were called B2, during the adsorption tests.

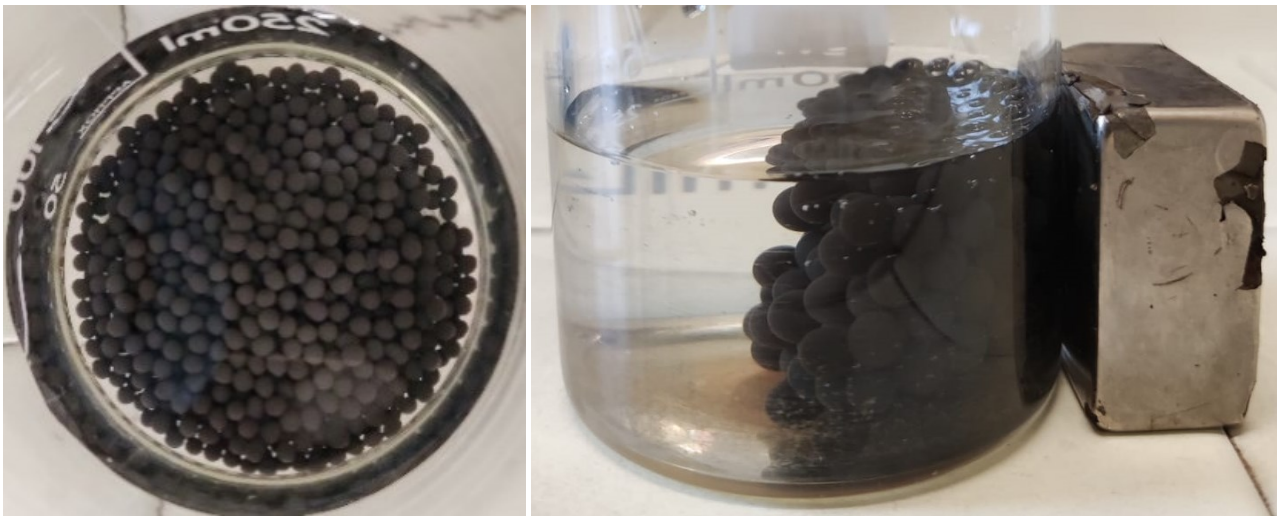

Figure 8.9: Beads with magnetite with a concentration of Fe_3O_4 nanoparticles of 5mg/mL.

Considering the beads of type II, the concentration of nanoparticles was 5 mg/mL (0.1503 g in 30 mL of alginate solution) and the dissolved amount of calcium chloride was 1 g, in 100 mL of deionized water. The homogenous suspension of nanoparticles and sodium alginate were added drop by drop in the calcium solution with no stirring. Once the drops fell from the burette in the calcium solution the beads were formed and were immediately collected and transferred in a beaker with only deionized water. Once all the beads were formed, the liquid phase was changed with fresh deionized water and the beads were left stirring for 30 minutes. They were stored in a Falcon® (Figure 8.10). These types of beads were called B1, during the adsorption tests.

Figure 8.10: Beads stored in the falcon with deionized water.

8.2.4 Beads without only sodium alginate

We also produced pure SA beads in order to visualize the adsorption process of copper ions. The beads were produced as usual, dropping a sodium alginate solution in a beaker containing a calcium solution (100 mL of deionized water and 3 g of calcium chloride).

8.2.5 Beads with Fe_3O_4@GO

In 30 mL of alginate solution, 0.1498 g of the Fe_3O_4@GO composite were added (concentration of 5 mg/mL). In the hardener solution, 1 g of calcium chloride was dissolved (10 mg/mL). The beads were extracted immediately after they were formed. After they was put in a beaker with only deionized water, washed two times with deionized water, and left stirring for the night. During this time, they started to break, and lost their sphericity. So, we proceeded to preparate more resistant and mechanical stable beads.

Two new different paths were tried:

1. increase of the concentration of calcium salt in the hardener solution. Beads with an unvaried concentration of nanoparticles were produced in a solution with a concentration of 30 mg/mL of calcium chloride;
2. decrease of the nanoparticles concentration. Beads with a nanoparticles concentration of 2.5 mg/mL were prepared in a solution with an unvaried concentration of calcium (10 mg/mL). These types of beads were called B3, during the adsorption tests.

Both these new types of beads remained stable in the long term after washing with deionized water for 3 times.

8.3 Characterization

All the adsorbents were characterized morphologically either by TEM or ESEM while those with magnetic nanoparticles were also characterized magnetically.

8.3.1 Magnetic measurements

The magnetic properties of the samples were studied with a Quantum Design superconducting quantum interference device (SQUID) magnetometer, operating in the 6–300 K temperature range (maximum applied field 50 kOe). The effects of the field and of the temperature on the magnetic properties of the adsorbents were investigated. The measurements were conducted by Prof. Federico Spizzo and Prof. Lucia Del Bianco, from the Physics and Earth Science Department of the University of Ferrara, Italy.

8.3.2 TEM characterization

For appreciating the morphology of the obtained systems, the characterization of the magnetite nanoparticles and of the graphene oxide sheets decorated with nanoparticles were conducted using the Transmission Electron Microscope (TEM FEI Tecnai G12 of the Laboratory of Microscopy in the Biology Department). For preparing the sample, 0.01 g of material was dispersed in 1 mL of deionized water. A single drop of nanoparticles suspension was deposited on a 400-mesh carbon-coated copper grid. The excess solution was removed from the grid and the sample was dried at room temperature.

8.3.3 ESEM characterization

ESEM (Environmental Scanning Electron Microscopy) analyses of the three typologies of beads have been performed at the CEASC (Centro di Analisi e Servizi Per la Certificazione) Laboratory of the University of Padova, using a FEI-QUANTA 200 variable pressure-environmental instrument, equipped with backscattered electron (BSE) detector. The sample was prepared positioning the beads on the support that will be insert inside the machine (Figure 8.11).

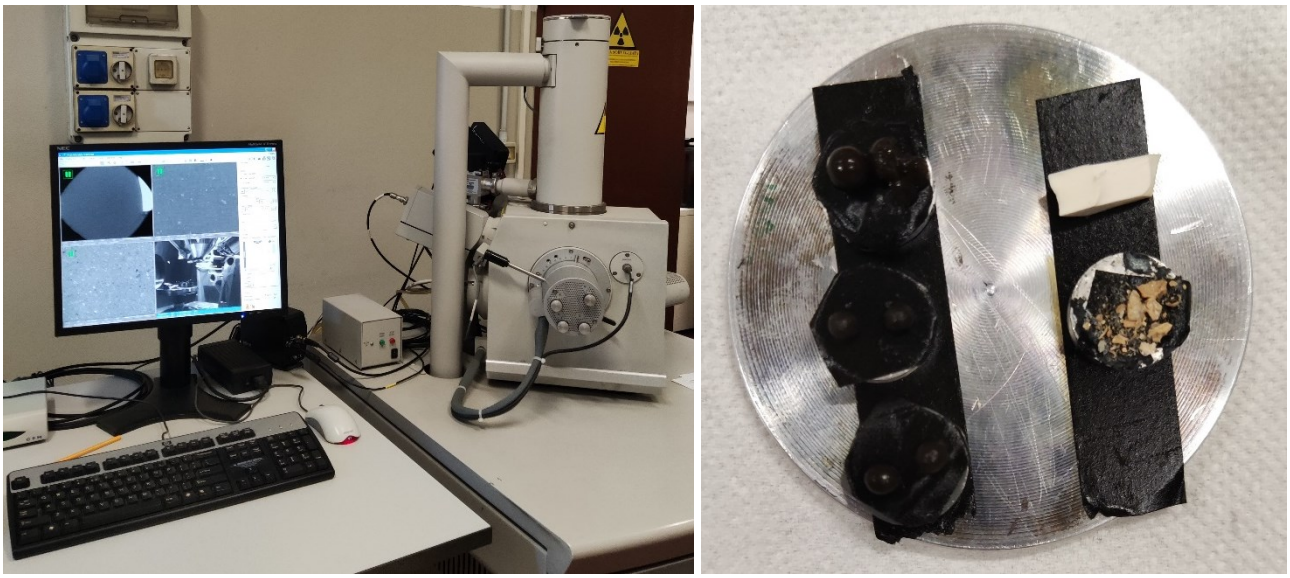

Figure 8.11: FEI-QUANTA 200 variable pressure-environmental instrument, equipped with backscattered electron (BSE) detector (on the left). Prepared sample (on the right).

8.4 Adsorption tests with heavy metal ions

The adsorption tests were articulated in isothermal and dynamic tests. Both these tests were conducted with magnetic composite adsorbent Fe_3O_4@GO and with beads containing Fe_3O_4 or Fe_3O_4@GO. The studied metal ions were chromium(III) and nickel(II) as chlorides, and copper(II) as nitrate.

8.4.1 Materials

Table 8.3: Materials used.

Composites	**Chemical formula**	**Molecular weight (g/mol)**	**Purity (%)**	**Productor**
Chromium(III) chloride	$CrCl_3 \cdot 6H_2O$	266.45	98%	Carlo Erba
Copper(II) nitrate	$Cu(NO_3)_2 \cdot 3H_2O$	241.60	99.5%	Merck
Nickel(II) chloride	$NiCl_2 \cdot 6H_2O$	237.70	99%	Carlo Erba

8.4.2 Preliminary adsorption tests with copper nitrate

1 M solution of copper nitrate was produced dissolving 24.1772 g of salt in 100 mL of deionized water.

1 mL of the stock solution and 9 mL of deionized water were put in two Falcon® tubes (dilution 1:10). In one,10 B2 beads were added. The stock solution kept in the second falcon was used as reference solution. The tubes were kept stirring for 15 minutes.

The second test was done with the beads made only of SA. In this way the eventual change of colour could be clearly seen. 20 beads were put in a beaker containing 1 mL of stock solution and 9 mL of deionized water. Each half an hour 5 beads were collected, and their colour was analysed. Once three samplings had been conducted (at 30 min, 1 h, 1 h and a half), the last five beads were put in a calcium solution with a concentration of 0.3 g/L of calcium chloride, for testing their regeneration capacity.

8.4.3 Isotherm adsorption tests

8.4.3.1 Adsorption isotherms for single elements using nanoparticles

For the selected ions, the adsorption isotherms were experimentally evaluated. The adsorbent/solution ratio was kept constant at 1 mg/mL. Tests were performed in a stirred glass flask (100 mL nominal volume for chromium and 50 mL for nickel and copper). After loading the nanoparticles in the solution, the vessel was kept at room temperature and stirred for 30 min. The removal of the adsorbent was carried out by using a standard Neodymium magnet. The treated liquid was also filtered, on filter paper, to eliminate any possible traces of the adsorbents. An Inductively Coupled Plasma Optical Emission Spectroscopy (ICP-OES) (Perkin Elmer Optima 4200DV by Perkin Elmer Italia S.p.A., Milano, Italy) was used for the concentration measurements. Every test was performed preparing a series of solutions at different target initial concentration (Table 8.4). After adding the nanoparticles (100 mg for the test with chromium and 50 mg for the tests with nickel and copper) to the solution, they were stirred at 100 rpm and, after 30 minutes, separated using a magnet and filtered.

Table 8.4: Tested concentrations for each heavy metal ions.

Chromium (µg/L)	Copper (µg/L)	Nickel (µg/L)
440	296	935
580	501	1900
1060	690	3980

Chromium (µg/L)	Copper (µg/L)	Nickel (µg/L)
1810	1020	5120
4990	2000	
	6430	

8.4.3.2 Adsorption isotherms for single elements using the beads

Isotherm adsorption tests were extended to the beads, operating on solutions containing different concentrations of nickel(II), copper(II) and chromium(III) salts as showed in Table 8.5.

Table 8.5: Tested concentrations for each heavy metal ions.

Chromium (µg/L)	Copper (µg/L)	Nickel (µg/L)
139	123	443
225	302	1020
273	587	1060
423	838	2120
605	928	2166
1915	2380	4250
	2770	4394
	4820	5123
		6125

The objective was to study the adsorption capacity of the different types of beads, with respect to the selected metal ions. The metal solutions were prepared by dilution from concentrated mother solutions and volumes of 2 mL, at the desired concentration, were used in the tests.

In every test we considered 5 beads in a vial, with 2 mL of the selected solution (Figure 8.12). The vials were homogenously stirred for all the time interval of testing (10 min). After that, a sample of the treated solution was taken from each vial with a micropipette. The liquid samples were analysed at ICP-OES to determine the concentration of pollutant present after the treatment with the adsorption medium. Moreover, all the stock solutions were also analysed in order to define the exact starting concentration in the solution to be treated.

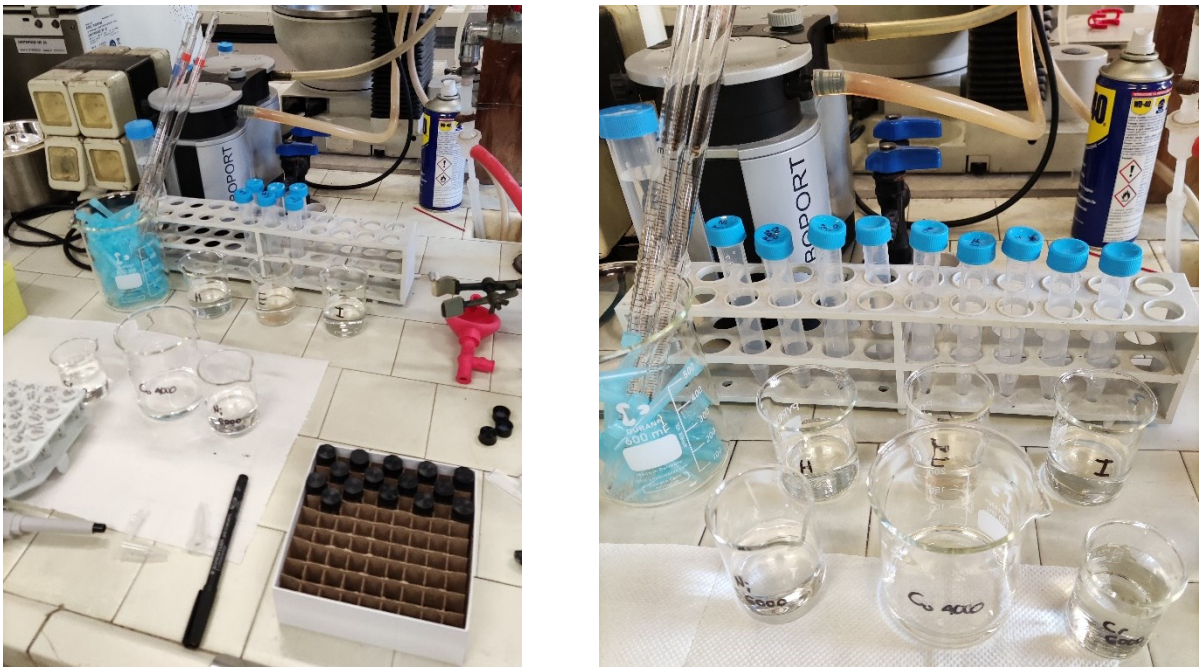

Figure 8.12: Test apparatus for the isotherm tests with the beads.

8.4.4 Kinetic adsorption tests

8.4.4.1 Adsorption kinetics using nanoparticles

We performed adsorption kinetic tests on six solutions: three single elements solutions (respectively with chromium, copper, and nickel) and three mixtures.

20 mg of Fe_3O_4@GO nanoparticles were put in each beaker, with 20 mL of the solution to be treated. The composition of the six solutions (3 single elements and 3 mixtures) has been analysed at 30 sec, 1 min, 2.5 min, 5 min, 7.5 min and 10 min.

The studied concentration for the single element solutions is 3635 µg/L, 1890 µg/L and 2740 µg/L for nickel, copper and chromium, respectively.

The mixed ions solutions were prepared starting from 3 solutions of the three single heavy metals in the correct ratio to obtain the following mixtures (Table 8.6).

Table 8.6: Metal ion concentration in the mixture.

	Ni (µg/L)	Cu (µg/L)	Cr (µg/L)
H	2360	494	1805
E	1250	301	395
I	5600	980	4770

The solution was added to 20 mg of nanoparticles in a glass beaker, with a pipette. The solution was kept under homogenous stirring for the entire duration of the test. After the desired time interval, the solution was filtered on paper under vacuum. (Figure 8.13) and stored in plastic Falcon® tubes for the analyses through ICP-OES.

Figure 8.13: Filtration apparatus (on the left). Test apparatus for adsorption tests with nanoparticles (on the right).

8.4.4.2 Adsorption kinetics using the beads

Metal ions solutions of the same concentrations, both for single elements and mixtures, have been treated also with the different types of beads as adsorption medium. The tests were performed using the three different types of beads (B1, B2, B3), previously synthesized.

The time intervals selected for the analysis of the treated solutions are: 30 sec, 1 min, 2.5 min, 5 min, 10 min, 15 min, 3 h and 24 h.

In vials containing 5 beads each of the same type, 2 mL of solution to be treated were added.

The solution treated with the beads was kept under homogeneous stirring for all duration of the test (Figure 8.14). At the end of each interval, 1 mL of treated solution was taken with the micropipette and stored for the ICP-OES analysis.

Figure 8.14: Vials containing the solution that has to be treated and the beads.

9 Results

In this section, the main results obtained are illustrated and discussed. First, the amount of product obtained from each synthesis is reported, in correlation with the quantity of reagents used. Then, the morphological and magnetic characterization of the produced nanoparticles is presented. The adsorbents were characterized by TEM and ESEM analysis. Finally, the results of the adsorption tests are described. For each adsorbent, both adsorption isotherm and kinetic tests were carried out, and the adsorption capacity was calculated.

9.1 Synthesis of the nanomaterials and adsorbents

In this section, we report the results of the synthesis previously described in the Experimental part.

9.1.1 Synthesis of Fe_3O_4 nanoparticles and GO composite

The procedure for the synthesis of the magnetite nanoparticles was based on a known coprecipitation method (Ghasemi et al., 2008) with some modification. In fact, we didn't proceed to the functionalization with oleic acid which would reduce the agglomeration of the nanoparticles in suspension, but also make them less dispersible in aqueous solution.

The synthesis was performed under nitrogen atmosphere because oxygen would oxidize Fe(II), especially when it is in solution, while the air humidity would modified Fe(III), which is really hygroscopic.

The synthetic procedure of the last composite sample has been carried out with one quarter of the initial concentrations of iron salts for the same mass of GO in order to reduce the superficial decoration of the sheet and have a higher area available for pollutants adsorption. In fact, with the concentrations initially used, the composite obtained showed an extremely high degree of decoration. The high amount of nanoparticles on the graphene oxide surface can decrease the adsorption capacity of the composite, considering that there is only a small fraction of the superficial are of graphene oxide able to adsorb the pollutant molecules.

Table 9.1 summarizes the amount of reagent used for the synthesis of magnetite nanoparticles, the amount of product obtained and the yield of the reaction, based on the following stoichiometric reaction:

$$2FeCl_3 \cdot 6H_2O + FeCl_2 \cdot 4H_2O + 8NH_4OH \rightarrow Fe_3O_4 + 20H_2O + 8NH_4Cl$$

Table 9.1: Summary of the magnetite synthesis.

Synthesis of Fe_3O_4	Mass of Fe(III) salts initially used (g)	Mass of Fe(II) salts initially used (g)	Moles of Fe(III) initially used (mol)	Mass of product obtained (g)	Moles of Fe(III) obtained (mol)	Yield (%)
#1	2.7813	1.0301	0.0051	1.2386	0.0053	97.1

Table 9.2 summarizes the amount of reagents used for the synthesis of Fe_3O_4@GO nanoparticles, and the amount of product obtained.

Table 9.2: Summary of the synthesis Fe_3O_4@GO synthesis.

Synthesis of Fe_3O_4@GO	Mass of GO (mg)	Mass of Fe(III) salts initially used (g)	Mass of Fe(II) salts initially used (g)	Mass of product obtained (g)
#1	55.75	1.6038	0.4029	0.5405
#2	55.75	1.6001	0.3933	0.5288
#3	55.75	1.5098	0.4040	0.5188
#4	55.75	0.2642	0.1011	0.1716

9.1.2 Production of the sodium alginate beads

The advantages of the type II beads are the use of less calcium salt (economy of material), and the presence of more free coordination sites useful for bonding the metal ions in the contaminated solution that needs treatment. Thus, they should be better in the treatment of heavy metal contaminated solution. Despite the lower degree of crosslinking, the beads properly formed. The only disadvantages is a loss in mechanical stability, since the internal crosslinking of the bead is less strong and stable.

During the first synthesis of the beads containing the Fe_3O_4@GO composite, it can be noticed that the use of a so small quantity of calcium salt and a reduced crosslinking time are evidently not sufficient for producing stable beads. This could be due also to the presence of the 2D graphene oxide sheet that reduce the crosslink ability of the alginate, interfering with the functional groups on the GO sheets.

9.2 Characterization

The magnetic characterization has been performed only on the magnetite nanoparticles. While the TEM characterization was conducted on both magnetite nanoparticles and graphene oxide decorated with magnetic nanoparticles. The ESEM characterization was conducted on all the types of beads produced.

9.2.1 Magnetic characterization of magnetic nanoparticles

By using a Quantum Design superconducting quantum interference device (SQUID) magnetometer the magnetization of the nanoparticles has been measured. From Figure 9.1, it can be seen that the main effect induced by a temperature increase is a reduction of the magnetization. The magnetization decrease, with respect to the 6 K value, is ~ 15 % whilst, as a reference, in bulk magnetite the decrease is ~ 6 %. This difference can be ascribed to the presence of a higher degree of surface structural disorder, in the nanoparticles, with respect to the bulk system. In fact, the magnetic moments in a nanometric dimension are characterized by a less ordered disposition, and a higher relative number of surface atoms ions, with respect to a more extended bulk system. The effect of non-alignment of the magnetic moment is a reduced total magnetization of the nanoparticles.

The magnetization values measured at 50 kOe are always smaller than the saturation magnetization values extrapolated from the magnetization loops (the loops were measured at 6 K, 20 K, 50 K, 100 K, 200 K, 300 K). So, at all the temperatures, the saturation of the sample is not obtained within the range of applied magnetic fields. The value of the saturation magnetization (M_{sat}) extrapolated from the 6 K loop is ~ 70 emu/g. At 300 K, M_{sat} is between 58 and 60 emu/g, which is smaller than reported value for bulk magnetite (92-100 emu/g) (Niculescu et al., 2022).

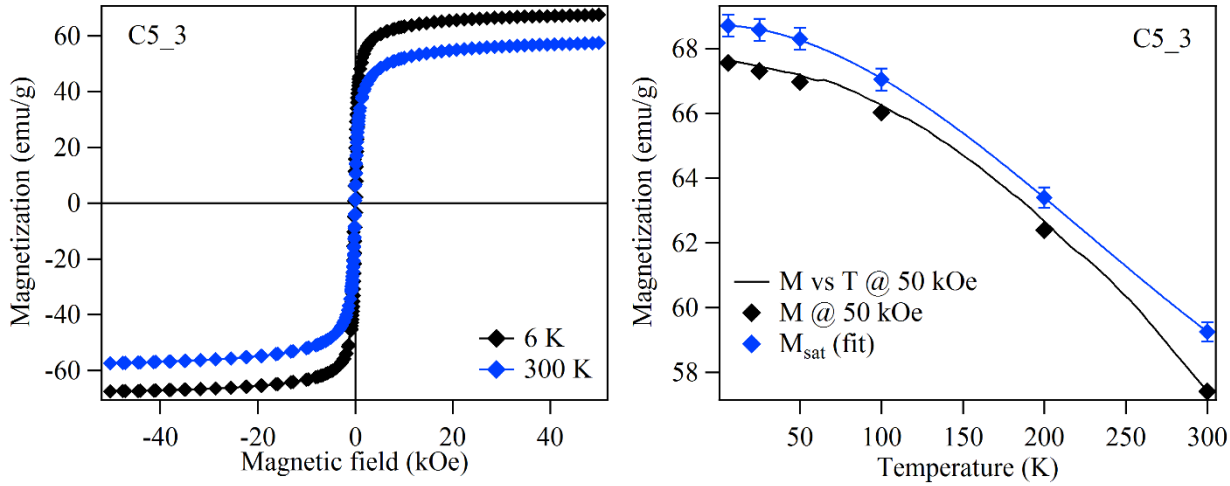

Figure 9.1: Behaviour of the magnetization recorded at 6 K and 300 K on magnetite nanoparticles (on the left). Behaviour of the magnetization recorder at 50 kOe on magnetite nanoparticles. The blue diamonds are saturation magnetization values (on the right).

It has to be evidenced that, once the magnetite nanoparticles are deposited on the graphene oxide sheets, the global magnetization of the composite is expected to be lower than that of the starting single magnetic nanoparticles, due to the fact that the carbonaceous support is not magnetic.

9.2.2 TEM characterization

9.2.2.1 Characterization of the Fe_3O_4 nanoparticles

Figure 9.2 shows the TEM images of the magnetite nanoparticles. It can be seen that they have a rounded shape and with a wide size distribution going from 3.8 nm to 15.4 nm.

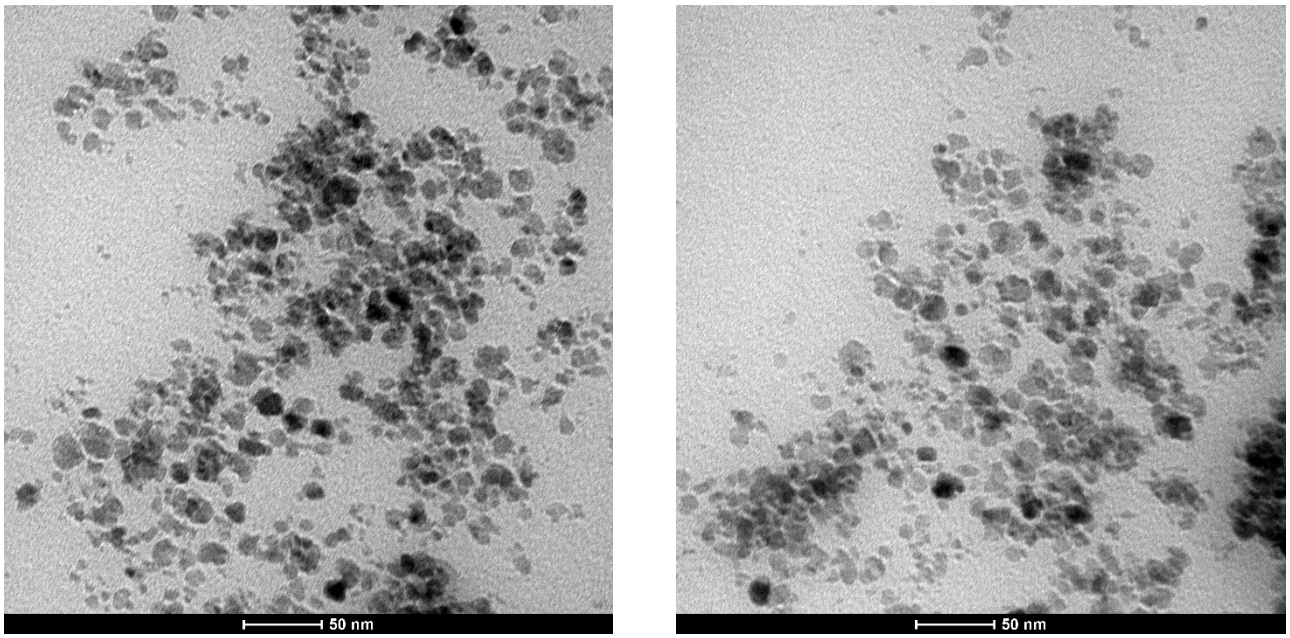

Figure 9.2: TEM characterization of magnetite nanoparticles.

In Figure 9.3 the size distribution is reported, from which an average diameter of 7.23 can be determined (about 400 nanoparticles were measured). The standard deviation of the sample is 2.824.

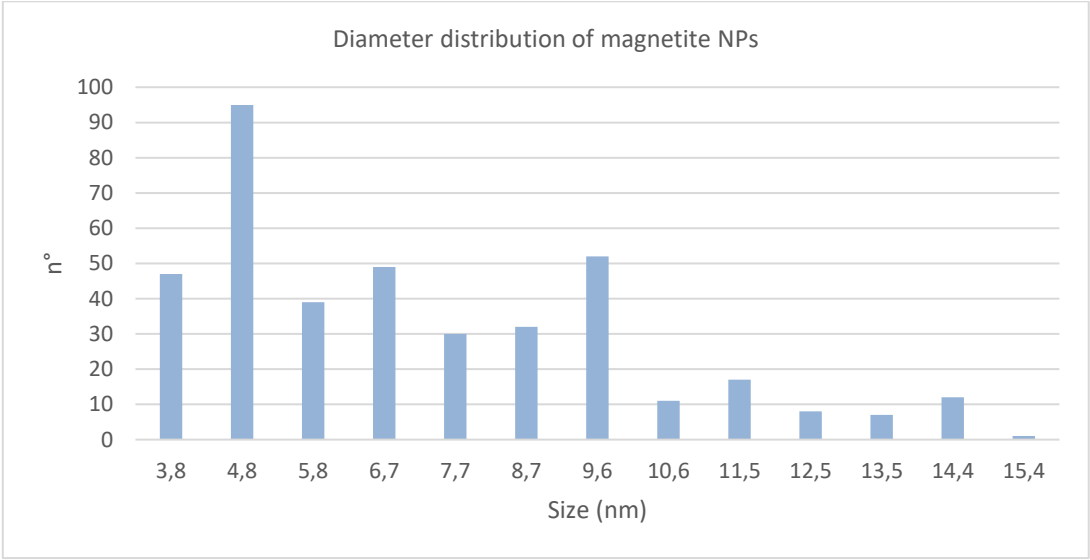

Figure 9.3: Diameter distribution of the magnetite nanoparticles.

9.2.2.2 Characterization of the Fe_3O_4@GO nanoparticles

The chosen synthesis based on the coprecipitation of Fe_3O_4 nanoparticles in presence of GO should favour the interaction of the nanoparticles with the anionic oxygenated groups on the graphene oxide present in the basic solution used. In Figure 9.4 we can recognize the carbonaceous support (grey sheet) on which the nanoparticles are attached (black dots). It can be observed that the degree of decoration of the composite is extremely high. The GO sheet, acting only as a support, is completely

covered by the magnetic material. With the idea of using also the adsorbent capacity of the graphene oxide itself, we decided to attempt a new synthesis, using a smaller amount of iron salts (1/4 of the previous concentration). In this way we could obtain a less functionalized compound, in which the GO sheets have some free active sites that could be used as adsorbent. It is interesting to see the effect that this smaller amount of iron inside the nanoparticles will have on the distribution of the magnetite nanoparticles on the GO surface but also on the dimensions of the Fe_3O_4 nanoparticles.

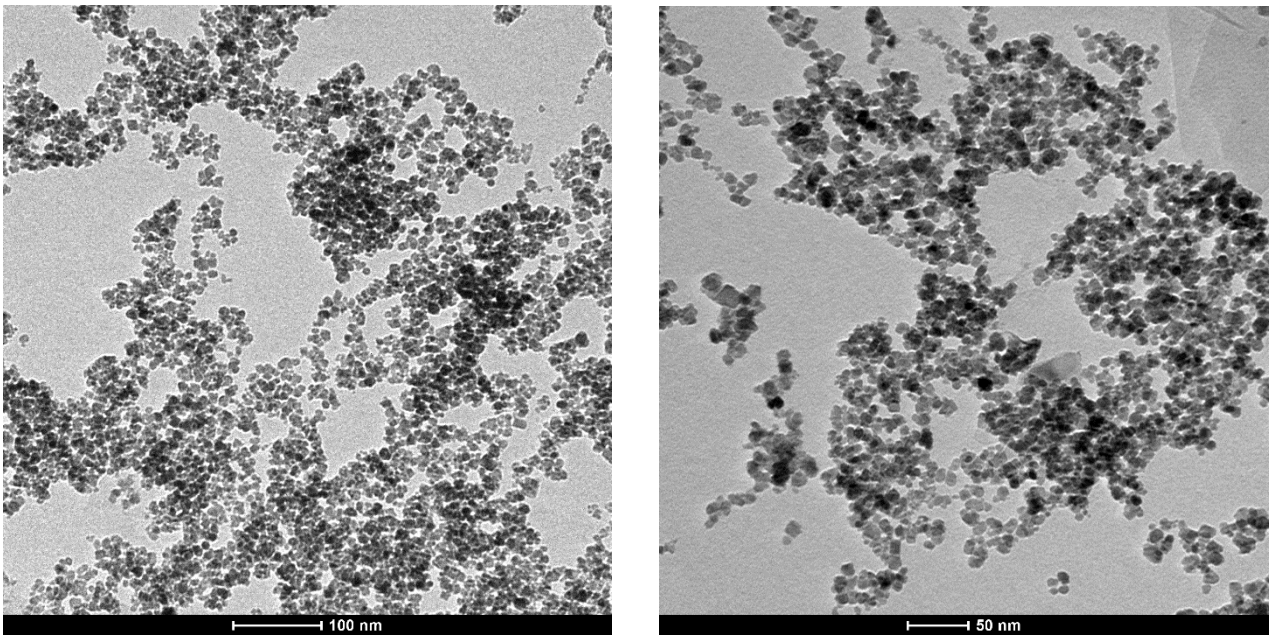

Figure 9.4: TEM images of Fe_3O_4@GO with the normal synthesis procedure.

The magnetite nanoparticles show generally a rounded shape, and a size distribution centered around 7.18 nm (about 350 nanoparticles were measured). The standard deviation of the sample is 2.418 (Figure 9.5).

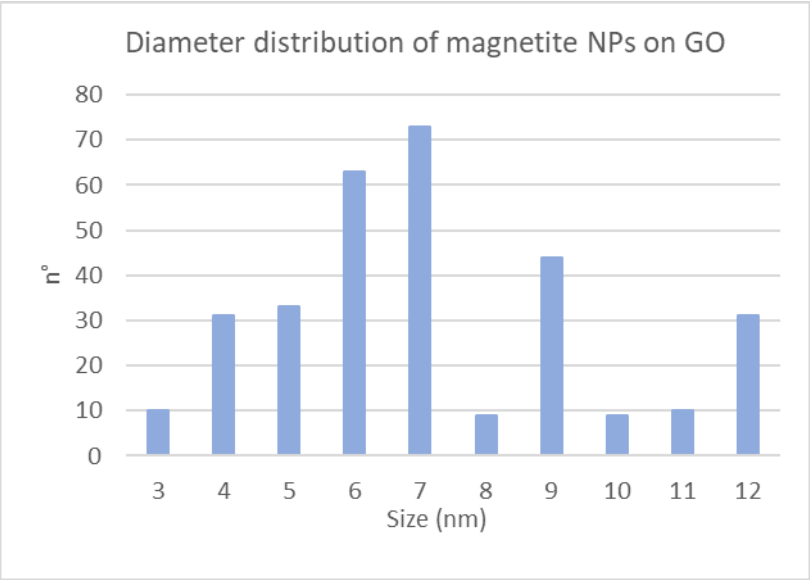

Figure 9.5: Diameter distribution of the magnetite nanoparticles on the graphene oxide sheet.

TEM images of the Fe_3O_4@GO at different magnification were shown. In Figure 9.6 it can be clearly seen that the graphene oxide sheets are less decorated by magnetite nanoparticles, confirming the assumptions made originally This comports a smaller nanoparticles' agglomeration and a free superficial area of the GO sheet, that can act as adsorbent for the heavy metal ions present in the aqueous solution.

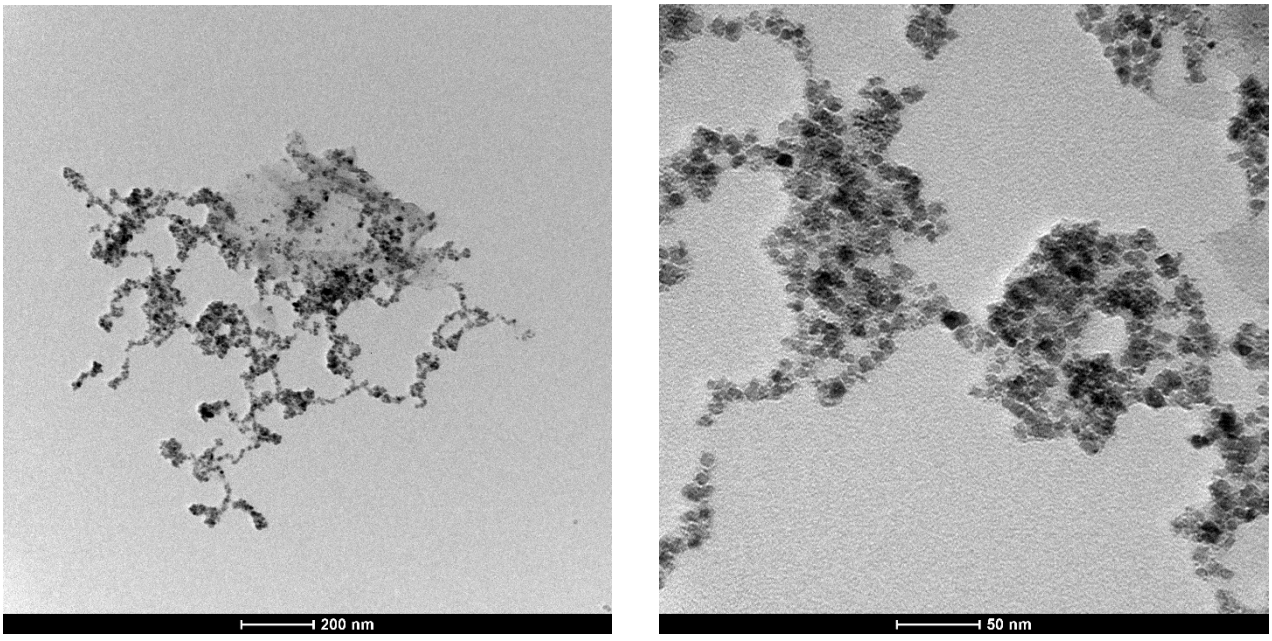

Figure 9.6: TEM images of Fe_3O_4@GO for the synthesis with a reduced iron amount.

The GO nanosheets have irregular shape and sizes ranging from 200 to 500 nm. The Fe_3O_4@GO are composed of a few sheets of GO with bounded magnetic nanoparticles which are not evenly distributed in the GO surface but tend to form aggregates closer to the sheet's borders, were the higher

concentration of oxygenated functional groups are expected. This leaves wide sections of the surface areas of GO free for adsorption.

9.2.3 ESEM characterization of the beads

9.2.3.1 Characterization of beads with Fe_3O_4

The ESEM (environmental scanning electron microscopy) coupled with EDX (x-ray energy dispersive analysis) is a technique that allow to collect both micrographic pictures of a sample and to perform surface elemental analysis on it. The term "environmental" comes from the use of non ultra high vacuum for the measurement, working at around 10-200 Pa on wet and uncoated samples.

The images show the external structure of the beads produced dispersing magnetite in the alginate solution. The obtained images are of the samples which did undergo a little partial evaporation of the water due to the sampling and the effect of the low pressure in the specimen chamber. This effect depends on how much time the sample is under vacuum at the moment in which the electron beam scans its surface. For this reason, their structure seems corrugated in the images.

Figure 9.7 reports the ESEM images of B1 beads. The analysed bead is not dehydrated yet, but fissures due to the vacuum are clearly visible. Through these fissures we can visualize the internal polymeric fibrous structure of the alginate matrix. In fact, once the alginate solution came in contact with the calcium solution, a reticulate structure was instantaneously formed.

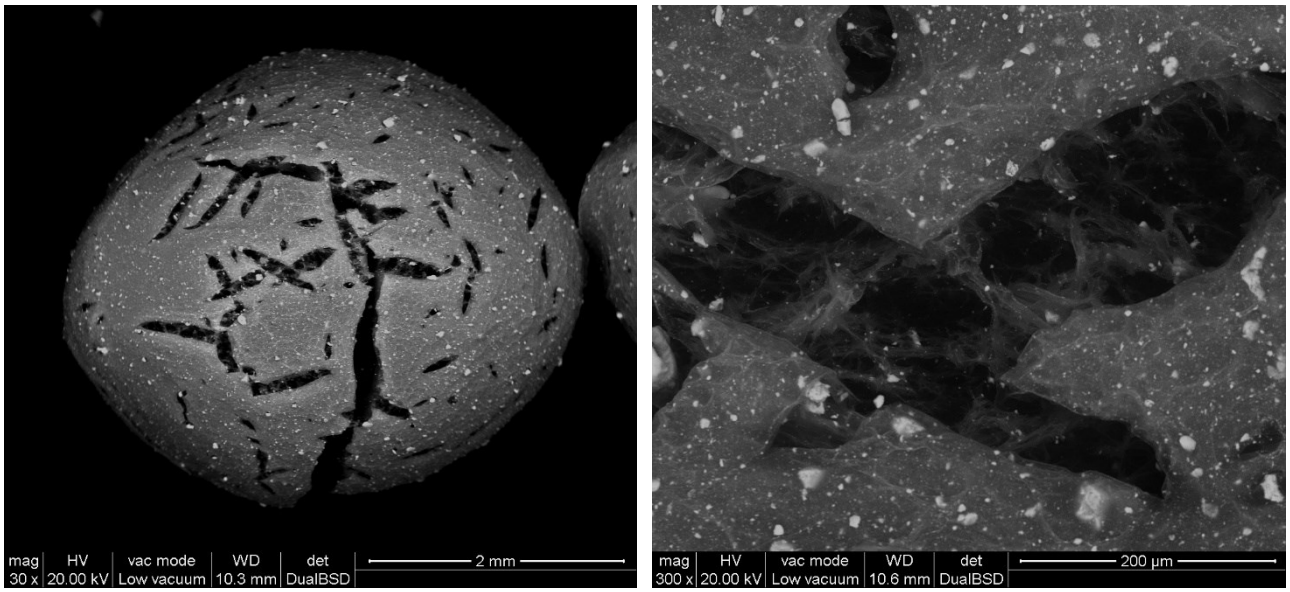

Figure 9.7: ESEM characterization of beads with magnetite (B1).

Figure 9.8 shows the average elemental analysis of a superficial spot on the beads surface. The graph qualitatively indicates the presence of both calcium and iron.

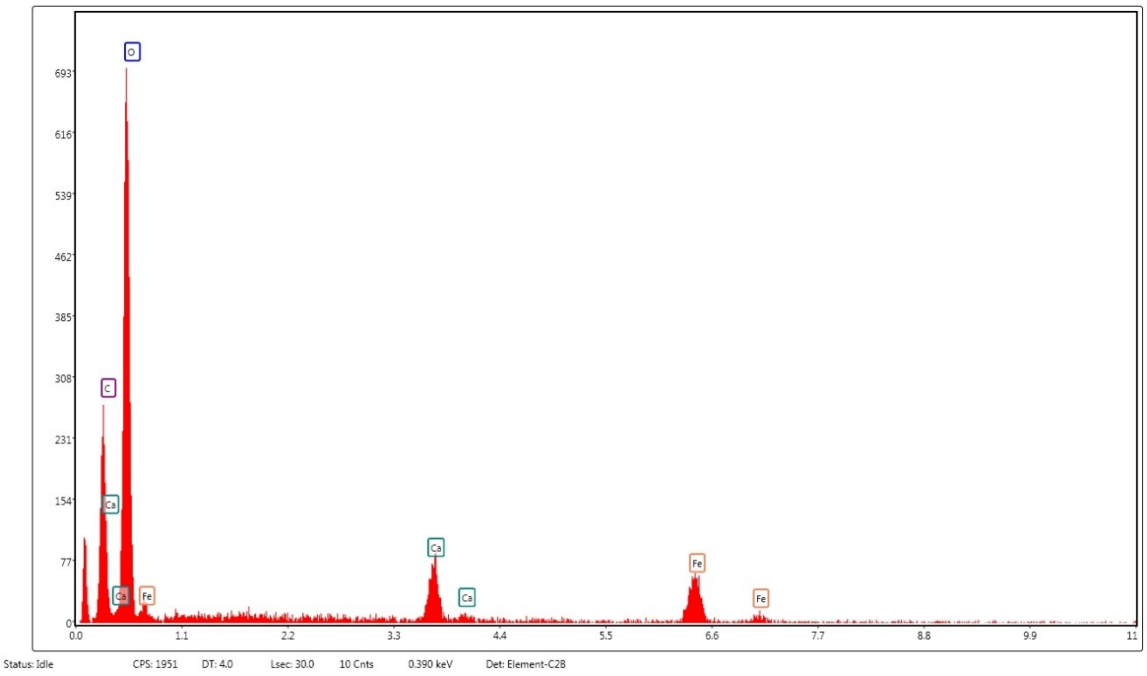

Figure 9.8: Medium analysis on a point of the bead's surface (B1).

Table 9.3 report the EDX elemental analysis of the bead B1.

Table 9.3: EDX elemental analysis of the bead B1.

Element	Weight %
C	22.08
O	61.65
Ca	5.87
Fe	10.4

Figure 9.9 reports the ESEM images of B2 beads. For the analysed bead the effect of the dehydration process is clearly visible. The minor grade of cracking of B2 with respect to B1 can be associated to the higher reticulation grade of B2. In fact, B2 beads were produced with a higher calcium concentration in the hardener solution and with a higher contact time. The highly concentrated white dots on the surface of the beads are the magnetite nanoparticles present in the adsorbent.

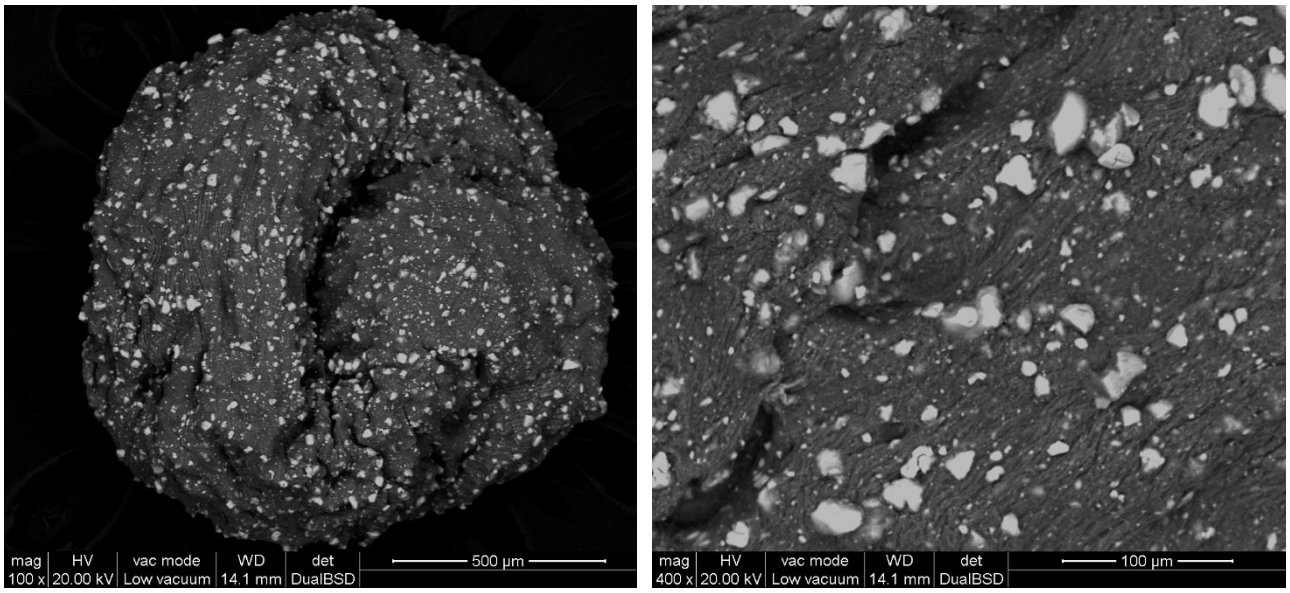

Figure 9.9: ESEM characterization of the beads with magnetite (B2).

Figure 9.10 reports the average analysis of a superficial spot on the beads surface. Also in this case, the graph qualitatively indicates the presence of both calcium and iron.

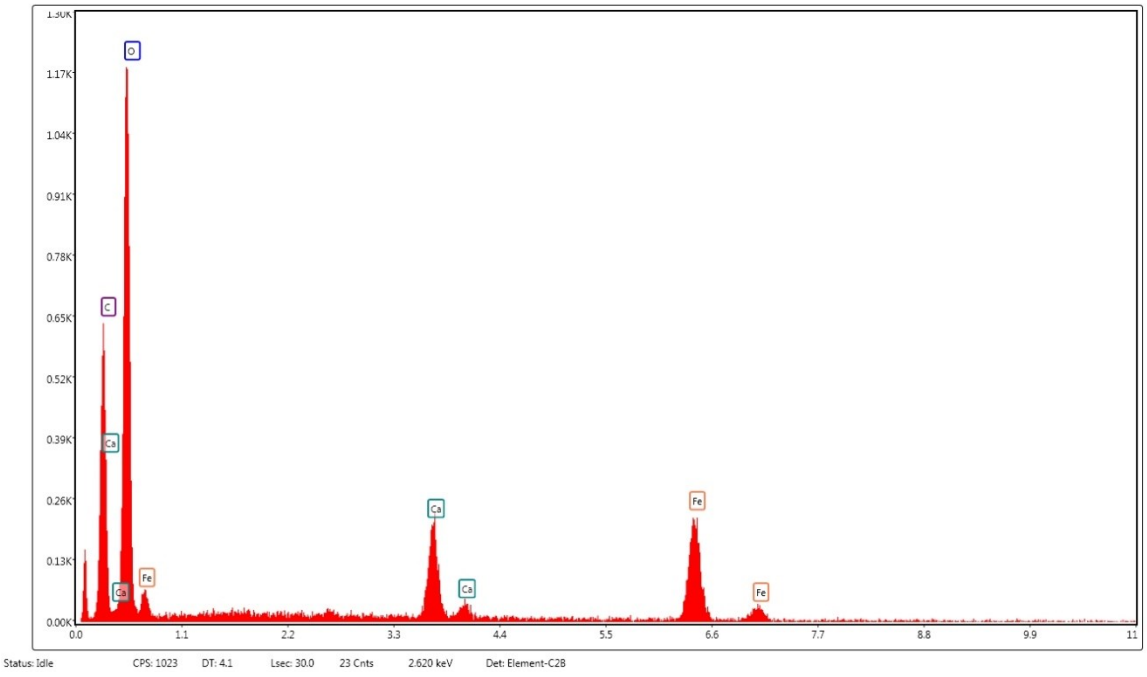

Figure 9.10: Medium analysis on a point of the beads' surface (B2).

Table 9.4 reports the EDX elemental analysis of the bead B2. It can be noticed that the presence of calcium and of iron is quite similar to that obtained for B1 beads (Table 9.3). This is justified for the iron, considering that the sodium alginate nanoparticles solutions were prepared with the same concentration of Fe_3O_4 nanoparticles. Instead, the same percentage of calcium in the two types of beads can be explained considering that this is a superficial analysis. From the results, it can be concluded that the concentration of calcium in the hardener solution is sufficient in both cases for a

complete crosslinking of the superficial part of the bead. A lower amount of calcium ions should be appreciable inside the beads, so it would be necessary to perform an ESEM-EDX analysis of an internal section of the bead. Another technique for appreciating the effect of the reduced concentration of calcium in this type of beads can be the ICP analysis, which would give the total concentration of Ca in the sample, averaging the outer and the inner parts of the beads. Moreover, the showed results come from a partial analyse conducted on a single spot of the sample. An averaged analysis on a higher number of spots could be considered.

Table 9.4: EDX elemental analysis of the bead B2.

Element	Weight %
C	26.06
O	55.57
Ca	5.62
Fe	12.76

9.2.3.2 Characterization of beads with Fe_3O_4@GO

Concluding the ESEM characterization, *Figure 9.11* reports the ESEM images of B3 beads. The analysed bead is almost completely dehydrated. For this reason, its surface appears extremely rough and irregular. This is probably due also to the presence of the graphene oxide 2D sheet structure, which can interfere with the organization of the polymer fibres and their ionic interactions.

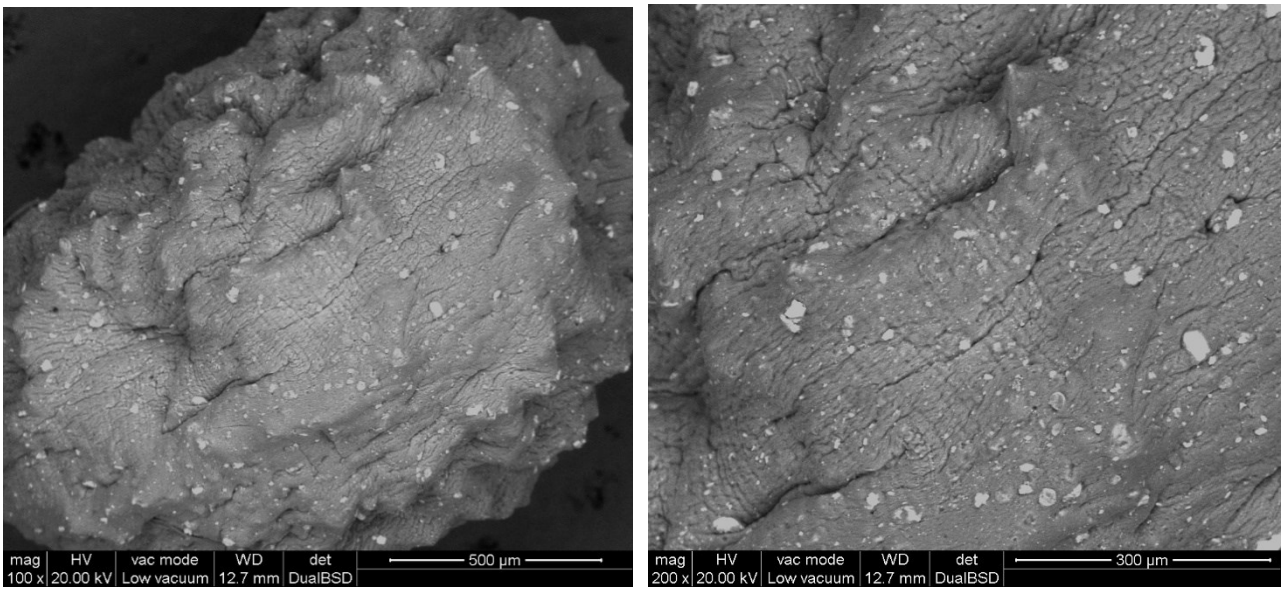

Figure 9.11: ESEM characterization of beads with GO (B3).

Figure 9.12 reports the average analysis of a superficial spot on the beads surface. Also in this case, the graph qualitatively indicates the presence of both calcium and iron.

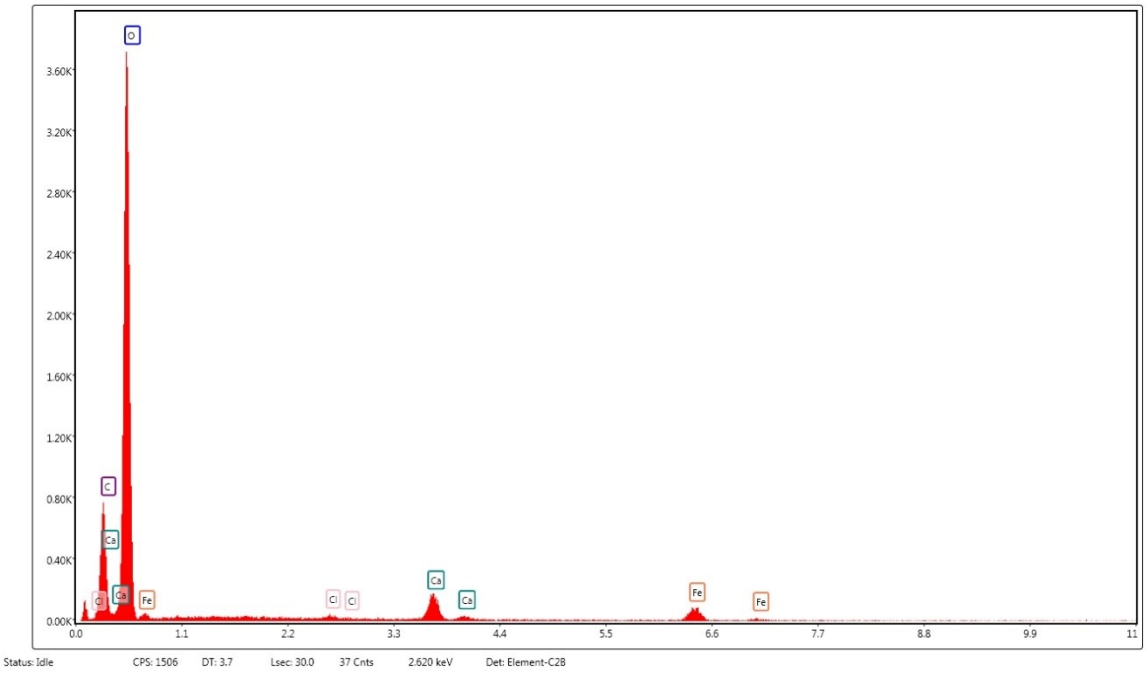

Figure 9.12: Medium analysis on a point of the beads' surface (B3).

Table 9.5 reports the EDX elemental analysis of the bead B3.

Table 9.5: EDX elemental analysis of the bead B3.

Element	Weight %
C	12.77
O	83.21
Ca	2.03
Fe	1.99

9.3 Adsorption tests with heavy metal ions

The results of the adsorption tests are subdivided both in isotherm test and kinetic test for each kind of adsorbent medium. The tests were conducted separately for the single elements and the mixtures of all the three heavy metals copper(II), chromium(III), and nickel(II).

9.3.1 Preliminary adsorption tests with copper nitrate

For what regard the preliminary test, conducted with pure sodium alginate beads, already after less than 10 min all the beads become light blue and, after this time, they did not change colour. This could mean that in 10 min they were already near the saturation concentration.

Concerning the preliminary test regarding the regeneration capacity of this adsorption medium, the beads left for the night in a calcium solution, released the copper(II) and returned transparent (Figure 9.13).

Figure 9.13: Beads removed from the solution after respectively 30 min, 1 h and 1 h and 30 min (on the left). Regenerated beads in calcium solution (on the right).

9.3.2 Isotherm adsorption tests

9.3.2.1 Adsorption isotherms for single elements using nanoparticles

Table 9.6 reports in detail the results for the isotherm adsorption of chromium(III). It is possible to see that with concentrations below 1100 µg/L, the adsorption efficiency is always above 97%. This means that the saturation is reached at higher concentrations. Instead, above 1100 µg/L, the removal decreases progressively down to 45% for 5000 µg/L (where a maximum load of 2.23 mg/g is reached).

Table 9.6: Results for chromium(III) adsorption.

Chromium(III)	**#1**	**#2**	**#3**	**#4**	**#5**
C_0 (µg/L)	440	580	1060	1810	4990
C_0 (µmol/L)	8.46	11.15	20.39	34.81	95.97
C_{end} (µg/L)	10	10	17.3	370	2760
η (mg/g)	0.43	0.57	1.04	1.44	2.23
Removal (%)	98	98	98	80	45

Figure 9.14 reports the removal of chromium(III) depending on the starting concentration of the heavy metal in solution (C_o). It is clearly visible as the value decreases with the increases of the initial concentration, but the adsorption efficiencies remain high.

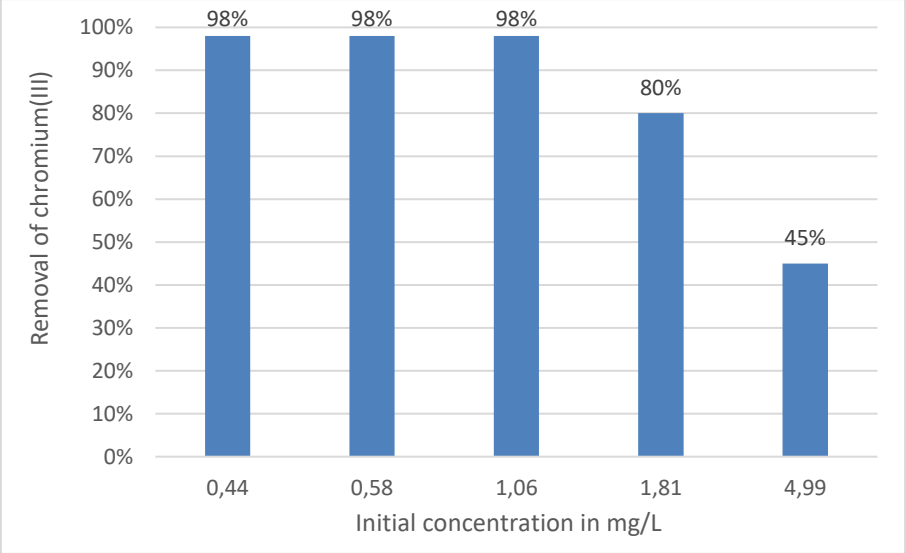

Figure 9.14: Removal of chromium(III) depending on the starting concentration of the heavy metal in solution.

Table 9.7 reports the results for copper(II). Results are similar to chromium, but the efficiency appears to be lower at lower starting concentrations. At 6.43 mg/L of Cu(II), the adsorption capacity is 4.56 mg/g, with a removal efficiency equal to 71%.

Table 9.7: Results for copper(II) adsorption.

Copper(II)	**#1**	**#2**	**#3**	**#4**	**#5**	**#6**
C_o (µg/L)	296	501	690	1020	2000	6430
C_o (µmol/L)	4.66	7.88	10.86	16.05	31.47	101.19
C_{end} (µg/L)	25.9	4502	48.6	53.9	185	1865
η (mg/g)	0.27	0.46	0.64	0.97	1.81	4.56
Removal (%)	91	91	93	95	91	71

Figure 9.15 reports the removal of copper(II) depending on the starting concentration of the heavy metal in solution (C_o).

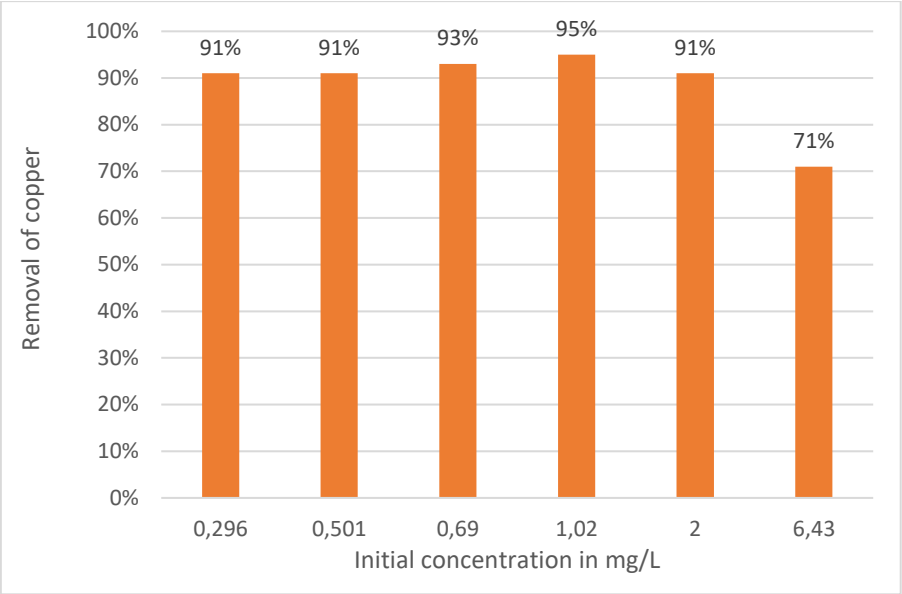

Figure 9.15: Removal of copper(II) depending on the starting concentration of the heavy metal in solution.

Table 9.8 reports the results for nickel. Adsorption efficiency steadily increases with the increase of the initial concentration: 91.4% at 935 µg/L and 56.6% at 5120 µg/L, respectively. The maximum achieved load of nickel(II) was found to be 2.90 g/mg, which is higher if compared with chromium's under similar starting concentrations.

Table 9.8: Results for nickel(II) adsorption.

Nickel(II)	**#1**	**#2**	**#3**	**#4**
C_o (µg/L)	935	1900	3980	5120
C_o (µmol/L)	15.93	32.37	67.81	87.23
C_{end} (µg/L)	80.4	298	1700	2220
η (mg/g)	0.85	1.60	2.28	2.90
Removal (%)	91	84	57	57

Figure 9.16 reports the removal of nickel(II) depending on the starting concentration of the heavy metal in solution (C_o).

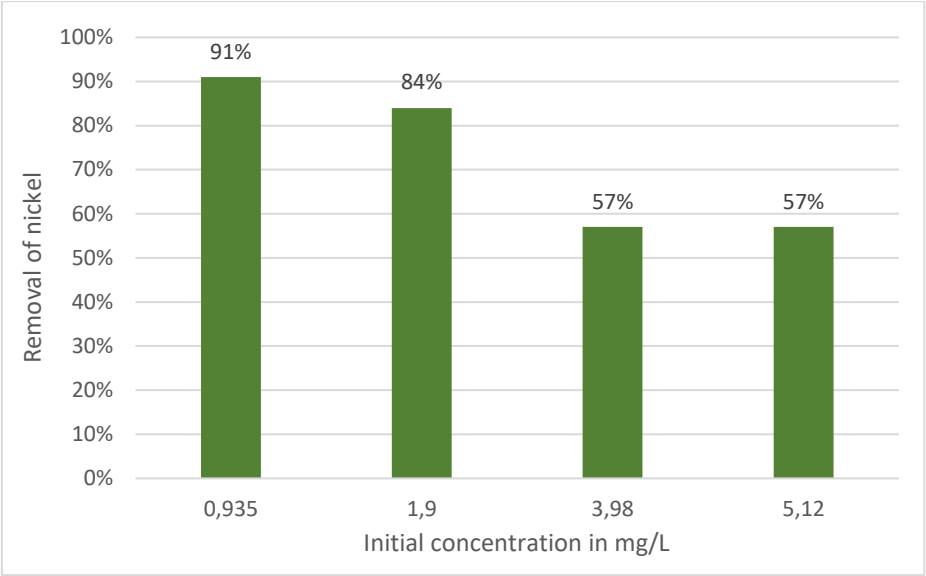

Figure 9.16: Removal of nickel(II) depending on the starting concentration of the heavy metal in solution.

Based on the difference between initial and final concentrations, the corresponding adsorption isotherms were developed. All the adsorption parameters were fitted from the experimental data using a Langmuir model, which is expected to give the best physical description of the adsorption process even if such a model was originally developed for the description of gas adsorption on solid phases (as activated carbons). But this model is very versatile and can be simply extended to characterize different adsorption processes, as the adsorption of metal ions dissolved in aqueous solutions on magnetic nanoparticles. Referring to the adsorption of different metal ions (Cu^{2+}, Cr^{3+}, and Ni^{2+}) on the nanoadsorbent dispersed in an aqueous solution, the equation is the following:

$$\eta = \frac{Q_{max} \cdot b \cdot C_o}{1 + b \cdot C_o} = \frac{(C_{end} - C_o) \cdot V_{sol}}{m} \quad [9]$$

where Q_{max} and b are constants; C_o represents the initial concentration of the metal ions in the solution, C_{end} is the final concentration of metal ion in the fluid phase, V_{sol} is the volume of the aqueous solution, m is the mass of magnetic nanoparticles used for a single treatment, and η is the final load of metal ion, which is adsorbed on the nanoparticles. The removal efficiency, χ, is evaluated as it follows:

$$\chi = \frac{C_0 - C_{end}}{C_0} \quad [10]$$

The design variables (Q_{max} and b) to be found are the coefficients of the Langmuir model. They were designed to minimize two objective functions: (f_1) the sum of the square of the point to difference of

the N measured valued with respect to the one evaluated by the model at different C_o and (f_2) the minimization of the maximum of the point to point difference between the measured values and the ones evaluated by the model. The optimization problem is based on the following objective functions to be minimized:

$$f_1 = \sum_{i=1}^{N} \left(X_{m,i}([C_{0,i}]) - X_{f,i}([C_{0,i}])\right)^2 \quad [11]$$

$$f_2 = \max_{i=1,\dots N} \left(\left|X_{m,i}([C_{0,i}]) - X_{f,i}([C_{0,i}])\right|\right) \quad [12]$$

where X_m is the experimental value of η_{end} as derived from the right side of the Langmuir equation and X_f is the value of η_{end} as estimated by the Langmuir model (left side of Langmuir equation). The optimization problem is solved by using a genetic algorithm in the class of Non-dominated- Sorting-Genetic Algortim (NSGA) with the collaboration of Prof. Elisabetta Sieni and Prof. Sabrina Copelli of the University of Insubria.

Figure 9.17 shows the results of the fitting of the Langmuir isotherm with the experimental data. The results, which are in accordance with the Langmuir hypothesis, highlight the prevalence of monolayer adsorption as the controlling mechanism for the adsorbent tested. It is reasonable to assume that Cu(II) adsorption capacity may still increase at higher concentration values.

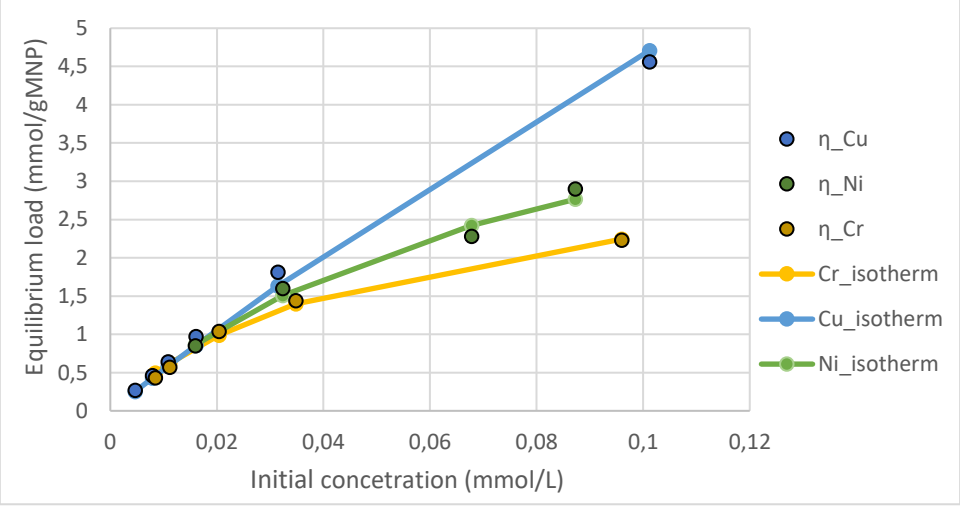

Figure 9.17: Fitting of the Langmuir isotherm of the experimental data, for the three different metal ions.

The values that have been used for fitting the experimental data by means of the Langmuir function are that reported in Table 9.9.

Table 9.9: Langmuir fitting parameters from the NSGA optimization algorithm for the investigated ions.

	Chromium	Copper	Nickel
Q_{max} (mg/gMNA)	3.42	31.1	5.45
b (L/mmol)	19.9	1.75	11.8

The Langmuir model shows a very good agreement with experimental data. A minimizing function f_l always lower than $2 \cdot 10^{-5}$ and a correlation coefficient also always equal or greater than 0.99 evidence a single layer adsorption, which is well-described by the Langmuir model. The maximum monolayer adsorption capacity ranges between 3.42 and 31.3 $mg/g_{(MNA)}$. The maximum value found is for copper(II), which possesses a significantly higher compatibility with the nanoadsorbents studied.

9.3.2.2 Adsorption isotherms for single elements using the beads

Table 9.10 reports the results for chromium(III). The removal efficiency of the different types of beads could be investigated.

Table 9.10: Results for chromium(III) adsorption with beads.

(mg/L) not treated solution	(mg/L) solution treated with B1	(mg/L) solution treated with B2	(mg/L) solution treated with B3
0.139 ± 0.01	0.033 ± 0.005	0.029 ± 0.005	0.065 ± 0.005
0.225 ± 0.01	0.035 ± 0.005	0.076 ± 0.005	0.046 ± 0.005
0.273 ± 0.01	0.105 ± 0.01	0.026 ± 0.005	0.045 ± 0.005
0.423 ± 0.01	0.018 ± 0.005	0.029 ± 0.005	0.056 ± 0.005
0.605 ± 0.01	0.023 ± 0.005	0.015 ± 0.005	0.071 ± 0.005
1.915 ± 0.1	0.067 ± 0.005	0.062 ± 0.005	0.120 ± 0.01

Figure 9.18 reports the removal efficiencies of each kind of beads, in dependence to the initial concentrations of chromium present inside the non-treated solution.

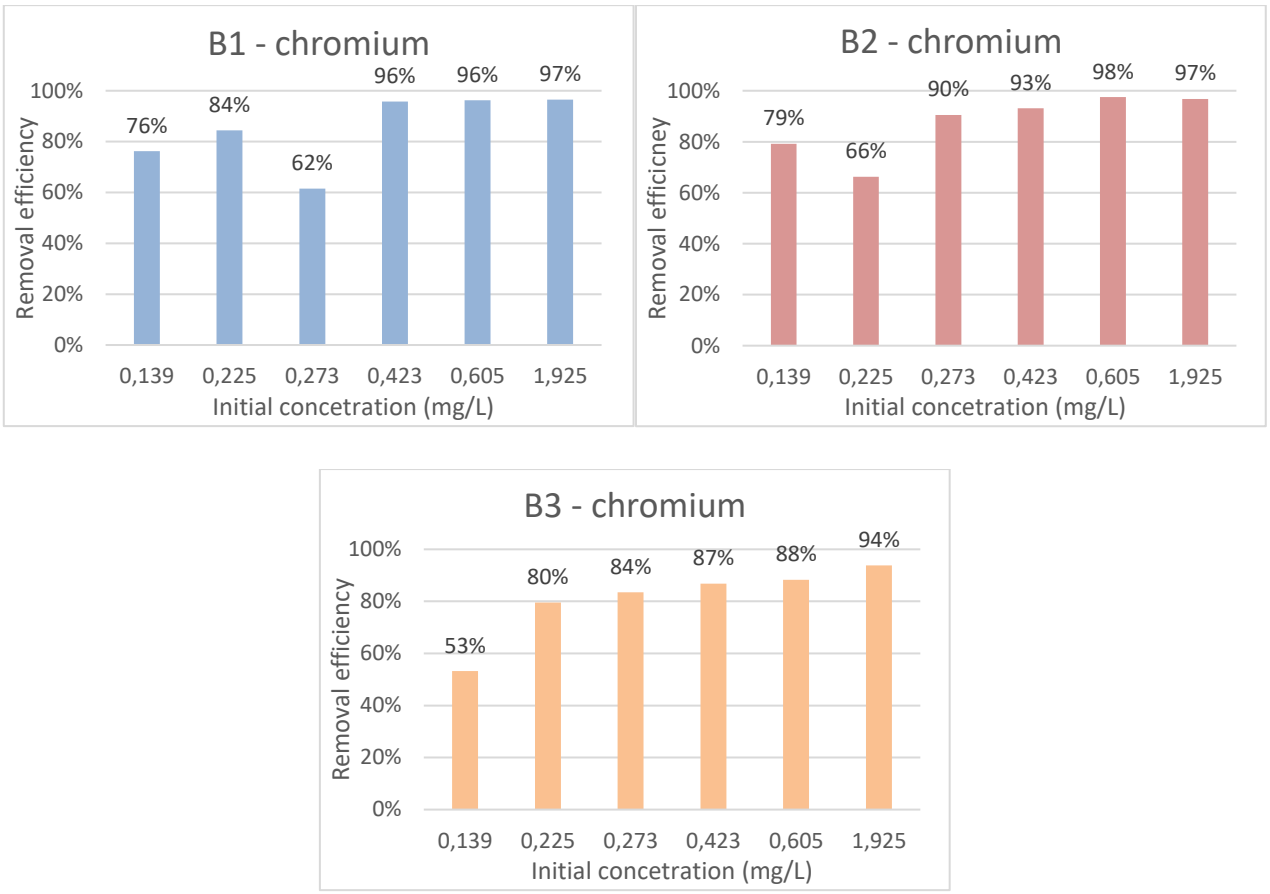

Figure 9.18: Comparison between the performance of different kinds of beads for the adsorption of chromium.

Table 9.11 reports the results for copper. The removal efficiency of the different types of beads could be investigated.

Table 9.11: Results for copper(II) adsorption with beads.

(mg/L) not treated solution	**(mg/L) solution treated with B1**	**(mg/L) solution treated with B2**	**(mg/L) solution treated with B3**
0.123 ± 0.01	0.024 ± 0.005	0.015 ± 0.005	0.036 ± 0.005
0.302 ± 0.01	0.053 ± 0.005	0.030 ± 0.005	0.060 ± 0.005
0.587 ± 0.01	0.088 ± 0.005	0.082 ± 0.005	0.082 ± 0.005
0.838 ± 0.01	-	0.152 ± 0.01	0.062 ± 0.005
0.928 ± 0.05	0.156 ± 0.01	-	-
2.380 ± 0.05	0.383 ± 0.01	-	-
2.770 ± 0.1	-	0.311 ± 0.01	0.615 ± 0.01
4.820 ± 0.1	0.648 ± 0.01	0.652 ± 0.01	0.755 ± 0.01

Figure 9.19 reports the removal efficiencies of each kind of beads, in dependence to the initial concentrations of copper present inside the non-treated solution.

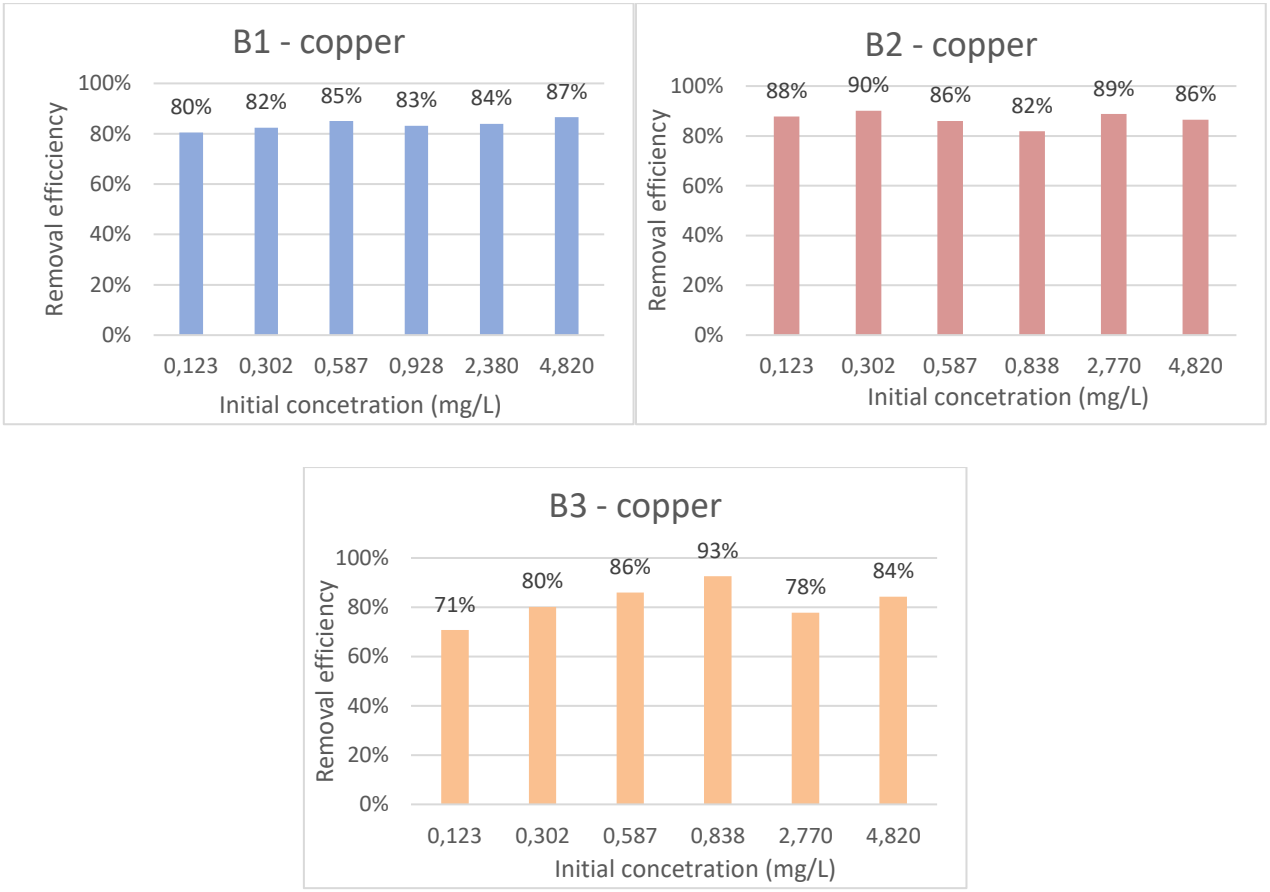

Figure 9.19: Comparison between the performance of different kinds of beads for the adsorption of copper.

Table 9.12 reports the results for nickel. The removal efficiency of the different types of beads could be investigated.

Table 9.12: Results for nickel(II) adsorption with beads.

(mg/L) not treated solution	**(mg/L) solution treated with B1**	**(mg/L) solution treated with B2**	**(mg/L) solution treated with B3**
0.443 ± 0.01	0.082 ± 0.005	0.093 ± 0.005	0.196 ± 0.01
1.020 ± 0.1	-	0.415 ± 0.01	0.172 ± 0.01
1.060 ± 0.05	0.193 ± 0.01	-	-
2.120 ± 0.1	-	0.881 ± 0.01	0.100 ± 0.01
2.166 ± 0.05	0.364 ± 0.01	-	-
4.250 ± 0.1	1.053 ± 0.05	-	-
4.394 ± 0.1	-	2.022 ± 0.1	0.621 ± 0.01
5.123 ± 0.1	-	2.171 ± 0.1	0.990 ± 0.01
6.125 ± 0.1	0.982 ± 0.05	-	-

Figure 9.20 reports the removal efficiencies of each kind of beads, in dependence to the initial concentrations of nickel present inside the non-treated solution.

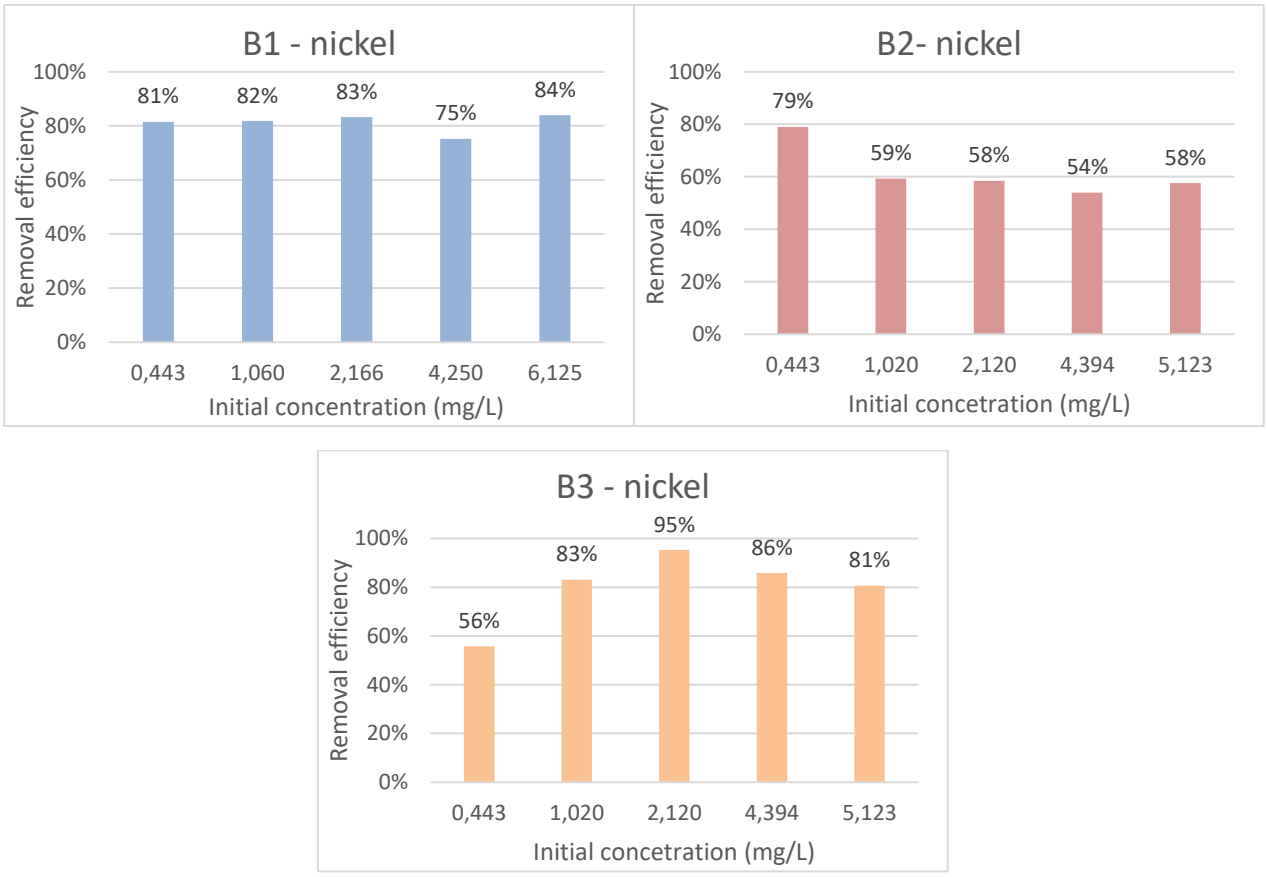

Figure 9.20: Comparison between the performance of different kinds of beads for the adsorption of nickel.

9.3.3 Kinetic adsorption tests

9.3.3.1 Adsorption kinetics using nanoparticles

Kinetic tests using nanoparticles have been conducted both on single elements solution and toward their mixtures.

9.3.3.1.1 Single elements adsorption kinetics using nanoparticles

Table 9.13 reports the results for the adsorption of single elements over time, until 10 min.

Table 9.13: Results for the kinetic tests conducted on the adsorption of single elements.

Element	0''	30''	1 min	2.5 min	5 min	7.5 min	10 min
Cu (µg/L)	1890	748	413	-	257	-	108
Removal		60%	78%	-	86%	-	94%
Cr (µg/L)	2740	822	233	148	0	0	0

Removal		70%	92%	95%	100%	100%	100%
Ni (µg/L)	3635	2655	2165	-	1730	-	1675
Removal		27%	40%	-	52%	-	54%

Note: 0 means <10

Figure 9.21 shows the decreasing concentration during the time interval of the test, for each of the three selected heavy metal ions.

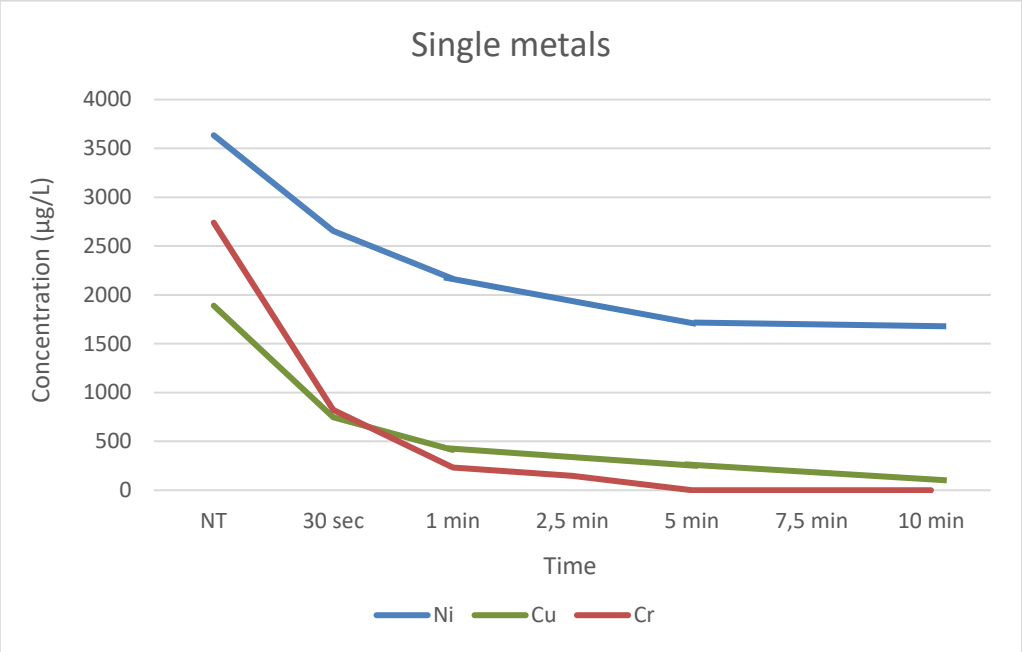

Figure 9.21: Kinetic adsorption curves for the three heavy metal ions Ni^{2+}, Cu^{2+}, and Cr^{3+}.

9.3.3.1.2 Mixtures adsorption kinetics using nanoparticles

The results regarding the mixtures analyses prove the decrease in concentration of all the elements present in the solution over time, until 10 min.

9.3.3.1.2.1 Mixture H

Table 9.14 reports the results for the adsorption of each element in mixture H, over time.

Table 9.14: Results for the kinetic tests conducted on the adsorption of mixture H.

Element	**0''**	**30''**	**1 min**	**2.5 min**	**5 min**	**7.5 min**	**10 min**
Cu (µg/L)	494	104	31.9	28.1	15.1	0	30.4
Removal		79%	94%	94%	97%	100%	94%
Cr (µg/L)	1805	651	352	45.5	33.6	13.3	23.2

Removal		64%	81%	98%	98%	99%	99%
Ni (µg/L)	2360	1560	1295	985	868	737	817
Removal		34%	45%	58%	63%	69%	65%

Note: 0 means <10

Figure 9.22 shows the decreasing trend of the concentration during the time interval of the test, for each one of the three selected heavy metal ions contained in mixture H.

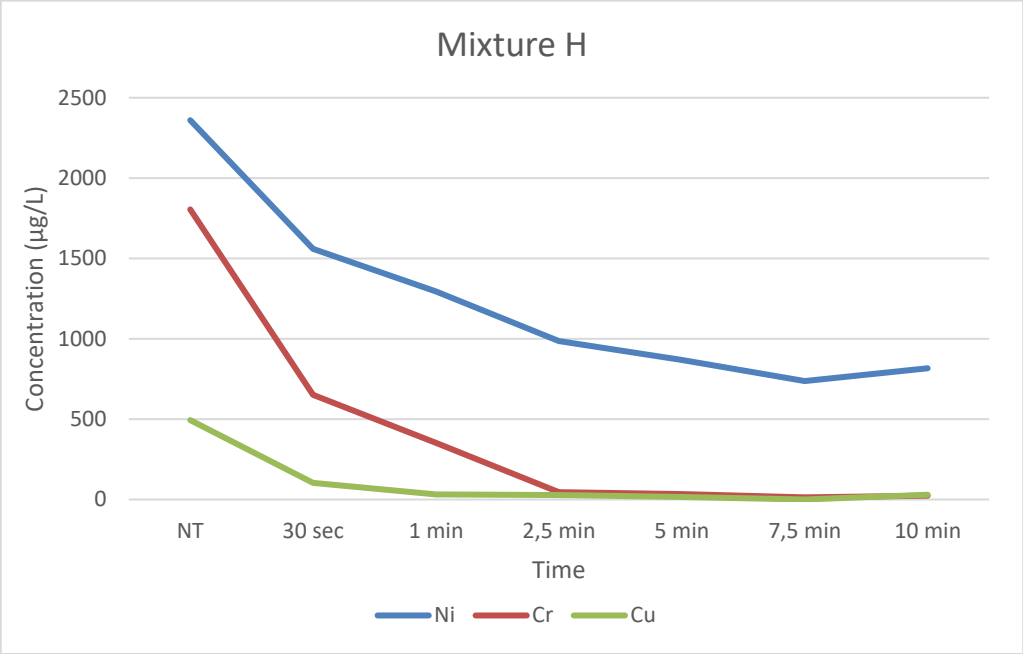

Figure 9.22: Kinetic adsorption curves for mixture H.

9.3.3.1.2.2 Mixture E

Table 9.15 reports the results for the adsorption of each element in mixture E, over time.

Table 9.15: Results for the kinetic tests conducted on the adsorption of mixture E.

Element	**0''**	**30''**	**1 min**	**2.5 min**	**5 min**	**7.5 min**	**10 min**
Cu (µg/L)	301	42.2	107	0	0	0	0
Removal		86%	65%	100%	100%	100%	100%
Cr (µg/L)	395	0	15.8	0	0	0	0
Removal		100%	96%	100%	100%	100%	100%
Ni (µg/L)	1250	265	191	141	135	105	63.3
Removal		79%	85%	89%	89%	92%	95%

Note: 0 means <10

Figure 9.23 shows the decreasing trend of the concentration during the time interval of the test, for each one of the three selected heavy metal ions contained in mixture E.

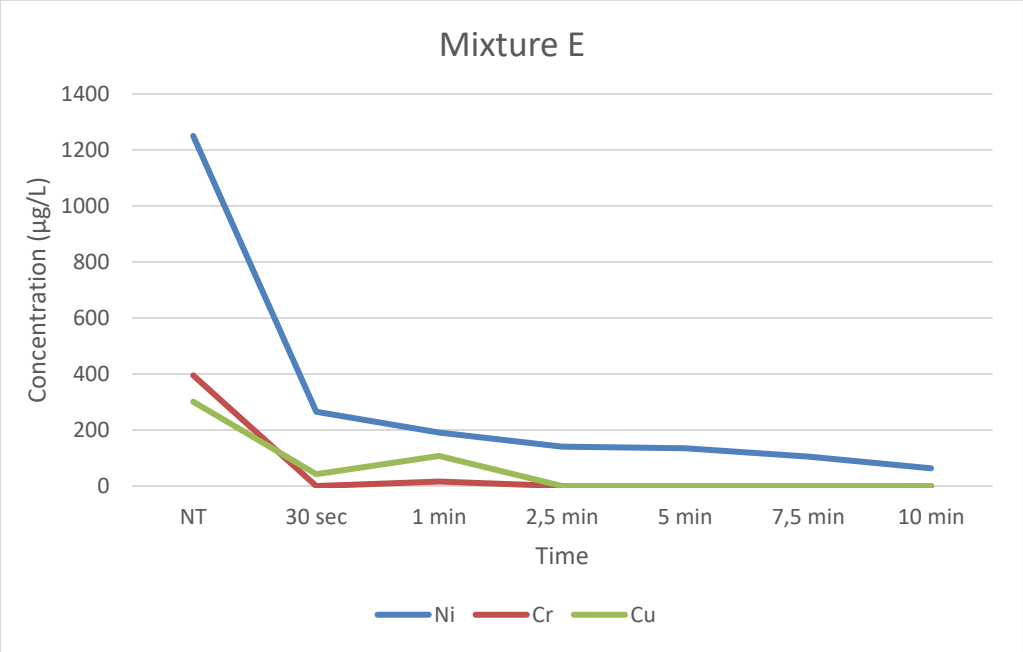

Figure 9.23: Kinetic adsorption curves for mixture E.

9.3.3.1.2.3 Mixture I

Table 9.16 reports the results for the adsorption of each element in mixture I, over time.

Table 9.16: Results for the kinetic tests conducted on the adsorption of mixture I.

Element	0''	30''	1 min	2.5 min	5 min	7.5 min	10 min
Cu (µg/L)	980	526	456	273	287	170	145
Removal		46%	53%	72%	71%	83%	85%
Cr (µg/L)	4770	3280	3030	2400	2120	1730	1280
Removal		31%	37%	50%	56%	64%	73%
Ni (µg/L)	5600	4830	4660	4550	4680	4700	4580
Removal		14%	17%	19%	16%	16%	18%

Note: 0 means <10

Figure 9.24 shows the decreasing trend of the concentration during the time interval of the test, for each one of the three selected heavy metal ions contained in mixture I.

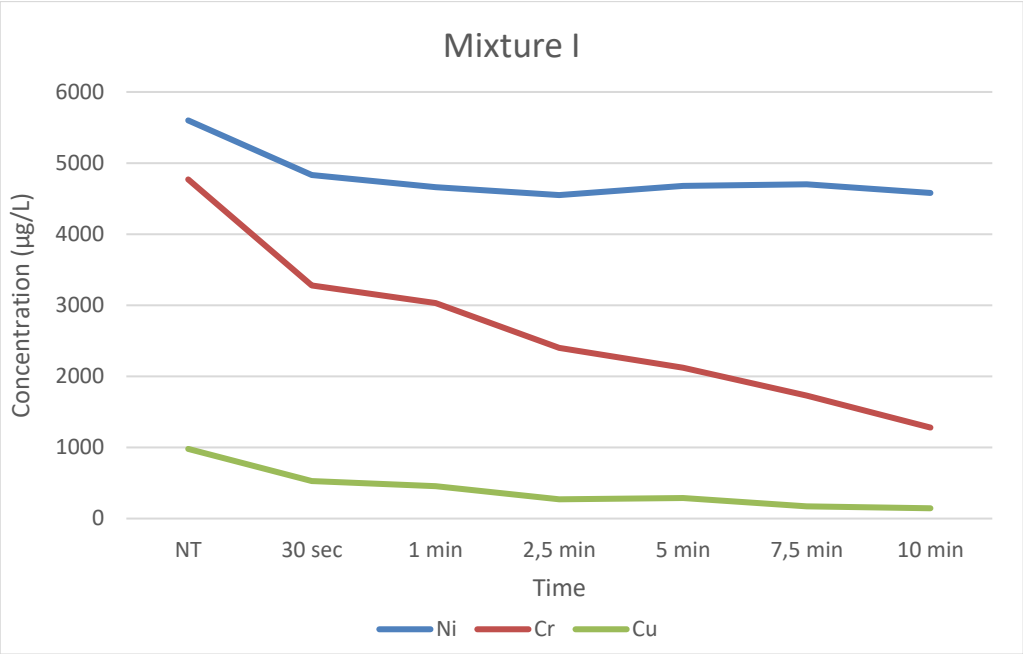

Figure 9.24: Kinetic adsorption curves for mixture I.

9.3.3.2 Adsorption kinetics using the beads

The clearest evidence from the analysis of the adsorption kinetics tests is that the beads of type B1 are less mechanically stable than the other types. In fact, during the longest tests (3 h and 24 h), B1 started to decompose, while beads of type B2 and B3 remained in their form (Figure 9.25). It can be clearly seen that the vials containing the beads B1, after the tests, contains a dark suspension, with respect to the vials containing beads B2. This is due to the fact that B1 adsorbed less calcium during the formation/crosslinking process (as they were immediately removed from the hardener solution). Moreover, the greatest instability was seen in the treatment of the sample with chromium(III). This is due to the fact that chromium(III) being a trivalent metal needs the exchange of more calcium atoms for its adsorption. Instead, copper(II) and nickel(II) can substitute a single Ca^{2+} ion each.

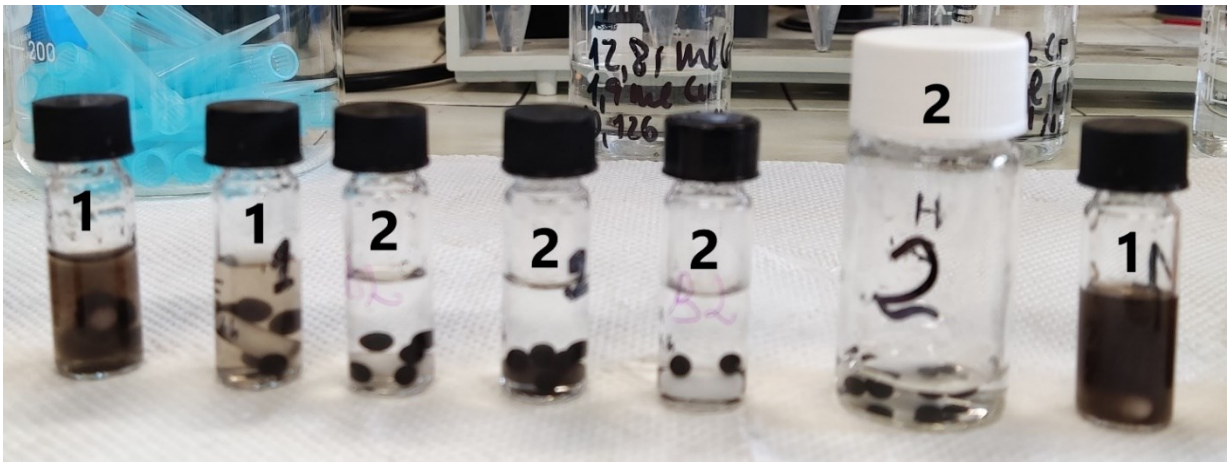

Figure 9.25: Vials with B1 or B2, after the test lasting 3 h or 24 h.

The lower mechanical resistance of the B1 beads indicates that the crosslinking process conducted with a lower calcium concentration produces beads which are not suitable for the envisaged application.

10 Conclusions and future perspectives

Water scarcity will constantly increase in the foreseeable future, so the recovery and purification of wastewater will be fundamental. This thesis studied some new magnetic nanocomposites for heavy metals removal from wastewater. The synthesis and functionalization processes are easy to implement, and the starting materials have limited costs. The nanocomposites' magnetic properties allow their separation from the water streams by applying a simple magnet. These nanocomposites may therefore be implemented in a simple device where they would be injected in the wastewater stream, mixed, and magnetically removed.

The adsorption efficiency of the nanoparticles has been tested on single heavy metals (Cu^{2+}, Ni^{2+}, and Cr^{3+}) and their mixtures. Their efficiency steadily increases with the increase of the initial concentration. However, below 1100 µg/L the removal is always higher than 91%. Up to an initial concentration of 6500 µg/L the removal remains higher than 45 %. Copper(II) possesses a significantly greater compatibility with the studied nanoparticles. At 6.43 mg/L of Cu(II), the adsorption capacity is 4.56 mg/g, with a removal efficiency of 71%. The Langmuir adsorption model shows a very good agreement with the experimental data. The results highlight the prevalence of monolayer adsorption as the controlling mechanism for the nanoadsorbent tested.

The removal efficiencies of the beads are higher than 60% with any initial concentration of the heavy metal ions. The beads show a slightly lower compatibility towards nickel(II) ions. This behavior is evidenced also in the trend obtained from the adsorption kinetics of the nanoparticles.

The adsorption kinetic tests of the nanoparticles show a consistently decreasing trend of the concentration of the heavy metal ions over time, both considering the single heavy metals and their mixtures. The lower selectivity for nickel(II) is confirmed, with respect to the other two heavy metals.

This work could be further developed investigating the results obtained for the adsorption kinetic of the beads. Moreover, a characterization of the internal structure of the beads should be conducted, for a better understanding of the effect of the different concentrations of calcium ions in the hardener solution. The concentration which maximizes the adsorption capacities of the adsorbent without compromising its mechanical stability could be determined.

In a longer perspective, different chemical modifications of the alginate structure could also be studied, in order to optimize the adsorption properties. Considering the use of pristine nanoparticles, some variations can be introduced by adding surface functionalities or coordinating molecules to reduce the agglomeration and increase their dispersibility in polar solutions. Selected MOFs could

also be considered for the incorporation in the alginate matrix and the creation of a more porous system with active sites for the adsorption of other pollutants (e.g. organic species). The adsorption kinetics and the subsequent regeneration process for the different alginate materials will have to be tested with different simulated wastewater systems, determining the removal efficiency through ICP analyses or chromatographic techniques.

11 Bibliography

Agbovi, H. K., & Wilson, L. D. (2021). Adsorption processes in biopolymer systems: fundamentals to practical applications. In *Natural Polymers-Based Green Adsorbents for Water Treatment* (pp. 1–51). Elsevier. https://doi.org/10.1016/b978-0-12-820541-9.00011-9

Anirudhan, T. S., & Sreekumari, S. S. (2011). Adsorptive removal of heavy metal ions from industrial effluents using activated carbon derived from waste coconut buttons. *Journal of Environmental Sciences*, *23*(12), 1989–1998. https://doi.org/10.1016/S1001-0742(10)60515-3

Bilal, M., Ihsanullah, I., Younas, M., & Ul Hassan Shah, M. (2022). Recent advances in applications of low-cost adsorbents for the removal of heavy metals from water: A critical review. In *Separation and Purification Technology* (Vol. 278). Elsevier B.V. https://doi.org/10.1016/j.seppur.2021.119510

Bohli, T., Ouederni, A., Fiol, N., & Villaescusa, I. (2015). Evaluation of an activated carbon from olive stones used as an adsorbent for heavy metal removal from aqueous phases. *Comptes Rendus Chimie*, *18*(1), 88–99. https://doi.org/10.1016/j.crci.2014.05.009

Danesh, N., Hosseini, M., Ghorbani, M., & Marjani, A. (2016). Fabrication, characterization and physical properties of a novel magnetite graphene oxide/Lauric acid nanoparticles modified by ethylenediaminetetraacetic acid and its applications as an adsorbent for the removal of Pb(II) ions. *Synthetic Metals*, *220*, 508–523. https://doi.org/10.1016/j.synthmet.2016.07.025

Das, S. K., Ghosh, G. K., & Avasthe, R. (2021). Conversion of crop, weed and tree biomass into biochar for heavy metal removal and wastewater treatment. *Biomass Conversion and Biorefinery*. https://doi.org/10.1007/s13399-021-01334-y

Decreto Legislativo 3 aprile, n°152, parte terza, allegato 5, tabella 3, Pub. L. No. 152 (2006).

Duc, T. H., Vu, T. K., Dang, C. T., Nguyen, V. H., La, D. D., Kim, G. M., Chang, S. W., Bui, X. T., Dang, T. D., & Nguyen, D. D. (2021). Synthesis and application of hydrogel calcium alginate microparticles as a biomaterial to remove heavy metals from aqueous media. *Environmental Technology and Innovation*, *22*. https://doi.org/10.1016/j.eti.2021.101400

Gao, X., Guo, C., Hao, J., Zhao, Z., Long, H., & Li, M. (2020). Adsorption of heavy metal ions by sodium alginate based adsorbent-a review and new perspectives. In *International Journal of Biological Macromolecules* (Vol. 164, pp. 4423–4434). Elsevier B.V. https://doi.org/10.1016/j.ijbiomac.2020.09.046

Ghasemi, E., Mirhabibi, A., & Edrissi, M. (2008). Synthesis and rheological properties of an iron oxide ferrofluid. *Journal of Magnetism and Magnetic Materials*, *320*(21), 2635–2639. https://doi.org/10.1016/j.jmmm.2008.05.036

Giraldo, L., Erto, A., & Moreno-Piraján, J. C. (2013). Magnetite nanoparticles for removal of heavy metals from aqueous solutions: Synthesis and characterization. *Adsorption*, *19*(2–4), 465–474. https://doi.org/10.1007/s10450-012-9468-1

Granger, M., & Montalvo, D. (2018). *Industrial waste water treatment - pressure on Europe's environment*.

Ho, S. H., Chen, Y. di, Yang, Z. kai, Nagarajan, D., Chang, J. S., & Ren, N. qi. (2017). High-efficiency removal of lead from wastewater by biochar derived from anaerobic digestion sludge. *Bioresource Technology*, *246*, 142–149. https://doi.org/10.1016/j.biortech.2017.08.025

Huang, S. H., & Chen, D. H. (2009). Rapid removal of heavy metal cations and anions from aqueous solutions by an amino-functionalized magnetic nano-adsorbent. *Journal of Hazardous Materials*, *163*(1), 174–179. https://doi.org/10.1016/j.jhazmat.2008.06.075

Iconaru, S. L., Guégan, R., Popa, C. L., Motelica-Heino, M., Ciobanu, C. S., & Predoi, D. (2016). Magnetite (Fe3O4) nanoparticles as adsorbents for As and Cu removal. *Applied Clay Science*, *134*, 128–135. https://doi.org/10.1016/j.clay.2016.08.019

Jiang, H., Yang, Y., Lin, Z., Zhao, B., Wang, J., Xie, J., & Zhang, A. (2020). Preparation of a novel bio-adsorbent of sodium alginate grafted polyacrylamide/graphene oxide hydrogel for the adsorption of heavy metal ion. *Science of the Total Environment*, *744*. https://doi.org/10.1016/j.scitotenv.2020.140653

Jiao, C., Xiong, J., Tao, J., Xu, S., Zhang, D., Lin, H., & Chen, Y. (2016). Sodium alginate/graphene oxide aerogel with enhanced strength-toughness and its heavy metal adsorption study. *International Journal of Biological Macromolecules*, *83*, 133–141. https://doi.org/10.1016/j.ijbiomac.2015.11.061

Kim, E. J., Lee, C. S., Chang, Y. Y., & Chang, Y. S. (2013). Hierarchically structured manganese oxide-coated magnetic nanocomposites for the efficient removal of heavy metal ions from aqueous systems. *ACS Applied Materials and Interfaces*, *5*(19), 9628–9634. https://doi.org/10.1021/am402615m

Lim, J. Y., Mubarak, N. M., Abdullah, E. C., Nizamuddin, S., Khalid, M., & Inamuddin. (2018). Recent trends in the synthesis of graphene and graphene oxide based nanomaterials for removal

of heavy metals — A review. In *Journal of Industrial and Engineering Chemistry* (Vol. 66, pp. 29–44). Korean Society of Industrial Engineering Chemistry. https://doi.org/10.1016/j.jiec.2018.05.028

Liu, D., Zhu, Y., Li, Z., Tian, D., Chen, L., & Chen, P. (2013). Chitin nanofibrils for rapid and efficient removal of metal ions from water system. *Carbohydrate Polymers*, *98*(1), 483–489. https://doi.org/10.1016/j.carbpol.2013.06.015

Liu, W., Yang, L., Xu, S., Chen, Y., Liu, B., Li, Z., & Jiang, C. (2018). Efficient removal of hexavalent chromium from water by an adsorption-reduction mechanism with sandwiched nanocomposites. *RSC Advances*, *8*(27), 15087–15093. https://doi.org/10.1039/c8ra01805g

Lo, S. F., Wang, S. Y., Tsai, M. J., & Lin, L. D. (2012). Adsorption capacity and removal efficiency of heavy metal ions by Moso and Ma bamboo activated carbons. *Chemical Engineering Research and Design*, *90*(9), 1397–1406. https://doi.org/10.1016/j.cherd.2011.11.020

Ma, H., Yang, J., Gao, X., Liu, Z., Liu, X., & Xu, Z. (2019). Removal of chromium (VI) from water by porous carbon derived from corn straw: Influencing factors, regeneration and mechanism. *Journal of Hazardous Materials*, *369*, 550–560. https://doi.org/10.1016/j.jhazmat.2019.02.063

Ma, H., Yang, Y., Yin, F., Zhang, X. F., Qiu, J., & Yao, J. (2022). Integration of thermoresponsive MIL-121 into alginate beads for efficient heavy metal ion removal. *Journal of Cleaner Production*, *333*. https://doi.org/10.1016/j.jclepro.2021.130229

Mahesh, N., Balakumar, S., Shyamalagowri, S., Manjunathan, J., Pavithra, M. K. S., Babu, P. S., Kamaraj, M., & Govarthanan, M. (2022). Carbon-based adsorbents as proficient tools for the removal of heavy metals from aqueous solution: A state of art-review emphasizing recent progress and prospects. *Environmental Research*, 113723. https://doi.org/10.1016/j.envres.2022.113723

Majdoub, M., Amedlous, A., Anfar, Z., Jada, A., & el Alem, N. (2021). Engineering of amine-based binding chemistry on functionalized graphene oxide/alginate hybrids for simultaneous and efficient removal of trace heavy metals: Towards drinking water. *Journal of Colloid and Interface Science*, *589*, 511–524. https://doi.org/10.1016/j.jcis.2021.01.029

Ni, B. J., Huang, Q. S., Wang, C., Ni, T. Y., Sun, J., & Wei, W. (2019). Competitive adsorption of heavy metals in aqueous solution onto biochar derived from anaerobically digested sludge. *Chemosphere*, *219*, 351–357. https://doi.org/10.1016/j.chemosphere.2018.12.053

Niculescu, A. G., Chircov, C., & Grumezescu, A. M. (2022). Magnetite nanoparticles: Synthesis methods – A comparative review. *Methods*, *199*, 16–27. https://doi.org/10.1016/j.ymeth.2021.04.018

Pendolino, F., Parisini, E., & lo Russo, S. (2014). Time-Dependent Structure and Solubilization Kinetics of Graphene Oxide in Methanol and Water Dispersions. *The Journal of Physical Chemistry*, *28*(162).

Rahbari, M., & Goharrizi, A. S. (2009). Adsorption of Lead(II) from Water by Carbon Nanotubes: Equilibrium, Kinetics, and Thermodynamics. *Water Environment Research*, *81*(6), 598–607. https://doi.org/10.2175/106143008x370511

Raychaudhuri, S. sen, Pramanick, P., Talukder, P., & Basak, A. (2021). Polyamines, metallothioneins, and phytochelatins—Natural defense of plants to mitigate heavy metals. In *Studies in Natural Products Chemistry* (Vol. 69, pp. 227–261). Elsevier B.V. https://doi.org/10.1016/B978-0-12-819487-4.00006-9

Sardella, F., Gimenez, M., Navas, C., Morandi, C., Deiana, C., & Sapag, K. (2015). Conversion of viticultural industry wastes into activated carbons for removal of lead and cadmium. *Journal of Environmental Chemical Engineering*, *3*(1), 253–260. https://doi.org/10.1016/j.jece.2014.06.026

Shahrokhi-Shahraki, R., Benally, C., El-Din, M. G., & Park, J. (2021). High efficiency removal of heavy metals using tire-derived activated carbon vs commercial activated carbon: Insights into the adsorption mechanisms. *Chemosphere*, *264*. https://doi.org/10.1016/j.chemosphere.2020.128455

Shen, H., Chen, J., Dai, H., Wang, L., Hu, M., & Xia, Q. (2013). New insights into the sorption and detoxification of chromium(VI) by tetraethylenepentamine functionalized nanosized magnetic polymer adsorbents: Mechanism and pH effect. *Industrial and Engineering Chemistry Research*, *52*(36), 12723–12732. https://doi.org/10.1021/ie4010805

Shen, H., Pan, S., Zhang, Y., Huang, X., & Gong, H. (2012). A new insight on the adsorption mechanism of amino-functionalized nano-Fe 3O 4 magnetic polymers in Cu(II), Cr(VI) co-existing water system. *Chemical Engineering Journal*, *183*, 180–191. https://doi.org/10.1016/j.cej.2011.12.055

Shi, T., Xie, Z., Zhu, Z., Shi, W., Liu, Y., & Liu, M. (2022). Highly efficient and selective adsorption of heavy metal ions by hydrazide-modified sodium alginate. *Carbohydrate Polymers*, *276*. https://doi.org/10.1016/j.carbpol.2021.118797

Sikder, M. T., Mihara, Y., Islam, M. S., Saito, T., Tanaka, S., & Kurasaki, M. (2014). Preparation and characterization of chitosan-caboxymethyl-β-cyclodextrin entrapped nanozero-valent iron composite for Cu (II) and Cr (IV) removal from wastewater. *Chemical Engineering Journal*, *236*, 378–387. https://doi.org/10.1016/j.cej.2013.09.093

Singh, K., Renu, N. A., & Agarwal, M. (2017). Methodologies for removal of heavy metal ions from wastewater: an overview. *Interdisciplinary Environmental Review*, *18*(2), 124. https://doi.org/10.1504/ier.2017.10008828

Stafiej, A., & Pyrzynska, K. (2007). Adsorption of heavy metal ions with carbon nanotubes. *Separation and Purification Technology*, *58*(1), 49–52. https://doi.org/10.1016/j.seppur.2007.07.008

Sutirman, Z. A., Sanagi, M. M., & Wan Aini, W. I. (2021). Alginate-based adsorbents for removal of metal ions and radionuclides from aqueous solutions: A review. In *International Journal of Biological Macromolecules* (Vol. 174, pp. 216–228). Elsevier B.V. https://doi.org/10.1016/j.ijbiomac.2021.01.150

Tafjord, J., Rytter, E., Holmen, A., Myrstad, R., Svenum, I. H., Christensen, B. E., & Yang, J. (2021). Transition-Metal Nanoparticle Catalysts Anchored on Carbon Supports via Short-Chain Alginate Linkers. *ACS Applied Nano Materials*, *4*(4), 3900–3910. https://doi.org/10.1021/acsanm.1c00294

Thakur, A. K., Singh, R., Teja Pullela, R., & Pundir, V. (2022). Green adsorbents for the removal of heavy metals from Wastewater: A review. *Materials Today: Proceedings*, *57*, 1468–1472. https://doi.org/10.1016/j.matpr.2021.11.373

Tu, Y. J., Chan, T. S., Tu, H. W., Wang, S. L., You, C. F., & Chang, C. K. (2016). Rapid and efficient removal/recovery of molybdenum onto ZnFe2O4 nanoparticles. *Chemosphere*, *148*, 452–458. https://doi.org/10.1016/j.chemosphere.2016.01.054

Tu, Y. J., You, C. F., & Chang, C. K. (2013). Conversion of waste Mn-Zn dry battery as efficient nano-adsorbents for hazardous metals removal. *Journal of Hazardous Materials*, *258–259*, 102–108. https://doi.org/10.1016/j.jhazmat.2013.04.029

Tu, Y. J., You, C. F., Chen, M. H., & Duan, Y. P. (2017). Efficient removal/recovery of Pb onto environmentally friendly fabricated copper ferrite nanoparticles. *Journal of the Taiwan Institute of Chemical Engineers*, *71*, 197–205. https://doi.org/10.1016/j.jtice.2016.12.006

Verma, M., Tyagi, I., Chandra, R., & Gupta, V. K. (2017). Adsorptive removal of Pb (II) ions from aqueous solution using CuO nanoparticles synthesized by sputtering method. *Journal of Molecular Liquids*, *225*, 936–944. https://doi.org/10.1016/j.molliq.2016.04.045

Verma, R., Asthana, A., Singh, A. K., Prasad, S., & Susan, M. A. B. H. (2017). Novel glycine-functionalized magnetic nanoparticles entrapped calcium alginate beads for effective removal of lead. *Microchemical Journal*, *130*, 168–178. https://doi.org/10.1016/j.microc.2016.08.006

Wadhawan, S., Jain, A., Nayyar, J., & Mehta, S. K. (2020). Role of nanomaterials as adsorbents in heavy metal ion removal from waste water: A review. In *Journal of Water Process Engineering* (Vol. 33). Elsevier Ltd. https://doi.org/10.1016/j.jwpe.2019.101038

Wang, B., Wan, Y., Zheng, Y., Lee, X., Liu, T., Yu, Z., Huang, J., Ok, Y. S., Chen, J., & Gao, B. (2019). Alginate-based composites for environmental applications: a critical review. *Critical Reviews in Environmental Science and Technology*, *49*(4), 318–356. https://doi.org/10.1080/10643389.2018.1547621

Wang, J., Guo, M., Luo, Y., Shao, D., Ge, S., Cai, L., Xia, C., & Lam, S. S. (2021). Production of magnetic sodium alginate polyelectrolyte nanospheres for lead ions removal from wastewater. *Journal of Environmental Management*, *289*. https://doi.org/10.1016/j.jenvman.2021.112506

Xu, P., Zeng, G. M., Huang, D. L., Lai, C., Zhao, M. H., Wei, Z., Li, N. J., Huang, C., & Xie, G. X. (2012). Adsorption of Pb(II) by iron oxide nanoparticles immobilized Phanerochaete chrysosporium: Equilibrium, kinetic, thermodynamic and mechanisms analysis. *Chemical Engineering Journal*, *203*, 423–431. https://doi.org/10.1016/j.cej.2012.07.048

Zhang, W., Ou, J., Wang, B., Wang, H., He, Q., Song, J., Zhang, H., Tang, M., Zhou, L., Gao, Y., & Sun, S. (2021). Efficient heavy metal removal from water by alginate-based porous nanocomposite hydrogels: The enhanced removal mechanism and influencing factor insight. *Journal of Hazardous Materials*, *418*. https://doi.org/10.1016/j.jhazmat.2021.126358